Universidad Autónoma de Madrid
Programa de Doctorado en Biociencias Moleculares

Molecular Mechanisms Underlying Cardiometabolic Disease in Aging

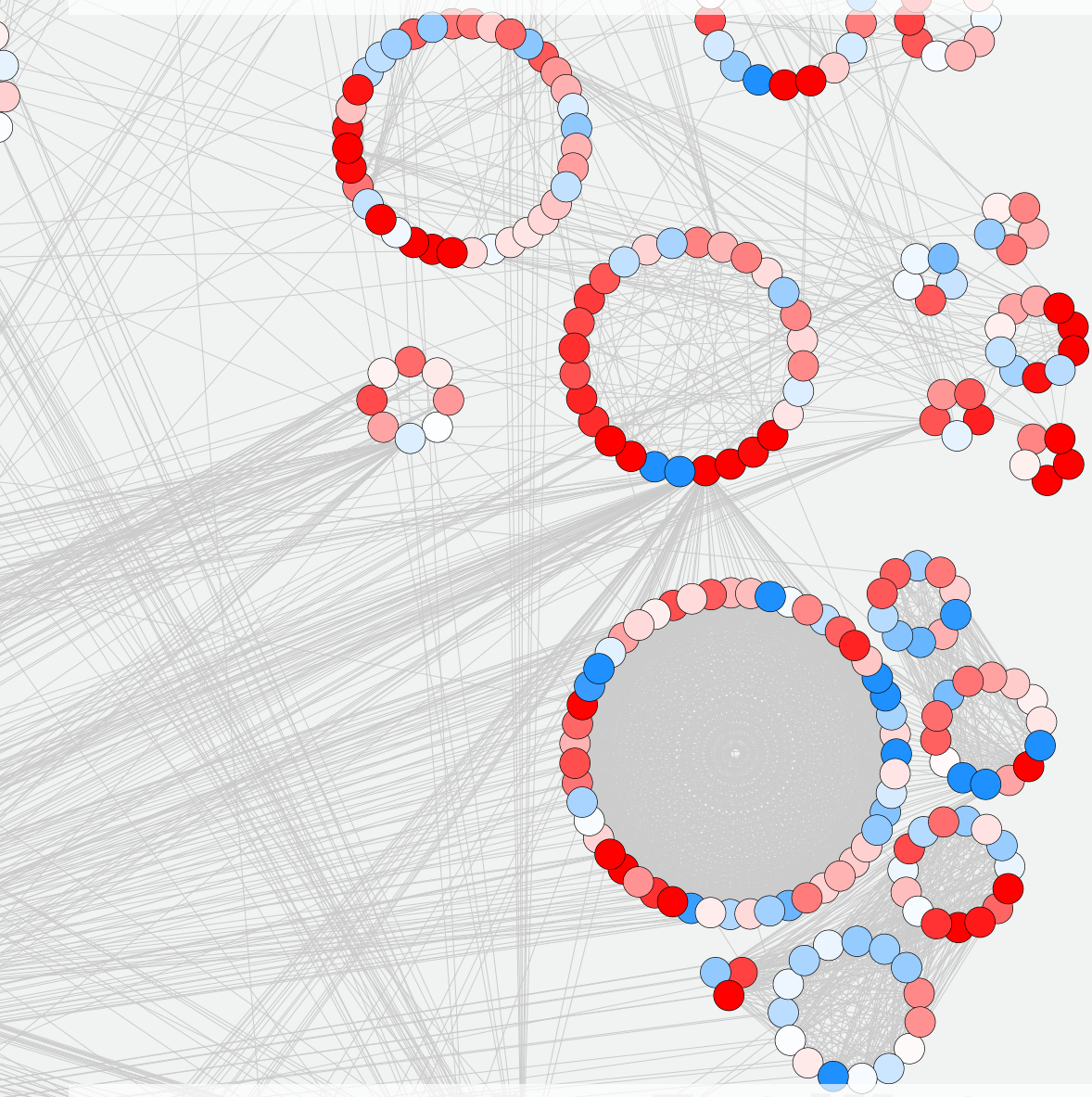

Víctor Fanjul Hevia

Madrid, 2019

Universidad Autónoma de Madrid

Departamento de Bioquímica

Facultad de Medicina

Doctoral Thesis

Molecular Mechanisms Underlying Cardiometabolic Disease in Aging

Víctor Fanjul Hevia

Licentiate in Biology

Supervisors Vicente Andrés García

Vascular Pathophysiology Area

Centro Nacional de Investigaciones Cardiovasculares Carlos III (CNIC)

Carlos López-Otín

Departamento de Bioquímica y Biología Molecular

Universidad de Oviedo

Madrid, 2019

Víctor Fanjul Hevia

Molecular Mechanisms Underlying Cardiometabolic Disease in Aging

Doctoral Thesis, Madrid, 2019

Supervisors: Vicente Andrés García & Carlos López-Otín

Universidad Autónoma de Madrid

Facultad de Medicina

Departamento de Bioquímica

Calle del Arzobispo Morcillo, 4

28029 Madrid

D. Vicente Andrés García, Doctor por la Universidad de Barcelona , y **D. Carlos López Otín**, Doctor por la Universidad Complutense de Madrid,

CERTIFICAN:

Que D. **Víctor Fanjul Hevia**, licenciado en Biología por la Universidad de Oviedo ha realizado bajo su dirección el trabajo de Tesis Doctoral que lleva por título ***Molecular Mechanisms Underlying Cardiometabolic Disease in Aging***.

Revisado el presente trabajo, expresan su conformidad para la presentación del mismo por considerar que reúne los requisitos necesarios para ser sometido a discusión ante el Tribunal correspondiente, para optar al grado de Doctor por la Universidad Autónoma de Madrid.

En Madrid, a 25 de febrero de 2019

Fdo.: Vicente Andrés García

Investigador principal

Centro Nacional de Investigaciones Cardiovasculares Carlos III (CNIC)
Melchor Fernández Almagro 3, 28029 Madrid
+34 914 531 200
vandres@cnic.es

Fdo.: Carlos López Otín

Catedrático de Bioquímica y Biología Molecular
Facultad de Medicina, Universidad de Oviedo, Instituto Universitario de Oncología del Principado de Asturias
33006-Oviedo
+34 985 104 201
clo@uniovi.es

To all who fight selflessly
to make *this* a better World
for *everyone*

> *I don't know where I'm going from here, but I promise it won't be boring.*
>
> **— David Bowie**

Acknowledgements / Agradecimientos

Recuerdo a mi yo de hace casi 10 años: ni siquiera había empezado segundo de carrera, pero quería participar como voluntario en el congreso de Bioquímica que iba a celebrarse en Oviedo. Con esto en mente, aproveché que Carlos estaba en el comité organizador para ir a conocerle en persona. Llevaba tiempo esperando la ocasión, pues sentía gran admiración por su investigación y filantropía. Para mi sorpresa, él ya sabía quien era yo y me esperaba para enseñarme el laboratorio. Así fue cómo (¿por serendipia?) comenzó el camino que hoy culmina con la presentación de esta Tesis Doctoral.

Carlos, estaré eternamente agradecido por la confianza que depositaste en mí aquel día. Siempre encuentras tiempo para los demás y sabes ver exactamente qué necesitamos para convertirnos en la mejor versión de nosotros mismos. Gracias también por animarme a hacer estancias y por avalarme. Recuerdo con gran cariño mis veranos en los laboratorios de Sandy y de Juan. Y como dicen que a la tercera va la vencida, fue durante la tercera estancia cuando conocí a Vicente y el lugar que (casi literalmente) se ha convertido en una casa para mí: el CNIC.

Vicente, recuerdo perfectamente cuando me llamaste por la beca Cicerone, porque me sorprendió mucho tu cercanía, que lo hizo todo más fácil. Muchas gracias por interesarte tan rápidamente en mí y por acogerme en tu laboratorio durante todos estos años. También por la libertad que me has brindado para diseñar y realizar experimentos, y por siempre tener la puerta abierta para recibirme cuando lo he necesitado.

Sois muchas las personas que habéis causado impacto en mi vida durante estos años. Haré lo posible por reconocer al menos a los que habéis contribuido directamente al desarrollo de mi Tesis. A todos los que por extensión del texto no pueda mencionar, sabed que igualmente soy consciente de vuestra aportación a esta historia.

Empecemos por el **laboratorio del CNIC**. Queridas María Jesús, Cris y Elba: no sé cómo agradecer vuestra inconmensurable ayuda. Entre otras muchas cosas, habéis genotipado unos 2.800

animales y tomado más de 4.200 pesos para mis proyectos. Sí, los he contado. Vuestra labor es imprescindible y he aprendido mucho de vosotras trabajando a vuestro lado.

También me gustaría agradecer el apoyo de mis compañeros de fatigas. Amanda, gracias por todas tus conversaciones sobre ideas, proyectos, temas banales... Tenerte a mi izquierda estos años ha significado mucho para mí. Sé que puedo contar contigo para lo que necesite. Alberto, currantes como tú hay pocos. Gracias por tu disposición, siempre ayudando en lo que puedes y hasta en lo que no puedes. Tenemos que repetir ese finde de esquí tan estupendo. Raquel, mi querida compañera de estancia, somos personas muy diferentes, pero hemos sabido encontrarnos. Gracias por todos tus consejos, me habría perdido sin ellos. Rosa, a veces no te entiendo cuando hablas, pero me lo paso muy bien contigo. Gracias por esas conversaciones vespertinas que me dan las fuerzas para rematar el día. Ana, gracias por hacer de reportera oficial. Eres una fotógrafa magnífica y le das al laboratorio ese toque artístico que es tan necesario. Aprovecha ese don, la creatividad es fundamental en ciencia y creo que te llevará muy lejos. Marta, Bea, Yaazan: no hemos hablado tanto, pero siempre estáis dispuestos a escuchar. Vuestra disposición no puede ser mejor y siento que, con vosotros, el laboratorio está en buenas manos.

No me puedo olvidar de los más *adultos* del grupo. Álvaro, gracias por tu carisma y humildad, haces que el laboratorio sea un lugar realmente acogedor. Iñaki, tu inquietud me inspira; creo que tienes unas ideas fantásticas. Gracias por compartirlas conmigo y por motivarme a pensar en grande. Pilar, tu sabiduría es inmensa, admiro tu capacidad para dar a cada cosa la importancia justa. Gracias por ayudarme a no perder la perspectiva. Rosa, hemos coincidido poco pero hemos congeniado enseguida. Gracias por comprender y aceptar mi sentido del humor. Bea, sin ti este equipo no funcionaría. Velas por que todas las piezas estén en su lugar y mantienes la cohesión. Muchas gracias por escuchar y por ayudarme a encontrar una solución para cada problema al que me he enfrentado.

A lo largo de mi estancia en el CNIC han pasado otras muchas personas por el grupo. José María, eres un fenómeno. Gracias por decirme siempre las cosas como son y por tus sabios consejos. Lara, echo de menos tenerte a mi derecha. Gracias por tus innumerables conversaciones sobre ciencia; has sabido motivarme en las etapas más difíciles. Magda, eres una persona brillante y muy rigurosa. Gracias por ayudarme a ver con claridad mis objetivos. José, ya te fuiste hace mucho, pero no me olvido de que sentaste las bases de alguno de mis proyectos. También querría mencionar a Carlos, Ricardo, Cris, Rapha, Pedro, Vane, Oscar, Marta y Laia, con los que coincidí en las etapas iniciales. Y, de todos los estudiantes que han circulado por el laboratorio, querría destacar a Carla, Raquel, Alba y Jaime (grado/máster); Rossella, Vero y Maria Pia

(internacionales); y Pablo, Dani y Zaira (residentes). He compartido muy buenos momentos con vosotros y estoy seguro de que os espera un brillante futuro.

Si tuviera que agradecer todo lo que me habéis aportado los compañeros del **laboratorio de Oviedo**, la Tesis sería el doble de larga. Xurde, me considero privilegiado por ser tu compañero, trabajar contigo me ha hecho mejor científico y mejor persona. David, estoy muy orgulloso de ti, vas a llegar muy lejos. Gloria, tu ayuda y tu afecto han sido clave en esta última etapa. Gracias por estar ahí. José Mari y Xosé, sois unos profesores y mentores extraordinarios, he aprendido infinito con vosotros. Jorge, Jandro y Ángela: vosotros me habéis enseñado lo que significa trabajar en un laboratorio, jamás lo olvidaré. Fer, Clea, Pedro, Ana, Álvaro, Guille, David, Víctor, Olaya, Alicia: no os imagináis cómo valoro todas nuestras conversaciones, han sido tremendamente enriquecedoras. Y a la otra treintena que no he nombrado, pero que he tenido el honor de conocer, ¡gracias!

Jesús, Inma, Emilio, Aleks y el resto de compañeros de **proteómica** del CNIC, gracias por acogerme y por todo lo que me habéis enseñado. Colaborando con vosotros me he sentido como uno más del grupo. Y tuve la suerte de experimentar esa misma sensación durante las estancias. *Prof. Priori, sono eternamente ringraziato per la possibilità di fare un breve soggiorno a **Pavia** per imparare le tecniche di telemetria. L'Italia ha un posto molto speciale nel mio cuore e questo mi ha dato l'opportunità di imparare la cultura, la lingua e incontrare persone straordinarie come Andrea, Rossana, Alessandra, Silvia, Giulia, Damiano, Serena e tutte le altre Gine. Vorrei ringraziare anche Andrea, Marco e Francesca per aver reso possibile tutto questo.* Y no me olvido del grupo satélite en Madrid que tanto ha ido creciendo (especialmente de Deme y Francy). *Je voudrais également remercier Philippe de l'invitation à votre laboratoire à **Oslo**. Votre énergie et votre enthousiasme n'ont pas de rival. Nolwenn, merci pour tout ce que tu m'as appris, ainsi que pour ta patience et ta compréhension. During this stay, I fell in love with Norway and met my friends Anna and Tarvesh, and Ninin, Frida, Torunn, Cohen, Erwan, Annaël, Kristin, Marie-Odile, Jonas... I am especially grateful to Sumithra and Anita, you are life savers. Tusen takk!*

En cuanto al resto de amigos y **compañeros del CNIC**, resulta tremendamente difícil condensarlos a todos en media página. Eeva, Ana, Anabel, Edu (y en general el personal de administración): estoy convencido de que tenéis superpoderes, ¡me habéis salvado en más de una ocasión! Santi, Ana, Rubén y vuestros compañeros de animalario: muchas gracias por vuestra disposición y ayuda, sé que no os lo he puesto fácil. También debo mencionar a Eva, Virginia, Laura, Frank, Lorena y Marta, pues sin vuestro curro los proyectos con animales no habrían sido posibles. Entre las unidades técnicas, estoy especialmente agradecido a Antonio y sus compañeros de histología (sois unos máquinas), a Fátima (bioinformática) y a los grupos de Imagen Avanzada, pues me

habéis ayudado muchísimo: Manuel, María, Jesús, las Lorenas, Ana Vanesa, Dani, etc. Alicia y los de informática: habéis sido imprescindibles para mi supervivencia, al igual que Elena y su equipo de cafetería.

Durante este tiempo, he tenido la ocasión de interaccionar en el centro con mucha gente fantástica. Irene, Javi, Ana: gracias por vuestra compañía, siempre tendréis un sitio en mi mesa. También estoy muy agradecido a Edu, Roci, Agus, Javi, Eli y nuestros otros vecinos de los grupos de Borja, Enrique, Marta, David, Andrés y José Javier. Habéis ayudado a crear un ambiente excelente y demostráis cada día que el altruismo es uno de los pilares de la ciencia. En este sentido, debo agradecer las enseñanzas de Nuria, Ivana y Guada cuando decidimos aventurarnos en el campo del metabolismo. Del mismo modo, os agradezco a Aurora, José Luis y David vuestro compromiso y seguimiento de la Tesis.

Dani y Fran, gracias por todas esas meriendas, por prender en mí la llama del emprendimiento. A vosotros y a los demás *cicerones*: Laura, Arturo, Carlos, Rebe, José, Ángel, Sergio, Maruchi, Raquel, Lau, Fede, Paula, Noe... hemos crecido juntos y estoy seguro de que nuestra aventura no acaba aquí. Me siento orgulloso de contaros entre mis amigos. A mis compañeros del **PhDay** (algunos ya mencionados en este párrafo): entre todos pusimos en marcha esta iniciativa maravillosa que me ayudó a sobrellevar los momentos difíciles y que me enseñó todo lo que no se puede aprender en un laboratorio. Además, esto me llevó a congeniar con gente tan genial como Bárbara, Eli, Toñi, Sarah, Julio, Fidel, los Jesuses, los Álvaros, Josema, Antonio, Ana, Carla, las Marías, Nacho, Yoli y un largo etcétera.

Gracias a mi querido guiri Austin conocí a otros grandes **amigos**: Alba, Juanlu, Marta y Verdi. A los cinco os debo muchos cines, viajes y cenas. También estoy muy agradecido a mis compañeros de piso, especialmente a Jesús, por vuestra compañía y paciencia conmigo. Y por supuesto no puedo evitar mencionar a Ali, María, Pablo y todos mis amigos de QuinteScience y también de La Facultad Invisible o de Celera. Colaborar con vosotros de forma complementaria al doctorado es una de las mejores cosas que he hecho. Juntos llegaremos lejos.

Para terminar, me gustaría agradecer a **mi familia** todo el apoyo que me ha dado. A mis innumerables tíos y primos paternos, por seguir con tanto cariño mi carrera. Y especialmente a mi familia materna, que siempre ha estado ahí. Gracias, tía Cova, por tu generosidad ilimitada. Aspiro a ser un poco más como tú. Gracias, tía Paz, por siempre buscar un enfoque diferente y estimular mi creatividad. Gracias, queridos primos: Fer, Cova... y también Enric, de quien aún tengo mucho que aprender. Fer, mi admiración por ti me ha empujado a crecer como persona

desde que era pequeño. Cova, emanas sabiduría, no sabes lo que han significado tu guía y tus consejos estos últimos años.

Arís, como hermana pequeña, tu obligación siempre ha sido chincharme. Pero por alguna razón, te has desviado significativamente de tu misión y te has comportado como mi hermana mayor, protegiéndome de modelos inadecuados y enseñándome que ser *outlier* no es tan malo. Papá, mamá, gracias por empezar todo. Por transmitirme vuestros valores, por enseñarme (casi) todo lo que sé, por moldearme en la persona que soy. Sin vuestra dedicación no sé qué habría sido de mí.

Mercedes, me has cambiado la vida. Gracias por tu cariño, por tu curiosidad insaciable, por tu fascinación infinita, por siempre estar ahí, por tenderme una mano cada vez que tropiezo, por ayudarme a conocerme mejor, por acompañarme en esta aventura. Estoy ansioso por conocer la próxima.

Por último, siento que debo terminar por los primeros, que ya estaban ahí antes de que llegáramos los demás. Habéis tenido una vida llena de experiencias maravillosas y otras inimaginables, sois un ejemplo para todos nosotros. Abuela, eres la mejor. Tu carisma, rebeldía y resiliencia te han llevado ser extraordinaria. Sé que sientes que te has quedado sin genes, al dar el 25% a cada uno de tus cuatro nietos, pero créeme que están en buenas manos. Abuelo, has sido mi fuente de inspiración. Echo de menos nuestras conversaciones sobre ciencia y filosofía, construir figuras geométricas juntos, ver cómo con más de 90 años seguías cediendo el paso a la gente... Ojalá algún día llegue a ser una persona tan excepcional como tú.

Recuerdo a mi yo de hace casi 10 años. Jamás hubiera imaginado llegar hasta aquí, acompañado de experiencias y de personas tan extraordinarias.

Abstract

Aging is the main risk factor for developing cardiovascular and metabolic diseases, which have become a global concern as the world population is progressively aging. The identification of the hallmarks of aging and the cumulative knowledge on the molecular foundations underlying cardiometabolic diseases show that these processes are deeply interconnected and can be modulated. Many advancements have been made in this field through the study of Hutchinson-Gilford progeria syndrome (HGPS or progeria), an extremely rare genetic disease characterized by cardiometabolic disorders and premature aging. Interestingly, age-related comorbidities such as cancer or neurodegeneration are absent in progeria, and environmental risk factors seem to have a minimal implication in disease progression. Hence, the analysis of HGPS provides an opportunity to elucidate the molecular mechanisms that drive cardiometabolic diseases during aging. Consequently, HGPS animal models constitute a unique tool for this purpose and to develop rejuvenation strategies.

In this Doctoral Thesis we sought to evaluate cardiometabolic disease in mouse models of premature and normal aging, to identify which mechanisms are common or specific to each condition, and to study the interplay between the local and systemic environments during disease progression. We found that both premature and normal aging models present similar cardiac electrical abnormalities, and high throughput proteomics in the heart of these animals revealed increased global oxidation as well as deregulated energy metabolism, proteostasis, gene expression and cardiac muscle contraction. Nevertheless, while old mice become overweight, progeric mice develop cachexia and impaired body temperature regulation. Moreover, progeric mice develop bradycardia and lipodystrophy, which are promoted by systemic mechanisms, since these features are absent in mice with heart or adipose tissue-specific progerin expression. Finally, we propose the use of *Pparg* agonists as a new therapeutic strategy in HGPS, targeting adipose tissue to restore energy balance and alleviate age-related cardiometabolic disease.

Resumen

El envejecimiento es el principal factor de riesgo para el desarrollo de enfermedades cardiovasculares y metabólicas, que se han convertido en un problema grave ya que la población mundial está envejeciendo progresivamente. La identificación de las claves del envejecimiento y el conocimiento acumulado sobre los fundamentos moleculares de las enfermedades cardiometabólicas muestran que estos procesos están profundamente interconectados y pueden ser modulados. Se ha avanzado mucho en este campo gracias al estudio del síndrome de la progeria de Hutchinson Gilford (HGPS), una enfermedad genética extremadamente rara que se caracteriza por el desarrollo de patologías cardiometabólicas y envejecimiento prematuro. Curiosamente, la progeria no presenta algunas comorbilidades asociadas al envejecimiento fisiológico, como el cáncer o la neurodegeneración, y su progresión parece poco influida por factores ambientales. Así pues, investigar sobre progeria podría contribuir a elucidar los mecanismos moleculares que promueven las enfermedades cardiometabólicas durante el envejecimiento. Por tanto, los modelos animales de HGPS constituyen una herramienta única para este propósito y para desarrollar estrategias de rejuvenecimiento.

En esta Tesis Doctoral estudiamos la enfermedad cardiometabólica en modelos de envejecimiento normal y prematuro con el objetivo de identificar mecanismos comunes o específicos a cada condición, y para analizar la interacción entre los ambientes local y sistémico en sú progresión. Descubrimos que tanto los modelos de envejecimiento normal como prematuro presentan anormalidades eléctricas cardiacas similares, y mediante proteómica de alto rendimiento demostramos que el corazón de estos animales presenta un incremento en la oxidación global y una desregulación del metabolismo energético, de la proteostasis, de la expresión génica y de la contracción cardiaca. No obstante, mientras que los ratones viejos tienden al sobrepeso, los progéricos desarrollan caquexia y problemas en la regulación de la temperatura corporal. Además, estos últimos manifiestan bradicardia y lipodistrofia promovidas por mecanismos sistémicos, pues estas anomalías no se dan en ratones con expresión de progerina restringida a tejido cardiaco o adiposo. Por último, proponemos el uso de agonistas de *Pparg* como nueva estrategia terapéutica en HGPS para restaurar el tejido adiposo, recuperar el balance energético y aliviar la enfermedad cardiometabólica asociada a la edad.

Abbreviations

ACN acetonitrile. 38

AF3 ammonium formate (pH 3.0). 38

ALT alkaline phosphatase. 46

ALT alanine transaminase. 46

AST aspartate transaminase. 46

ATP adenosine triphosphate. 8, 9, 71

BAT brown adipose tissue. 31–33, 36, 53–55, 63–66, 72, 74, 77, 99

BSA bovine serum albumin. 37

CNIC Centro Nacional de Investigaciones Cardiovasculares Carlos III. i, 23, 29

CO cardiac output. 3, 28, 29, 44, 45, 57, 59

CR calorie restriction. 11

CRISPR clustered regularly interspaced short palindromic repeats. 15

CVD cardiovascular disease. 1

DMSO dimethyl sulfoxide. 33

DNA deoxyribonucleic acid. 6–9, 11, 12, 16, 34, 35

DTT dithiothreitol. 35, 37

ECG electrocardiography, electrocardiogram. 25–27, 29, 32, 41, 43, 44, 56–60, 64, 68, 74

ECM extracellular matrix. 2

EDTA ethylenediaminetetraacetic acid. 32, 33, 35, 37

EDV end-diastolic volume. 27, 29, 45, 68

EE energy expenditure. 4, 30, 31, 52–54, 58, 59, 65, 70–72, 76, 77, 99

EF ejection fraction. 2, 27, 29, 44, 45, 57, 58, 68

ESV end-systolic volume. 27

ET ejection time. 28, 58

FASILOX filter-aided stable isotope labeling of oxidized cysteines. 37, 39, 47

FASP filter-aided sample preparation. 37

FBS fetal bovine serum. 33

FDR false discovery rate. 40, 49, 68

FS fractional shortening. 27

FTI farnesyltransferase inhibitor. 15, 16

GO Gene Ontology. 40

GOT glutamic oxaloacetic transaminase. 46

GPT glutamate pyruvate transaminase. 46

GTT glucose tolerance test. 32, 45, 46

H&E hematoxylin and eosin (staining). 33

HDL high density lipoprotein. 5, 19, 70

HGPS Hutchinson-Gilford progeria syndrome. xiii, 11–21, 24, 43, 44, 56, 67–75

HR heart rate. 3, 24–29, 41, 43, 44, 58–61, 71, 73, 74, 78

HRP horseradish peroxidase. 37

IIS insulin and IGF1 signaling. 7, 9, 11

IPA Ingenuity Pathway Analysis. 40

iPSC inducible pluripotent stem cell. 10, 74

IQR interquartile range. 24

iTRAQ isobaric tag for relative and absolute quantitation. 38–40, 47

ITT insulin tolerance test. 32, 45, 46

IVSd end-diastolic inter ventricular septum thickness. 27, 68

iWAT inguinal (subcutaneous) white adipose tissue. 33, 63, 64

KH Krebs-Henseleit (buffer). 33

LAX long axis. 27–29

LC liquid chromatography. 38

LCS lamin C-stop. 14, 24, 72

LDL low density lipoprotein. 4, 19, 70

LV left ventricle. 2, 3, 19, 27–29, 44, 45, 58, 68

LVIDd end-diastolic left ventricle internal diameter. 27, 57

LVIDs end-systolic left ventricle internal diameter. 27

LVOTd left ventricle outflow tract diameter. 28

LVPWd end-diastolic left ventricle posterior wall thickness. 27, 68

MMTS s-methyl thiomethanesulfonate. 38

MRI magnetic resonance imaging. 23, 29, 41, 44, 45, 68

mRNA messenger ribonucleic acid. 35, 55, 62, 63

MS/MS tandem mass spectrometry. 38

MV mitral valve. 2, 19, 28, 58, 68

NAD^+ nicotinamide adenine dinucleotide. 8, 9

NEFA non-esterified fatty acid. 64

NMR nuclear magnetic resonance. 29, 44, 45

ORO Oil-Red O (staining). 34, 63

PAS Periodic acid–Schiff (staining). 33, 55

PAT pulmonary artery acceleration time. 28, 58

PBS phosphate-buffered saline. 32

PCR polymerase chain reaction. 34

PFA paraformaldehyde. 32, 34

PW pulsed wave. 27, 28

pWAT perigonadal (visceral) white adipose tissue. 33, 62–64, 74

RIPA radioimmunoprecipitation assay (buffer). 35

RNA ribonucleic acid. 15, 34, 35

ROS reactive oxygen species. 6, 8–10, 16

RQ respiratory quotient. 30, 31, 53, 58, 70, 71

RT-qPCR reverse transcription - quantitative PCR. 35, 36, 41, 55, 63, 101

RV right ventricle. 28, 29, 44, 45, 47, 58, 68

SASP senescence-associated secretory phenotype. 8, 9

SAX short axis. 27–29, 45

SDS sodium dodecyl sulfate. 35–37

SV stroke volume. 3, 28, 29, 44, 45

TAPSE tricuspid annular plane systolic excursion. 28, 58

TBS-T tris-buffered saline with Tween 20. 36, 37

Tm melting temperature. 36

TZD thiazolidinedione. 75

VAT visceral adipose tissue. 4, 10

VCO_2 CO_2 production. 31, 52, 59

VO_2 O_2 consumption. 31, 52, 59

VTI velocity time integral. 28

WAT white adipose tissue. 33, 34, 36, 62, 74, 77

WSPP Weighted Scan-Peptide-Protein. 40

ZMPSTE24 zinc metallopeptidase STE24. 11, 12, 17

Contents

1 Introduction

1.1 Cardiometabolic Disease in Aging

Humankind has long aspired to achieve immortality. Many authors and thinkers throughout history have extensively examined this topic in the literature, explorers like Ponce de León led expeditions searching for the Fountain of Youth and the alchemists pursued the creation of the Philosopher's Stone. Notwithstanding myths and promises, death remains inevitable, universal, final. Longevity, on the other hand, may be manipulated through the advancement of modern medicine, science and technology.

During the past two centuries life expectancy has therefore substantially increased (Christensen et al., 2009) and it is projected to continue increasing in most countries (Kontis et al., 2017). However, this increment in lifespan gives rise to the aging process, a progressive loss of physiological integrity and molecular harmony that leads to a decline in the quality of life and increased susceptibility to death (Kirkwood, 2005; Guzman-Castillo et al., 2017).

Aging is the main risk factor for the development of pathologies such as cardiovascular disease (CVD), cancer, metabolic disorders and neurodegeneration (Savji et al., 2013; Kennedy et al., 2014). Due to a progressively growing aged population, these diseases are on the rise, which imposes a grave health and financial problem worldwide (Dunbar et al., 2018). Among them, CVD is the leading cause of death in the developed countries (Roth et al., 2017).

Noteworthy, the development of CVD is accelerated by the presence of metabolic disorders like diabetes, obesity or dyslipidemia, which have reached epidemic proportions during the last years (Michalakis et al., 2013; Dietz et al., 2015; Chia et al., 2018). Furthermore, persistent exposure to unhealthy lifestyles (inadequate nutrition, sedentarism, stress, smoking...) drastically increases the risk of developing cardiac, vascular and metabolic disorders (Fontana, 2018). Since these pathologies are multifactorial and share common mechanisms and manifestations, we may refer to them collectively as cardiometabolic diseases.

Consequently, lifespan extension in our aging society comes at the expense of poor health and diminished quality of life within the geriatric population. Therefore, there is an urgent need to explore the mechanisms underlying age-related cardiometabolic diseases and to develop preventive and therapeutic strategies that may promote healthier aging.

1.1.1 Heart Disease

Aging is associated with increased collagen content in the myocardial extracellular matrix (ECM), which has been attributed to decreased ECM degradation and increased collagen cross-linking (Lima, 2017; Biernacka and Frangogiannis, 2011). The resulting **cardiac fibrosis** reduces the ability of the myocardium to conduct electrical impulses, relax, stretch and diffuse oxygen. This promotes cardiomyocyte cell death and the replacement of lost cells by fibrotic material, generating a vicious cycle that leads to cardiac dysfunction (Piek et al., 2016). Consequently, fibrosis predisposes to heart failure, left ventricle (LV) hypertrophy, valve dysfunction and arrhythmias (Horn, 2015).

Heart failure is a complex clinical syndrome in which impairment of ventricular filling or ejection causes insufficient perfusion of peripheral tissues (Yancy et al., 2013). Clinical manifestations are dyspnea, fatigue and fluid retention, which may lead to pulmonary or peripheral edema. Age-related heart failure is generally attributed to dysfunction in the diastolic filling of the LV rather than an impairment of systolic function, since ejection fraction (EF) is preserved (Wong et al., 2016; Lakatta, 2003). Diastolic dysfunction in aging is caused by stiffening of the cardiac muscle as a result of fibrosis and incomplete calcium recruitment by the myofilaments (Martos et al., 2007; Dai et al., 2012).

The prevalence of **LV hypertrophy**, defined as the thickening of the LV wall, increases dramatically with age and is associated with high blood pressure, obesity, valve disease and myocardial infarction (Levy et al., 1988; Eng et al., 2016). Age-associated LV hypertrophy is the result of a progressive pathologic cardiac remodeling involving cardiomyocyte hypertrophy and death as well as collagen deposition (Lakatta, 2003; Olivetti et al., 1995).

During aging, aortic and mitral valves (MV) become thicker and stiffer, leading to **cardiac valve disease** and regurgitation, which may provoke LV hypertrophy and heart failure (Horn, 2015; Spadaccio et al., 2016). The loss of elastomechanical force and the increased weakness and stiffening of the valves are driven by progressive alterations in the ECM, inflammation and calcification.

While cardiac output (CO) (volume of blood pumped by the heart per unit time) at rest is not modified during aging, as both stroke volume (SV) and heart rate (HR) are maintained, **heart rhythm alterations** arise in response to physical exercise, causing reduced physical performance and increased fatigue (Brubaker and Kitzman, 2011). Moreover, aging reduces the intrinsic pacemaker activity of the sinoatrial node, likely due to fibrosis and alterations in electrical conduction and in the sinus node action potential (Moghtadaei et al., 2016). The prevalence of atrial fibrillation also increases with age and is associated with hypertension, heart valve disease, and heart failure (Zoni-Berisso et al., 2014). Factors suggested to contribute to atrial fibrillation are overt sinus node dysfunction and altered autonomous nervous regulation (Nguyen et al., 2013).

Defective autonomic cardiac regulation during aging has a major impact on HR variability, myocardial contractility and myocardial relaxation. Age-related elevated sympathetic activity has been linked to increased plasma levels of catecholamines and decreased β-adrenergic sensitivity (Lakatta, 2003).

1.1.2 Vascular Pathologies

The aging-associated sympathetic hyperactivity also affects the vascular system, causing **deregulation of the blood flow**. Baroreflex sensitivity is reduced, leading to a decline in blood pressure variability (Monahan, 2007; Taylor and Tan, 2014). As a result, systemic pressure may increase with aging, even reaching the hypertension threshold (Lakatta, 2003).

Large-vessel **arterial stiffness** sets the stage for the initiation and progression of hypertension and atherosclerosis in the elderly by promoting cellular dysfunction in the vessel wall (Wang et al., 2014). Furthermore, vessel stiffness places a strain on the heart, leading to cardiac fibrosis, LV hypertrophy and heart failure (Biernacka and Frangogiannis, 2011). The mechanisms underlying age-induced arterial stiffness include increased inflammation as well as progressive collagen deposition and cross-linking in the tunica media (Sun, 2015; Kohn et al., 2015).

Aging is also associated with **endothelial dysfunction**, which alters the regulation of vascular tone. Moreover, decreased bioavailability of nitric oxide in dysfunctional endothelial cells increases vascular permeability and inflammation, and triggers a positive feedback loop that aggravates the phenomenon in the long term (Paneni et al., 2017; Huveneers et al., 2015).

Endothelial dysfunction is a major determinant of **atherosclerosis** initiation and progression, a degenerative process that occurs within arteries during aging and that increases the risk of myocardial infarction or stroke (Lakatta, 2003; Alenghat, 2016). Atherogenic plaque formation involves tunica intima thickening, leukocyte-mediated inflammation and the recruitment and transdifferentiation of vascular smooth muscle cells, that switch from a contractile to a secretory phenotype (Libby and Hansson, 2015; Fisher, 2010).

1.1.3 Metabolic Disorders

During aging, body composition changes. The main alterations include a reduction in bone (osteopenia) and muscle mass (sarcopenia), as well as a redistribution of fat from subcutaneous to visceral depots, infiltrating muscle, liver or bone marrow (Batsis and Villareal, 2018). Moreover, body fat increases eliciting **central obesity**, which is associated with increased risk for diabetes, hypertension, atherosclerosis, dyslipidemia, cancer and mortality (Shuster et al., 2012).

Obesity is the result of an imbalance between food intake and energy expenditure (EE) (Michalakis et al., 2013). During aging, the resting metabolic rate decreases, and arthrosis, sarcopenia and pulmonary or heart failure cause a reduction in physical activity capacity, eliciting sedentarism. EE is hence significantly reduced (Speakman and Westerterp, 2010; Volkert and Sieber, 2011). Notably, appetite and intestinal absorption also decrease with age, but intake is not severely compromised (Morley, 2013).

Different **hormonal alterations** promote obesity during aging. Thus, reduced thyroid function contributes to limiting EE; the decrease in blood levels of ghrelin and rise of leptin induce satiety; and insulin resistance is associated with a reduction in adiponectin levels (Michalakis et al., 2013). Furthermore, there is an increase in inflammation, mediated by visceral adipose tissue (VAT) secretion of TNFα, IL-6, C-reactive protein and other pro-inflammatory cytokines which reduce insulin sensitivity and inhibit adipogenesis (adipose cell differentiation) in subcutaneous depots (Pradhan et al., 2001; Caso et al., 2013). Consequently, adipose stem cells become senescent, fibrosis is induced and subcutaneous fat is loss, as in lipodystrophy (Tchkonia et al., 2013; Sun et al., 2013). Interestingly, age-related increased osteopontin secretion by the VAT promotes cardiac fibrosis (Sawaki et al., 2018).

Both lipodystrophy and obesity involve impaired fat deposition by adipocytes, which leads to increased lipolysis and dyslipidemia (Tchkonia et al., 2013). **Dyslipidemia** comprises high plasma levels of triglycerides (hypertriglycerolemia) and low density lipoprotein (LDL), as well

as low levels of high density lipoprotein (HDL). This deregulation of lipids in the blood promotes ectopic fat deposition (steatosis) and is linked to increased risk of atherosclerosis and diabetes (D'Agostino et al., 2008; Chait and Goldberg, 2017).

Liver and muscle steatosis impair insulin signaling, therefore evoking **insulin resistance**, which in turn reduces glucose tolerance (Samuel et al., 2010). During aging and in insulin resistance or inflammatory conditions, pancreatic secretion of insulin becomes compromised, contributing to hyperglycemia and giving rise to **type 2 diabetes**, a common cause of premature heart disease, stroke and dementia (Rao Kondapally Seshasai et al., 2011; Lee and Halter, 2017).

1.2 The Hallmarks of Aging

For decades, aging was thought to be caused by a progressive and stochastic accumulation of cellular damage (Hayflick, 2007; Kirkwood and Melov, 2011). However, the discovery of genetic mutations that extend lifespan in different model organisms helped to understand that aging is also driven by genetic programs and signaling pathways that promote the evolutionary adaptation of the organisms (Kenyon, 2010; Jones et al., 2014).

This finding led to the identification and categorization of the molecular and cellular foundations that characterize the process of aging, which have been defined as the hallmarks of aging (López-Otín et al., 2013). Each of the hallmarks fulfills three criteria: 1) it manifests during normal aging; 2) its experimental aggravation accelerates aging; and 3) its experimental amelioration retards the normal aging process, increasing healthspan. According to these three criteria, nine hallmarks have been proposed, grouped in three categories: primary hallmarks, antagonistic hallmarks and integrative hallmarks (Fig. 1).

The existence of a genetic program that regulates aging has raised many questions regarding the molecular causes of aging, the compensatory responses that try to reestablish homeostasis, the connection between cell-autonomous and systemic mechanisms, and the intervention strategies that could modulate and delay aging.

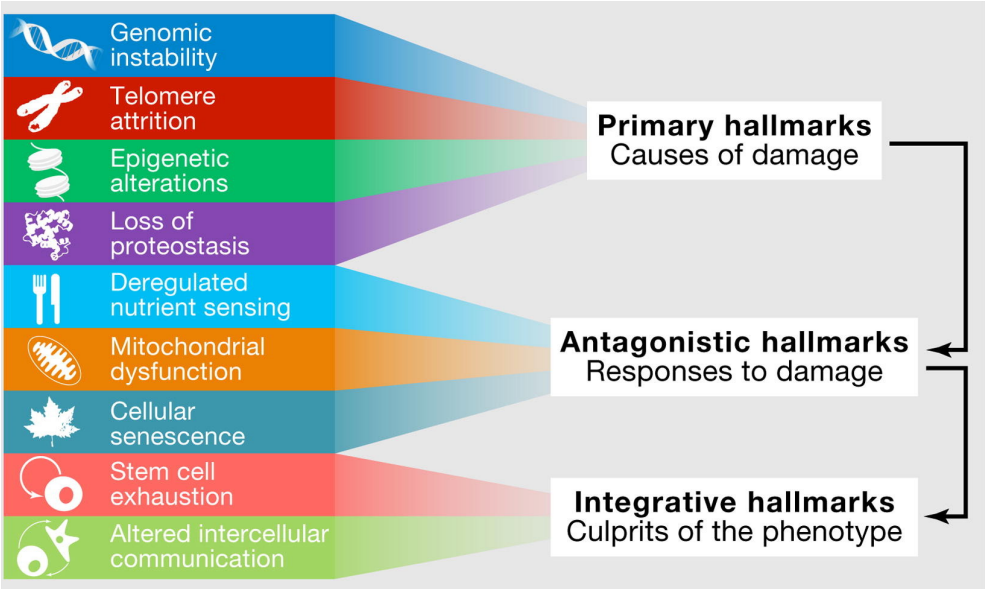

Figure 1: Functional Interconnections between the Hallmarks of Aging
The primary hallmarks are considered to be the initial causes of cellular damage. The antagonistic hallmarks involve compensatory responses to the damage that become deleterious when exacerbated or chronic. The integrative hallmarks are consequence of the previous hallmarks and ultimately responsible for the functional decline associated with aging. From López-Otín et al., 2013.

1.2.1 Primary Hallmarks

The primary hallmarks of aging cause detrimental effects for the cell and include deoxyribonucleic acid (DNA) damage, telomere shortening, epigenetic dysregulation, and defective protein homeostasis (Fig. 1).

Genomic instability comprises the accumulation throughout life of genetic damage in nuclear and mitochondrial DNA (Moskalev et al., 2013). Genetic lesions arise from extrinsic (physical, chemical and biological agents) and intrinsic sources (DNA replication errors, spontaneous hydrolytic reactions, and reactive oxygen species (ROS)) and include point mutations, chromosomal translocations an copy number variations, or gene disruption caused by transposons or viruses (Hoeijmakers, 2009). Organisms have evolved a complex network of DNA repair mechanisms that are collectively capable of repairing most of the damages inflicted to DNA (Lord and Ashworth, 2012). Nevertheless, defects on these mechanisms or in the nuclear architecture cause premature aging diseases such as Werner and Bloom syndromes and laminopathies (Burtner and Kennedy, 2010; Worman, 2012). Importantly, lifespan can be extended through the enhancement in DNA repair mechanisms (Baker et al., 2013; Vaidya et al., 2014).

The inability of DNA replication polymerases to copy the terminal ends of linear DNA molecules provokes **telomere attrition**. This process is performed by the telomerase, which is inactivated

after birth in most somatic cells. This leads to the gradual loss of telomeres during aging (Blackburn et al., 2006; Hayflick and Moorhead, 1961). Accordingly, telomerase deficiency is linked to defective tissue homeostasis (Armanios and Blackburn, 2012; Blasco et al., 1997), and activation of telomerase expression can extend lifespan (Jaskelioff et al., 2011).

Throughout life, cells and tissues are affected by a large diversity of **epigenetic alterations**: changes in DNA methylation patterns, chromatin remodeling and post-translational modifications of histones (Talens et al., 2012; Fraga and Esteller, 2007). The importance of the epigenetic regulatory mechanisms is evidenced by the deacetylase SIRT6, whose deficiency accelerates aging in mice (Mostoslavsky et al., 2006), whereas its overexpression extends lifespan. Consistent with this, some intervention strategies encompass the administration of epigenetic remodeling complex inhibitors (Krishnan et al., 2011) or activators of SIRT proteins (Houtkooper et al., 2012).

The **loss of proteostasis** (protein homeostasis) is related to an impairment in the pathways in charge of quality control and leads to an agglomeration of damaged or misfolded proteins that disrupt cell function (Baixauli et al., 2014; Powers et al., 2009). Deficiency in some chaperones, lysosomal proteins or in ubiquitin-proteasome system components causes accelerated aging in different animal models (Yun et al., 2008; Koga et al., 2011). Consequently, overexpressing some chaperones or stimulating proteolytic systems pharmacologically reverses age-associated defects and promotes longevity (Morrow et al., 2004; Zhang and Cuervo, 2008; Eisenberg et al., 2009).

1.2.2 Antagonistic Hallmarks

The second category includes those hallmarks that help the organism survive through harsh environmental conditions, but become deleterious and promote aging when exceed a certain threshold or manifest in a chronic way. This is the case for deregulation of nutrient sensing, mitochondrial dysfunction and cellular senescence (Fig. 1).

During aging and in metabolic syndromes, **nutrient sensing deregulation** compromises the ability of the organism to adapt its metabolism to energy availability (Efeyan et al., 2015; López-Otín et al., 2016). Some of the most studied nutrient sensors are AMPK, mTOR, the insulin and IGF1 signaling (IIS) and sirtuins (Kenyon, 2010; López-Otín et al., 2013). Remarkably, IIS inhibition by caloric restriction activates FOXO proteins and delays aging (Lapierre and Hansen, 2012). The mTOR inhibitor rapamycin also increases lifespan (Harrison et al., 2009). Conversely,

a constant inactivation of these pathways elicits cell growth arrest and is also associated with accelerated aging (Garinis et al., 2008; Mariño et al., 2010).

When the respiratory machinery efficacy is compromised, electron leakage increases, the nicotinamide adenine dinucleotide (NAD^+) pool is depleted and adenosine triphosphate (ATP) production is reduced (Green et al., 2011). Hence, **mitochondrial dysfunction** leads to reduced bioenergetics and increased production of ROS, which in turn activate a compensatory homeostatic response. During aging, ROS levels increase over the physiological threshold and ultimately exacerbate the age-associated damage (Hekimi et al., 2011). Moreover, DNA polymerase γ deficiency in mouse mitochondria leads to accelerated aging (Edgar et al., 2009).

Cellular senescence involves the arrest of proliferation and the manifestation of specific cellular features (flattening, multinucleation, vacuolation...) (Collado et al., 2007; Deursen, 2014). This mechanism is essential to protect against cancer progression and also contributes to tissue regeneration by preventing the propagation of damaged cells (Demaria et al., 2014). Nevertheless, an excessive accumulation of senescent cells may promote aging, whereas the clearance of senescent cells in aging mouse tissues delays age-associated diseases (Baker et al., 2011).

1.2.3 Integrative Hallmarks

This last category comprises stem cell exhaustion and altered intercellular communication, hallmarks that compromise tissue homeostasis and function due to the damage accumulated by other hallmarks (Fig. 1). **Stem cell exhaustion** leads to reduced tissue regenerative capacity during aging (Molofsky et al., 2006; Shaw et al., 2010; Conboy and Rando, 2012; Sousa-Victor et al., 2015). Consequently, rejuvenating stem cells by somatic reprogramming reverses aging at the organism level (Rando and Chang, 2012; Ocampo et al., 2016).

Aging also involves **altered intercellular communication**, characterized by the loss of neurohormonal signaling coordination in tissues, in favor of self-preservation mechanisms within cells (Russell and Kahn, 2007; Zhang et al., 2013). Inflammatory reactions increase with aging (Adler et al., 2007), the composition of the extracellular environment changes (Gutiérrez-Fernández et al., 2015) and circadian rhythm regulation is progressively lost (Zwighaft et al., 2015). Moreover, senescence is propagated to adjacent cells by direct contact or through senescence-associated secretory phenotype (SASP) (Baker et al., 2013). Interestingly, altered intercellular communication may be reverted through different genetic, pharmacological or nutritional approaches (Freije

and López-Otín, 2012). Notably, some studies have achieved rejuvenation mediated by different systemic factors (Conboy et al., 2005; Villeda et al., 2011; Loffredo et al., 2013).

1.2.4 Metabolic Impact of the Hallmarks of Aging

Besides influencing longevity, the hallmarks of aging are also associated with undesirable metabolic alterations that accumulate over time and collaborate in the physiological decline (López-Otín et al., 2016). In fact, mitochondrial dysfunction and deregulated nutrient sensing are tightly related to metabolic alterations.

Mitochondrial dysfunction is linked to aging and reduced bioenergetics through increased production of ROS and inhibition of ATP synthesis (Green et al., 2011). Moreover, electron leakage depletes the NAD^+ pool, which leads to NAD^+-dependent deacetylase SIRT1 inactivation and subsequent inhibition of the master metabolic regulator PGC1α (Lagouge et al., 2006). As a result, mitonuclear communication is hampered and both mitochondriogenesis and mitochondrial autophagy (mitophagy) are reduced (Quirós et al., 2016).

SIRT1 also acts as a nutrient sensor, repressing PPARγ in adipocytes to stimulate lipolysis during food deprivation (Picard et al., 2004). Nevertheless, the downregulation of sirtuins during aging interrupts this mechanism (Verdin, 2015). Other major nutrient sensors, such as IIS, AMPK and mTOR, also play a key role in the metabolic regulation of aging (López-Otín et al., 2016) (Section 1.2.2).

DNA damage blocks trophic signals that stimulate proliferation (insulin, IGF1, GH) and hyperactivates PARP1, which in turn inhibits SIRT1 (Garinis et al., 2008; Fang et al., 2014). Moreover, DNA damage and telomere attrition activate p53 signaling, causing the suppression of PGC1α and leading to senescence and inhibition of stem cell function (Yu et al., 2015; Sahin et al., 2011). Cellular senescence alters metabolism through the so-called SASP, as it prevents adipogenesis (in adipose tissue) and drives autophagy inhibition and a subsequent accumulation of the proinflammatory transcription factor GATA4 (Xu et al., 2015; Kang et al., 2015).

Stimulating autophagy in mice contributes to the restoration of protein and metabolic homeostasis, in part by removing aggregated proteins that inhibit the clearance of dysfunctional mitochondria and by improving insulin sensitivity (Pyo et al., 2013). Mitochondrial dysfunction also compromises epigenetic regulation during aging, since different epigenetic cofactors and substrates are obtained from the intermediate metabolism (Matilainen et al., 2017). Additionally,

gene expression varies with age, and the aging epigenome is associated with high blood pressure as well as elevated glucose and cholesterol levels in blood (Peters et al., 2015).

Finally, the integrative hallmarks of aging compromise local and systemic metabolism as a result of the alterations provoked by the other hallmarks. For instance, ROS accumulation and deregulated nutrient sensing impair stem cell quiescence and renewal (Sahin and Depinho, 2010; Jasper and Jones, 2010). Interestingly, age-associated inflammation and insulin resistance can be reduced by genetic ablation of the NLRP3 inflammasome or by preventing the accumulation of regulatory T lymphocytes in VAT (Goldberg and Dixit, 2015; Bapat et al., 2015). Moreover, adding polyamines to diet can restore circadian rhythms, which are also deregulated during aging in mice (Zwighaft et al., 2015).

All these data illustrate the need to expand the study of aging to include age-related metabolic alterations in order to understand the complex etiology of aging, and also to explore metabolic-based strategies to promote longevity.

1.2.5 Rejuvenation Strategies

The cumulative knowledge on the hallmarks of aging shows that aging can be modulated. Thus, identifying the molecular mechanisms that sustain aging could help design intervention strategies to prevent age-related diseases, extending both lifespan and healthspan. Moreover, since some species in nature do not age at all (Jones et al., 2014), it may be even possible to slow the rate of aging, uncoupling the biological aging process from chronological aging.

All age-associated marks are reverted naturally with fertilization. This reprogramming process may also be exploited in stem cell biology thanks to the development of inducible pluripotent stem cells (iPSCs) (Takahashi and Yamanaka, 2006). Although generation of iPSCs from centenarian donors has been achieved (Lapasset et al., 2011), the process is highly inefficient and it involves reversing not only the aging clock but the differentiation state as well. Other strategies have achieved rejuvenation in adult organisms, such as the elimination of unfit cells in tissues, heterochronic parabiosis, partial reprogramming to pluripotency or promoting reprogramming through inflammation inhibition (Merino et al., 2015; Conboy et al., 2005; Ocampo et al., 2016).

Given the implication of the hallmarks of aging on metabolism, recent studies are also focusing on metabolic interventions to reverse aging (López-Otín et al., 2016). Among them, it is worth

highlighting inhibition of trophic signaling by blocking IIS or mTOR (Ortega-Molina et al., 2015; Bitto et al., 2016), physical exercise (Neufer et al., 2015; Clark-Matott et al., 2015) and gut microbiome modulation (Cox et al., 2014; Li et al., 2016; Plovier et al., 2017).

Additionally, different types of dietary restrictions have arisen as key rejuvenation strategies. Calorie restriction (CR) (and variants such as intermittent fasting) can delay aging in numerous organisms by acting on several hallmarks through AMPK and SIRT1 activation and the inhibition of ISS and mTOR (Madeo et al., 2015; Longo and Panda, 2016; Mattison et al., 2017; Galluzzi et al., 2014). Less aggressive alternatives include protein or methionine restriction, which are associated with a lower incidence of age-associated diseases, such as cancer (Levine et al., 2014; Madeo et al., 2015). Another strategy to avoid the unpleasant application of CR to humans is the use of CR mimetics, compounds that emulate the effects of CR in different tissues reducing the availability of acetyl-CoA, which leads to a global protein deacetylation (Eisenberg et al., 2014; Madeo et al., 2014; Pietrocola et al., 2016).

1.3 Progeria in Aging Research

Our current understanding of the molecular mechanisms underlying aging has been in part possible through the research in progeroid syndromes, a group of sporadic genetic diseases that recapitulate the aging process precociously or in an exacerbated form (Gordon et al., 2014b). Many of these conditions are caused by mutations in DNA repair mechanisms and are characterized by DNA damage and genomic instability.

Laminopathies constitute the other main type of progeric syndromes. These pathologies are provoked by mutations in nuclear envelope components that lead to aberrant nuclear architecture and chromatin instability (Burtner and Kennedy, 2010; Carrero et al., 2016). Nestor-Guillermo progeria syndrome is caused by mutations in the gene encoding BAF, a nuclear protein that interacts with lamins at the nuclear envelope (Cabanillas et al., 2011; Puente et al., 2011); whereas mutations in the gene encoding the zinc metallopeptidase STE24 (ZMPSTE24), a protease involved in the maturation of lamins, is responsible for restrictive dermopathy and mandibuloacral dysplasia (Pereira et al., 2008; Cenni et al., 2018). Moreover, mutations in A-type lamins, key components of the nuclear lamina, are responsible for a broad range of disorders characterized by neurological, bone, adipose, muscular or cardiological alterations (Worman, 2012). Among these pathologies, HGPS is the most researched progeroid laminopathy.

1.3.1 Hutchinson-Gilford Progeria Syndrome

HGPS is an exceptionally rare, autosomal dominant disease caused by a point mutation in the *LMNA* gene, which encodes the intermediate filament proteins lamin A and lamin C. These two main components of the nuclear lamina play key roles in maintaining nuclear architecture and in the regulation of multiple cell functions, including DNA replication and repair, higher-order chromatin organization, signal transduction and gene transcription (Andrés and Gonzalez-Granado, 2009; Dittmer and Misteli, 2011; Gruenbaum and Foisner, 2015).

During protein maturation, (pre)lamin A undergoes a series of post-translational modifications, including the addition of C-terminal farnesyl and carboxymethyl groups (prenylation) followed by the cleavage of the prenylated 15 amino acids at the C-terminus by ZMPSTE24 (Sinensky et al., 1994; Pendás et al., 2002) (Fig. 2). Most HGPS patients carry a heterozygous *de novo* c.1824C>T (p.Gly608Gly) point mutation within exon 11 of the *LMNA* gene, which activates a cryptic splicing donor site that leads to the accumulation of progerin, a truncated form of the precursor prelamin A. Progerin lacks 50 amino acids of exon 11 encompassing the target sequence for ZMPSTE24 (Eriksson et al., 2003; De Sandre-Giovannoli et al., 2003) (Fig. 2).

The accumulation of progerin at the nucleus elicits a toxic effect on the cell, in part mediated by the retention of the farnesyl group, the altered three-dimensional structure of the protein and aberrant interactions with proteins such as lamin A/C (Pendás et al., 2002; Yang et al., 2011; Kalinowski et al., 2014; Lee et al., 2016). This causes structural defects (blebbing) of the nuclear envelope, chromatin disorganization and DNA damage, which in turn evoke chronic p53 activation, systemic inflammation and accelerated aging (Gordon et al., 2014b).

The prevalence of HGPS is 1 in 20 million and has no ethnic or gender bias (Hennekam, 2006). Affected children are normal at birth but within the first two years of life, they begin to present symptoms of the disease, such as failure to thrive and skin abnormalities. Patients progressively develop other signs of premature aging, including alopecia, loss of subcutaneous fat, joint stiffness and osteopenia (Hennekam, 2006; Merideth et al., 2008). Importantly, they show generalized arteriosclerosis, which leads to death from heart failure or stroke at an average age of 14.6 years (Gordon et al., 2014a; Ullrich and Gordon, 2015; Gordon et al., 2018a).

1.3.2 Animal Models of Progeria

There are less than 150 identified children living with HGPS worldwide (progeriaresearch.org). With such a small number of patients, conducting research and clinical trials has proven to be challenging. The development of appropriate models of the disease has thus been a critical

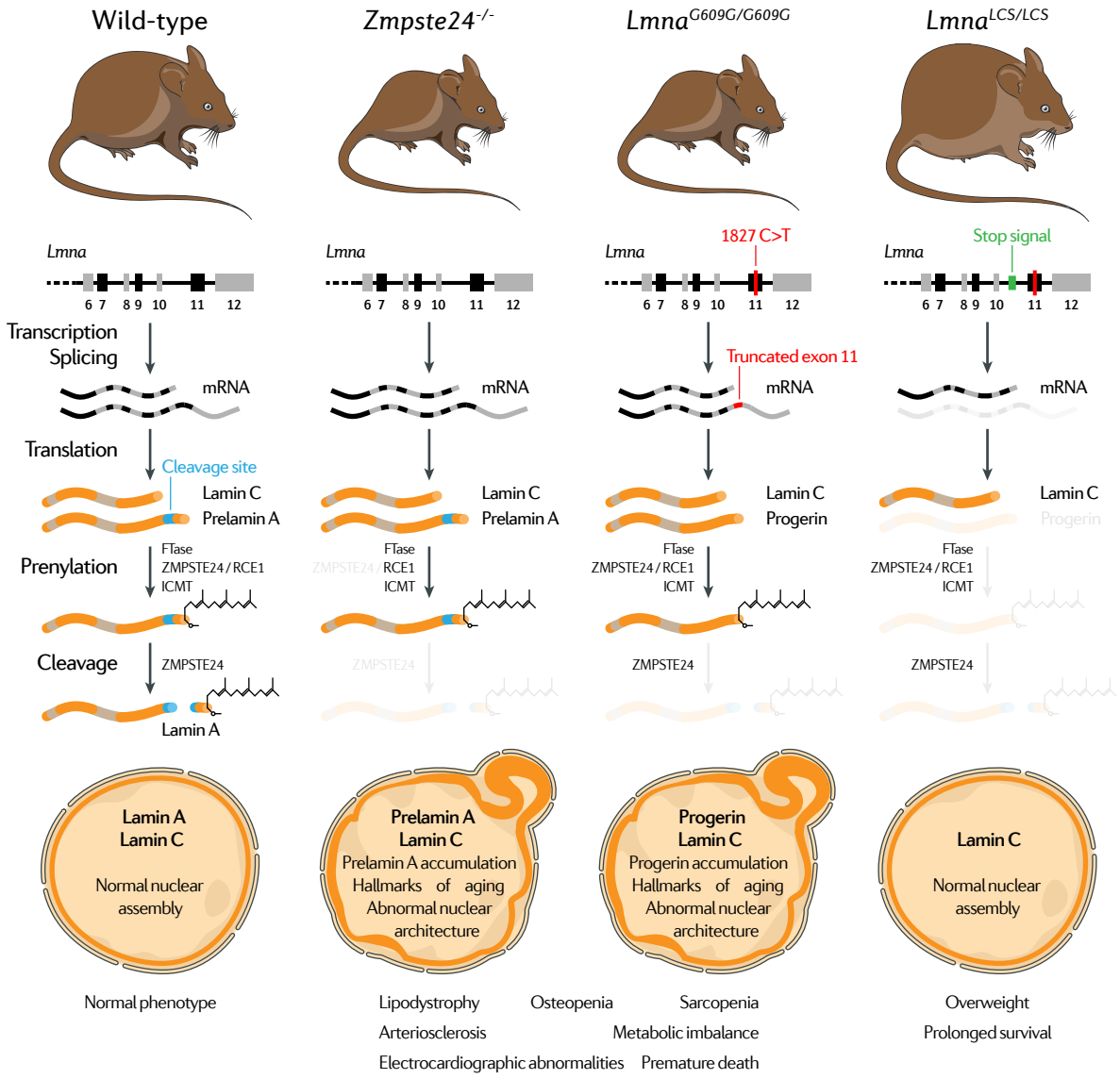

Figure 2: Animal models of Progeria
The *Lmna* gene encodes for both lamins A and C. Lamin A is translated as prelamin A, which undergoes post-translational modifications including prenylation and cleavage of the C-terminal region. *Zmpste24*$^{-/-}$ mice are deficient for the protease that mediates the last step, therefore uncleaved prenylated prelamin A accumulates in the cell, leading to progeria development. The *Lmna*$^{G609G/G609G}$ strain carries the HGPS mutation on the *Lmna* gene, which activates a cryptic splicing site in exon 11. This results in the accumulation of progerin, a truncated form of prelamin A that lacks the cleavage site and accelerates aging. *Lmna*$^{LCS/LCS}$ also carry the HGPS mutation, but a stop signal prevents progerin transcription. Hence, these mice express only lamin C and show no overt progeric phenotype.

step for understanding its etiology and developing therapeutical strategies. Cells derived from HGPS patients and reprogrammed have become a powerful tool in this regard (Lo Cicero and Nissan, 2015), but their translational potential is limited due to the lack of a complex systemic environment.

For this reason, over the last two decades various mouse models of HGPS have been created (Pendás et al., 2002; Bergo et al., 2002; Yang et al., 2005; Varga et al., 2006; Osorio et al., 2011; Lee et al., 2016). These differ on the strategies used for their generation (human or mouse transgenes, knock-in mutations, etc.), on the targeted genes (*Lmna* or *Zmpste24*) and the relative amount of toxic protein they accumulate (prelamin or progerin versus lamins A and C). The result is that not all models recapitulate to the same extent the phenotype observed in human patients. Furthermore, the existence of interspecific differences between mice and humans must be always considered (e.g., in atheroma plaque formation or tolerance to high levels of progerin), hence caution is advised when extrapolating observations from models to patients.

The most widely used models in HGPS studies are the *Zmpste24*-deficient and the $Lmna^{G609G/G609G}$ mouse strains, both generated in our laboratory at *Universidad de Oviedo* (Fig. 2). $Zmpste24^{-/-}$ mice are knock-out for the protease involved in the last step of the lamin A maturation process. This model accumulates prelamin A in the nucleus and phenocopies most of the alterations present in HGPS, including growth retardation, premature death, lipodystrophy, alopecia, skeletal and muscular atrophy, or altered heart repolarization (Pendás et al., 2002; Varela et al., 2005; Rivera-Torres et al., 2016).

It is noteworthy that *Zmpste24*-deficient mice do not reproduce the molecular alteration of HGPS patients at the *LMNA* locus, which is a limitation for studying and targeting *LMNA* splicing in this disease. Consequently, the $Lmna^{G609G}$ mouse strain was generated. This model carries the *Lmna* c.1827C>T (p.Gly609Gly) mutation (equivalent to c.1824C>T; p.Gly608Gly in humans) and accumulates progerin at the nuclear envelope. Homozygous $Lmna^{G609G}$ mice resemble $Zmpste24^{-/-}$ mice and recapitulate most of the characteristic symptoms in HGPS patients (Osorio et al., 2011; Balmus et al., 2018; Hamczyk et al., 2018b). In contrast, heterozygous $Lmna^{G609G}$ mice appear normal until eight months of age, when they start presenting a premature aging phenotype similar to that of homozygotes (Osorio et al., 2011; Villa-Bellosta et al., 2013).

$Lmna^{G609G}$ mice were generated by crossing $Lmna^{LCS}$ or lamin C-stop (LCS) mice with a germline-Cre-deleter mouse strain. $Lmna^{LCS}$ animals carry a conditional HGPS allele with a floxed cassette that prevents the formation of prelamin A but allows the expression of lamin C (Osorio et al., 2011) (Fig. 2). These mice are deficient for lamin A but show no overt progeric phenotype nor

the deleterious effects of suppressing both lamins A and C (López-Mejía et al., 2014; Sullivan et al., 1999).

The greatest advantage of the $Lmna^{LCS}$ model is that it can be crossed with different Cre-expressing strains to generate mice with tissue-specific progerin expression. This therefore allows to study how local and systemic environments contribute to progeria progression. Using this strategy, we obtained mice with progerin expression restricted to vascular smooth muscle cells, macrophages or endothelial cells to study how these compartments affect atherosclerosis and vessel stiffness progression in progeric mice (Hamczyk et al., 2018b; Del Campo et al., 2019).

1.3.3 Therapeutical Approaches in Progeria

Thanks to the availability of different models of progeria, several potential therapies for HGPS are being tested, some of which have reached clinical trials (Gordon et al., 2014b; Hamczyk et al., 2018a). The first approaches have focused on preventing prelamin A farnesylation using farnesyltransferase inhibitors (FTIs), which showed promising effects on HGPS cells and mice (Yang et al., 2005; Fong et al., 2006; Yang et al., 2006; Capell et al., 2008). However, later work showed that FTI treatment results in alternative prenylation of prelamin A, so a combined treatment of statins and bisphosphonates was designed to more efficiently block prelamin A prenylation and ameliorate the progeric phenotype in mice (Varela et al., 2008).

Other promising strategies that target the toxic effects of progerin are blocking prelamin A carboxymethylation or enhancing progerin clearance by inhibiting mTOR and promoting autophagy (Ibrahim et al., 2013; Cao et al., 2011; Graziotto et al., 2012). Nevertheless, efficacy of the latter approach is controversial, since this pathway is already active in progeria (Mariño et al., 2008).

Genetic therapy is rapidly becoming a promising alternative for progeria treatment as well. Prelamin ribonucleic acid (RNA) aberrant splicing may be blocked by antisense oligonucleotides, as shown in HGPS cells and mouse models (Scaffidi and Misteli, 2005; Osorio et al., 2011). Similarly, genome-editing technologies (clustered regularly interspaced short palindromic repeats (CRISPR)-Cas9) offer the possibility of directly repairing the HGPS mutation (Hsu et al., 2014; Liao et al., 2017; Santiago-Fernández et al., 2019; Beyret et al., 2019). Furthermore, metabolic intervention (Bárcena et al., 2018) and cell reprogramming are emerging as promising strategies for both progeria and rejuvenation (Ocampo et al., 2016; Balmus et al., 2018) (section 1.2.5).

Based on these findings, different clinical trials with HGPS patients have been conducted to test the therapeutic efficacy of the FTI lonafarnib, alone or in combination with statins (pravastatin) and bisphosphonates (zoledronate). Lonafarnib monotherapy provided some improvement in vascular stiffness, bone structure, audiological status and plasma proteins (Gordon et al., 2012; Gordon et al., 2018b). Additionally, this approach was estimated to significantly lower mortality rate (3.7% vs 33.3%) after a median of 2.2 years (Gordon et al., 2014a; Gordon et al., 2018a). Triple-drug therapy showed an additional improvement in bone mineral density, but there was no cardiovascular amelioration compared with lonafarnib monotherapy (Gordon et al., 2016). Recently, another clinical trial has started to test the combined effect of lonafarnib and everolimus (mTOR inhibitor) (NCT02579044).

1.3.4 Premature versus Normal Aging

HGPS animal models offer a unique opportunity to study physiopathological processes in premature aging and to test therapeutical approaches. The obvious questions are whether progeria provides insights into normal aging and the aging-related pathologies, and hence, whether progeria models may be used to develop rejuvenation and preventive strategies.

In the first place, it is noteworthy that all hallmarks of aging have been identified in HGPS (Burtner and Kennedy, 2010; López-Otín et al., 2013; Carrero et al., 2016; Folgueras et al., 2018) (Section 1.2). Progerin (or prelamin) accumulation in the nucleus causes blebbing among other defects in nuclear structure (Scaffidi, 2006; Righolt et al., 2011). This is linked to genomic instability due to inefficient recruitment of DNA repair factors and to increased susceptibility to ROS (Liu et al., 2005; Camozzi et al., 2014). In turn, the alterations in nuclear architecture lead to heterochromatin loss, which has been identified in progeria together with other epigenetic alterations such as aberrant histone acetylation and methylation (Shumaker et al., 2006; Osorio et al., 2010; Liu et al., 2013).

HGPS models also exhibit accelerated telomere attrition (Decker et al., 2009; Cao et al., 2011), miR-29/p53-mediated cellular senescence (Varela et al., 2005; Ugalde et al., 2011), mitochondrial dysfunction (Rivera-Torres et al., 2013) and loss of proteostasis through alterations in autophagy and protein translation (Mariño et al., 2008; Buchwalter and Hetzer, 2017). Moreover, the observed autophagy induction (linked to AMPK activation and mTOR inhibition) as well as the constant inactivation of the GH/IGF1 somatotroph axis are signs of deregulated nutrient sensing: these pro-survival mechanisms become detrimental when overinduced or overrepressed (Mariño et al., 2008; Mariño et al., 2010).

Stem cell depletion is also a feature of progeria, since progerin accumulation reduces the proliferative and differentiation capacity of multipotent mouse and human cells (Espada et al., 2008; Scaffidi and Misteli, 2008; Rosengardten et al., 2011; Pacheco et al., 2014). Lastly, altered intercellular communication in this disease is evoked through aberrant activation of NF-κB by ATM in progeric mice, which induces the overexpression of pro-inflammatory cytokines (Osorio et al., 2012).

Another resemblance between HGPS and physiological aging is that progerin is also produced at low levels in normally aging individuals. This occurs because the cryptic splice site present in exon 11 of the *LMNA* gene is sporadically activated in non-HGPS individuals (Scaffidi, 2006; McClintock et al., 2007; Rodriguez et al., 2009). Given its dominant-negative nature, low levels of progerin accumulating throughout life are likely sufficient to elicit cellular damage. Notably, prelamin A has been also detected in normal aging, presumably due to age-dependent downregulation of ZMPSTE24 (Ragnauth et al., 2010; Reddy and Comai, 2012).

The similarities between premature and normal aging extend beyond the molecular level. Some of the features that HGPS patients share with aged individuals are alopecia, altered skin pigmentation, scleroderma, low bone mineral density, sarcopenia, joint contractures, conductive hearing loss, atherosclerosis, heart disease, lipodystrophy and insulin resistance (Hennekam, 2006; Merideth et al., 2008; Ullrich and Gordon, 2015) (Fig. 3).

Nevertheless, there are some HGPS manifestations that differ from aging, such as growth impairment, skeletal dysplasia, and lack of secondary sex characteristics or abnormal pubertal development (Gordon et al., 2007; Gordon et al., 2011; Greer et al., 2018). These features are absent or modest in late-onset progeroid syndromes, indicating that these are consequence of HGPS manifesting during childhood (Martin, 2005).

More importantly, some key aspects of aging are not recapitulated in HGPS. Most prominent among these are the absence of neurodegeneration, immune system deficits and the low frequency of infiltrating tumors. Low progerin levels in the brain due to miR-9 prelamin A downregulation may explain the lack of dementia and other neurological pathologies in HGPS patients (Jung et al., 2012; Nissan et al., 2012). Low lamin A expression in immune cells could also account for the absence of immune system deficiencies (Gonzalez-Granado et al., 2014; Toribio-Fernández et al., 2018).

Despite the exacerbated genomic instability observed in premature and normal aging, HGPS patients are not predisposed to cancer. Interestingly, ZMPSTE24 mosaic mice have revealed

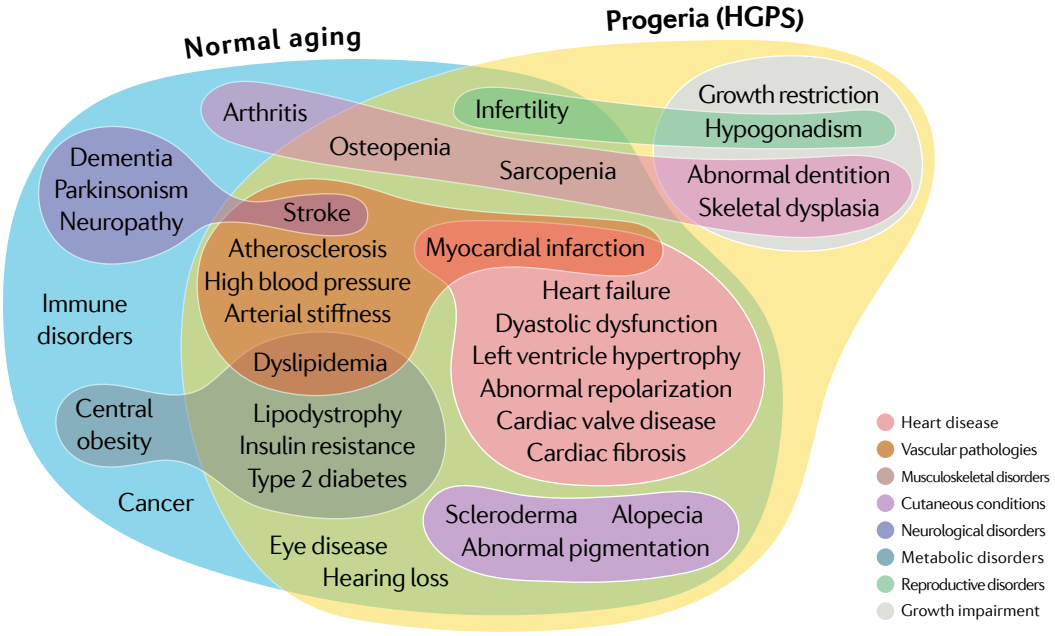

Figure 3: Premature versus normal aging
Euler diagram depicting the relations between normal aging, HGPS and associated pathologies. Note that the prevalence of the different disorders varies and that environmental factors interplay with the aging process.

that prelamin A accumulation prevents cancer invasion and reduces the incidence of infiltrating carcinomas (De la Rosa et al., 2013). Other studies find that HGPS patient cells are resistant to neoplastic transformation through BRD4-mediated inhibition of oncogenic dedifferentiation (Fernandez et al., 2014).

The aforementioned distinctions between HGPS and physiological aging evidence that HGPS is a segmental progeroid disease with partial representation of the multifactorial process of normal aging. However, elucidating the intersections between premature and normal aging may provide insight into both fields.

1.4 Progeria and Age-Related Cardiometabolic Disease

HGPS recapitulates many features present in age-related cardiovascular and metabolic diseases (Fig. 3). Therefore, progeria could be used as a model to study these pathologies typical in the elderly without interference from comorbidities such as neurodegeneration or cancer. Furthermore, isolated from environmental risk factors (smoking, sedentarism, environmental toxicants, unhealthy diet, etc.), the study of HGPS provides an opportunity to elucidate the molecular mechanisms that drive cardiometabolic diseases during aging.

As in normal aging, high blood pressure and carotid atherosclerotic plaques are prevalent in late-stage HGPS patients (Gerhard-Herman et al., 2012; Merideth et al., 2008; Gordon et al., 2016). Furthermore, arterial stiffness and stenosis affect HGPS patients of all ages (Gerhard-Herman et al., 2012). In addition to alterations typically seen in normal aging, such as inflammation, vascular smooth muscle cell loss, vascular calcification and plaque erosion, atherosclerotic vessels in HGPS also feature prominent adventitial thickening and fibrosis (Olive et al., 2010; Stehbens et al., 2001). Nevertheless, although there is evidence of peripheral artery disease in HGPS, endothelial vasomotor function seems to be preserved (Gerhard-Herman et al., 2012; Merideth et al., 2008; Nair et al., 2004).

Associated with both vascular disease and aging, clinically silent myocardial infarction or stroke are prevalent characteristics of HGPS (Hennekam, 2006). Stroke in HGPS patients can also provoke neurologic sequelae and represents one of the main causes of death in this disease (Silvera et al., 2013; Gordon et al., 2014a).

Regarding heart disease, the most prominent alteration in HGPS is LV diastolic dysfunction (Prakash et al., 2018). Other age-related cardiac alterations include LV hypertrophy, aortic and MV calcification (which causes aortic or mitral regurgitation), interstitial fibrosis and electrocardiographic repolarization abnormalities that could elicit arrhythmia, such as ST depression/elevation and T-wave flattening (Nair et al., 2004; Hennekam, 2006; Merideth et al., 2008; Hanumanthappa et al., 2011; Gerhard-Herman et al., 2012; Rivera-Torres et al., 2016; Prakash et al., 2018). Taken together, all these anomalies could lead to heart failure, the primary cause of death in HGPS (79.4% of the cases) (Gordon et al., 2018a).

Over the last few years, several studies have analyzed plasma levels of different protein and metabolite markers in HGPS patients (Gordon et al., 2005; Merideth et al., 2008; Gerhard-Herman et al., 2012; Gordon et al., 2018b). Interestingly, unlike in the elderly, dyslipidemia is not highly prevalent in HGPS. Although reduced HDL levels in blood is a common feature, it is rarely associated with increased plasma levels of LDL or triglycerides in these patients. C-reactive protein levels are normal, as well as those of thyroid or growth hormones.

Overt diabetes is very unusual in HGPS, although several patients display hyperglycemia or low glucose tolerance. Insulin levels are high and rise with disease progression very much like in age-associated insulin resistance. Additionally, plasma levels of leptin and adiponectin are low in HGPS patients and decrease with age, correlating with the development of subcutaneous lipodystrophy (Gordon et al., 2005; Merideth et al., 2008; Gerhard-Herman et al., 2012; Gordon

et al., 2018b). Subcutaneous loss of adipose tissue is also common in the elderly, as well as central obesity, which is absent in HGPS (Tchkonia et al., 2013).

Progeria animal models constitute an exceptional tool to elucidate the molecular mechanisms underlying cardiometabolic disease during aging, without interference from other comorbidities and risk factors. Much progress has been made regarding the age-related vascular pathology and the electrical cardiac alterations (Hamczyk et al., 2018a); nevertheless, little is still known about the mechanisms that drive cardiac and metabolic disorders, as well as their interplay at the local and systemic environments.

2

Objectives

Aging comprises the main risk factor for developing cardiovascular and metabolic diseases, which have become a global concern. The identification of the hallmarks of aging and the cumulative knowledge on the molecular foundations underlying cardiometabolic diseases show that these processes are deeply interconnected and can be modulated.

HGPS is characterized by premature aging and cardiometabolic disorders. Interestingly, comorbidities such as cancer or neurodegeneration are absent in progeria, and environmental risk factors have a minimal implication in the disease progression. Thus, HGPS mouse models constitute a unique tool to elucidate the molecular mechanisms that drive cardiometabolic disorders during aging and to develop rejuvenation strategies.

Recent studies from our laboratories have focused on the vascular pathology and cardiac electrical abnormalities in HGPS. Nevertheless, much remains to be interpreted regarding the age-related cardiac and metabolic disorders, as well as their interconnection. Therefore, the main objectives of this Doctoral Thesis were the following:

1. To characterize cardiometabolic alterations present in mouse models of premature and normal aging.

2. To identify proteomic changes in the mouse heart, common or specific to premature and normal aging.

3. To study the interplay between local and systemic mechanisms that promote cardiometabolic disease during aging.

3

Materials & Methods

3.1 Animal Model Methods

3.1.1 Animal Care and Models

All animal experiments were performed on mice following the guidelines of the Ethics Committee of CNIC, in accordance with to EU Directive 2010/63EU and Recommendation 2007/526/EC, enforced in Spanish law under Real Decreto 53/2013. Every effort was made to minimize the suffering of the mice.

Mice were housed separately by sex at the CNIC animal facility in specific pathogen free conditions. For the magnetic resonance imaging (MRI) and electrocardiographic telemetry experiments, mice were transferred to the conventional and quarantine areas (respectively) on account of the location of the equipment. Animals were maintained at a 12:12 h light-dark cycle with *ad libitum* access to food and water, and standard conditions of humidity and temperature (20-24 °C). For the thermoneutrality experiments, mice were caged separately by genotype and kept either in standard conditions or in a cabinet at 26-28 °C. In the cohousing study, each cage accommodated all studied genotypes and the control group was shared with the thermoneutrality study.

The mouse strains disclosed in table 1 were used for this project. Mice were maintained in a pure Charles River Laboratories C57BL/6N genetic background, except for the *αMHC-Cre* which originated from a CD1-mixed background, diluted in each generation. Cre transgenes were kept in heterozygosis to moderate recombinase expression. $Lmna^{G609G/G609G}$ mice were generated by intercrossing $Lmna^{G609G/+}$ animals to overcome fertility complications. *αMHC-Cre* and *aP2-Cre* mice were generously provided by the Juan Miguel Redondo and the Guadalupe Sabio groups at CNIC (respectively).

Table 1: **Mouse strains used for this project**

Alias	Strain	Phenotype	Reference
WT	*C57BL/6NCrl*	Wild-type	
Lmna^{LCS}	*Lmna*^{tm1Otin}	LCS. Expression of lamin C but not lamin A. Conditional ready targeted mutation of HGPS	Osorio et al., 2011
Lmna^{G609G}	*Lmna*$^{tm1.1Otin}$	Ubiquitous targeted mutation of HGPS (expression of progerin)	Osorio et al., 2011
αMHC-Cre	*Tg(Myh6-cre)2182Mds*	Cre recombinase under α-myosin heavy chain promoter for specific expression in myocardium	Agah et al., 1997
Lmna^{LCS} *αMHC-Cre*	*Lmna*^{tm1Otin}; *Tg(Myh6-cre)2182Mds*	Heart-specific expression of progerin in LCS background	
aP2-Cre	*Tg(Fabp4-cre)1Rev*	Cre recombinase under *FABP4* promoter for specific expression in (pre)adipocytes	He et al., 2003
Lmna^{LCS} *aP2-Cre*	*Lmna*^{tm1Otin}; *Tg(Fabp4-cre)1Rev*	Adipose tissue-specific expression of progerin in LCS background	

Official strain names and aliases are given, as well as a brief description of the phenotype and the reference to the article in which the lines were first described.

3.1.2 Longitudinal Studies

Starting at eight weeks of age, animals were weighed and inspected for health and survival at least once every three weeks. Checks became more frequent when the minimum lifespan was reached. Temperature was assessed concurrently by rectal probe (RET-3) and thermometer (Microtherma 2T, ThermoWorks). Animals that met humane end point criteria were euthanized and the deaths recorded. Animals euthanized because of hydrocephalus, malocclusion, intermale aggression, dermatitis or other reasons unconnected to phenotype were censored.

3.1.3 Heart Rate and Blood Pressure Measurement

HR and blood pressure were measured with a non-invasive automated tail-cuff device (BP2000, Visitech Systems) in conscious mice. Measurements were taken on a daily basis for two weeks at the same time in the morning. To improve accuracy, the first 10 of 20 measurements were discarded. The interquartile range (IQR) was calculated (difference between quartiles 3 and 1) and data points 1.5xIQR below the first quartile (Q1) or 1.5xIQR above the third quartile (Q3) were discarded as outliers. Values over 200 mm Hg in pressure measurements were considered

artifacts and therefore excluded. When blood pressure analysis was not required, tail cuff pressure was not applied and HR was measured only three consecutive days.

3.1.4 Electrocardiography

Mice were anesthetized with 1% to 2% isoflurane, and 4 ECG electrodes were inserted subcutaneously into the limbs (Fig. 4). 2 min ECG recordings were acquired at 2 KHz sweep-speed using a MP36R data acquisition workstation (Biopac Systems). ECG data were exported with AcqKnowledge software (Biopac Systems) and automatically analyzed using custom R scripts that 1) remove noise and baseline fluctuations; 2) detect heart beats, peaks and waves; 3) exclude artifacts; and 4) calculate HR, ECG intervals (PR, QRS, QT, QT_{90}, QT_e), JT gap and T-wave

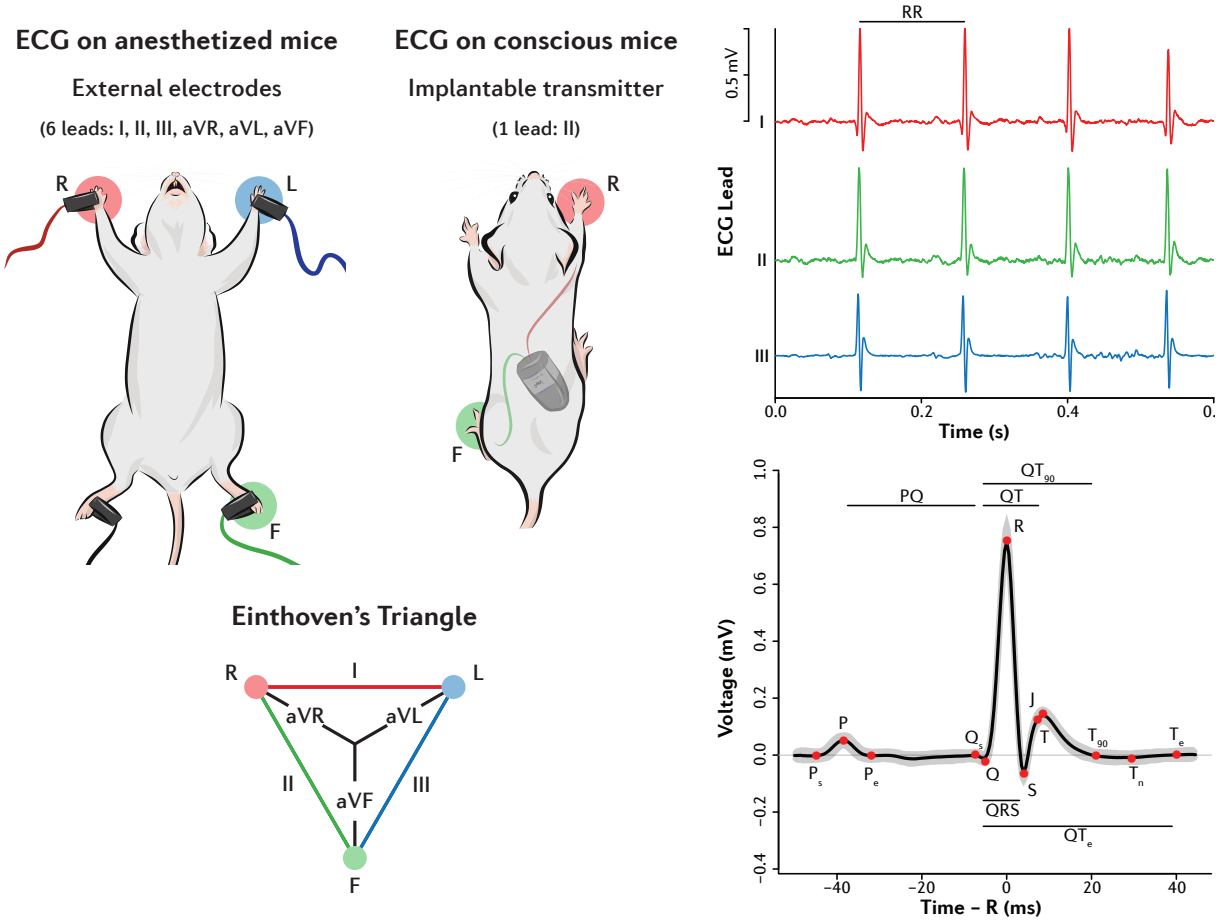

Figure 4: Electrocardiography experiments
Left panel: Electrocardiography (ECG) on anesthetized mice is performed by attaching external electrodes to each limb and allows 6-lead recordings. ECG on conscious mice requires subcutaneous implantation of a 1-lead transmitter through surgery. Leads I, II and III depict the voltage between limbs (L: left, R: right, F: foot), whereas augmented leads aVL, aVR and aVF are calculated from the former leads. Right panel: signal from limb leads and time interval calculations from lead II.

steepness. The second lead was selected for the study, since the signal was more stable in most experiments and therefore the identification of waves more robust using this channel.

HR is the inverse of the time difference between two consecutive R-wave peaks (RR). Since noise may interfere with the detection of the beginning of the P-wave (P_s), PR interval (or PQ interval) was measured from the P-wave peak to the beginning of the Q-wave (Q_s). The end of the S-wave (J) is not evident in mice because the ST segment is absent in this species and replaced by a J-wave corresponding to a positive segment of the T-wave (Speerschneider and Thomsen, 2013; Boukens et al., 2013; Boukens et al., 2014). Therefore, QRS complex was calculated from the Q_s to the S-wave minimum and the QT interval from the Q_s to the T-wave peak (also termed J-wave peak). The QT_{90} was defined as the interval between the Q_s and the point where the T-wave declines 90% (T_{90}) from the peak. QT_e was also measured, from the Q_s to the point where the negative component of the T-wave returned to the isoelectric line (T_e) (Fig. 4) (Speerschneider and Thomsen, 2013; Boukens et al., 2013; Boukens et al., 2014).

Adaptive HR-corrected QT values ($QT_{90}c$, QT_ec) were derived using a modification of Bazzet's formula for murine ECG (Mitchell et al., 1998). T-wave morphological alterations were quantified by defining the JT gap and the T-wave steepness. The JT gap measures the distance between the J point and the T-wave peak, typically coincidental in mice, allowing thus to detect delays in T-wave appearance. T-wave steepness serves as an indicator of T-wave flattening, for it represents the absolute value of the slope (difference in voltage divided by the difference in time) between the peak of the T-wave and the T_{90}.

$$RR\ (ms) = R_{n+1} - R_n \qquad HR\ (bpm) = \frac{60000\ ms}{1\ min \times RR}$$

$$PR\ (ms) = Q_s - P \qquad QRS\ (ms) = S - Q_s$$

$$QT\ (ms) = T - Q_s \qquad JT\ (ms) = T - J$$

$$QT_{90}\ (ms) = T_{90} - Q_s \qquad QT_{90}c\ (ms) = \frac{T_{90} - Q_s}{\sqrt{RR/100}}$$

$$QT_e\ (ms) = T_e - Q_s \qquad QT_ec\ (ms) = \frac{T_e - Q_s}{\sqrt{RR/100}}$$

$$T_{steepness}\ (mV/ms) = \left| \frac{{}_VT_{90} - {}_VT}{T_{90} - T} \right|$$

For ECG experiments on conscious mice, animals were anesthetized with 2% isoflurane, and ECG transmitters (TA11ETA-F10, Data Sciences International) were implanted subcutaneously (Fig.

4). ECG recording was performed on single-caged conscious mice with the HD-X11 PhysioTel Implantable Telemetry System (Data Sciences International). Basal measurements of HR, body temperature and physical activity were recorded during 1 h. In circadian experiments, telemetry was performed over 60 h. For drug response studies, baseline ECGs were recorded for 20 min in resting conditions followed by intraperitoneal delivery of 2 mg/kg epinephrine or atropine (B. Braun) injection and observation for additional 20 min.

3.1.5 Echocardiography

Transthoracic echocardiography was blinded performed by an expert operator using a high-frequency ultrasound system (Vevo 2100, VisualSonics) with a 40 MHz linear probe. Before echocardiography, animal fur was removed with a topical depilatory agent. Two-dimensional (2D) and M-mode echography were performed at a frame rate above 230 frames/sec, and pulsed wave (PW) Doppler was acquired with a pulse repetition frequency of 40 kHz. Mice were lightly anesthetized with 1-2% isoflurane in oxygen through a facial mask, adjusting the isoflurane delivery to maintain the HR at 450 $\pm$ 50 bpm. Mice were placed in supine position using a heating platform and warmed ultrasound gel was used to maintain normothermia. A base apex ECG was continuously monitored. Images were analyzed off-line using the Vevo 2100 Workstation software (VisualSonics).

For LV systolic function assessment, parasternal standard 2D and M-mode, long axis (LAX) and short axis (SAX) views were acquired (Moran et al., 2013). LV chamber dimensions were measured from these views, including the end-diastolic LV posterior wall thickness (LVPWd), the end-diastolic LV internal diameter (LVIDd), the end-systolic LV internal diameter (LVIDs) and the end-diastolic inter ventricular septum thickness (IVSd). These measurements served to calculate LV end-systolic volume (ESV) and end-diastolic volume (EDV), LV fractional shortening (FS), LV EF and LV (corrected) chamber mass (LV_{mass}, $LV_{mass}c$) (Foppa et al., 2005).

$$LVEDV\ (\mu l) = \frac{7\ LVIDd^3}{2.4 + LVIDd} \qquad LVESV\ (\mu l) = \frac{7\ LVIDs^3}{2.4 + LVIDs}$$

$$LVFS\ (\%) = \frac{LVIDd - LVIDs}{LVIDd}\ 100 \qquad LVEF\ (\%) = \frac{LVEDV - LVESV}{LVEDV}\ 100$$

Right ventricle (RV) systolic function was indirectly estimated using the tricuspid annular plane systolic excursion (TAPSE), obtained from a 4-chamber apical M-mode view, measuring maximum lateral tricuspidal annulus movement (Moran et al., 2013). MV inflow pattern was acquired using PW Doppler echography in the four-chamber apical view to assess diastolic function. The sample volume was positioned parallel to the blood flow, across the mitral orifice. Early and late diastolic velocity peak wave (E and A, respectively) to measure the E/A ratio (Schnelle et al., 2018).

$$LV_{mass}\ (mg) = 1.053\ [(LVIDd + IVSd + LVPWd)^3 - LVIDd^3]$$
$$LV_{mass}c\ (mg) = 0.8 \times 1.053\ [(LVIDd + IVSd + LVPWd)^3 - LVIDd^3] + 0.6$$

SV was calculated by measuring the area of the LV outflow tract diameter (LV outflow tract diameter (LVOTd)) and the velocity time integral (VTI). LVOTd was assessed from a 2D LAX view, at the level of the aortic valve annulus, after maximal systolic leaflet separation. VTI was obtained by tracing the LVOT flow signal envelope, which was acquired by aligning the PW Doppler beam with the LV outflow. CO was derived from the product of SV and HR (Zoghbi and Quinones, 1986).

To assess pulmonary pressures, the pulmonary artery flow was measured from a 2D SAX view, at the level of the aorta, optimized to visualize the pulmonary artery crossing the aorta and parallel to the ultrasound beams. PW Doppler was displayed just at the beginning of the artery. Pulmonary artery acceleration time (PAT) and ejection time (ET) were measured, and the ratio was calculated (Thibault et al., 2010).

$$MVE/A = \frac{MVE}{MVA} \qquad PAT/ET\ (\%) = \frac{PAT}{ET}\ 100$$
$$SV\ (\mu l/beat) = \frac{\pi}{4}\ LVOTd^2\ VTI \qquad CO\ (ml/min) = \frac{1\ ml}{1000\ \mu l}\ SV\ HR$$

3.1.6 Magnetic Resonance Imaging

MRI studies were performed at the CNIC Advanced Imaging Unit, using 7-T Agilent/Varian scanner (Agilent Technologies) equipped with a DD2 console. For the image acquisition, mice were sedated using 2% isoflurane in oxygen. Ophthalmic gel was applied to prevent retinal drying.

Cardiac MRI was performed using an actively shielded 115/60 gradient. A surface coil was used for MRI signal transmission and reception. MRI experiments were conducted by applying an ECG-triggered fast gradient echo cine sequence with the following imaging parameters: 125 ms repetition time (minimum values depending on HR and number of frames per heart cycle), 1.25 ms echo time, 30 x 30 mm field of view, 128 x 128 acquisition matrix, 15 ° flip angle, 4 averages, 20 cardiac phases and 12 0.8 mm slices (depending on heart size) with a 0.2 mm gap.

The examination began with the acquisition of survey chest images in the three orthogonal planes (transverse, coronal, and sagittal) to localize the heart and obtain images of two-chamber SAX view, the four-chamber view and the two-chamber LAX view. By using the four-chamber and two-chamber LAX views, a series of parallel SAX images (encompassing the entire LV from the base to the apex) were defined. The most apical slice of the multislice set was positioned inferior to the heart, and the most basal slice was positioned above the LV to ensure total coverage of the ventricles through the cardiac cycle.

Body fat mass was obtained by MRI and ^{1}H nuclear magnetic resonance (NMR) spectra. ^{1}H NMR spectra were acquired using an actively shielded 205/120 gradient with a volume transmit coil (MR Volume Resonator V-HQS-O70-00666 VO8). Spectra were obtained using a SPULS sequence with 5000 ms RT, 20 averages, 8192 complex points, 8 block size and a 10 kHz spectral width. Body fat imaging was acquired using a spin echo multi slice (SEMS) sequence with and without fat saturation and the following parameters: 533-884 ms repetition time (varies between with and without fat saturation), 10.44 ms echo time, 128 x 128 acquisition matrix, 90 ° flip angle, 1 average and 35 1 mm slices with a 1 mm gap.

Cine MRI was analyzed using the freely available software Segment software (Heiberg et al., 2010). On both ventricles, epicardial and endocardial borders were delineated manually on the SAX of each slide to measure total ventricular volumes and cardiac mass (Hernández-Porras et al., 2014). Cardiac function was assessed by calculating LV and RV EF, SV and CO from these measurements. Aditionally, the RV to LV EDV ratio and the Fulton index (RV / LV mass) were

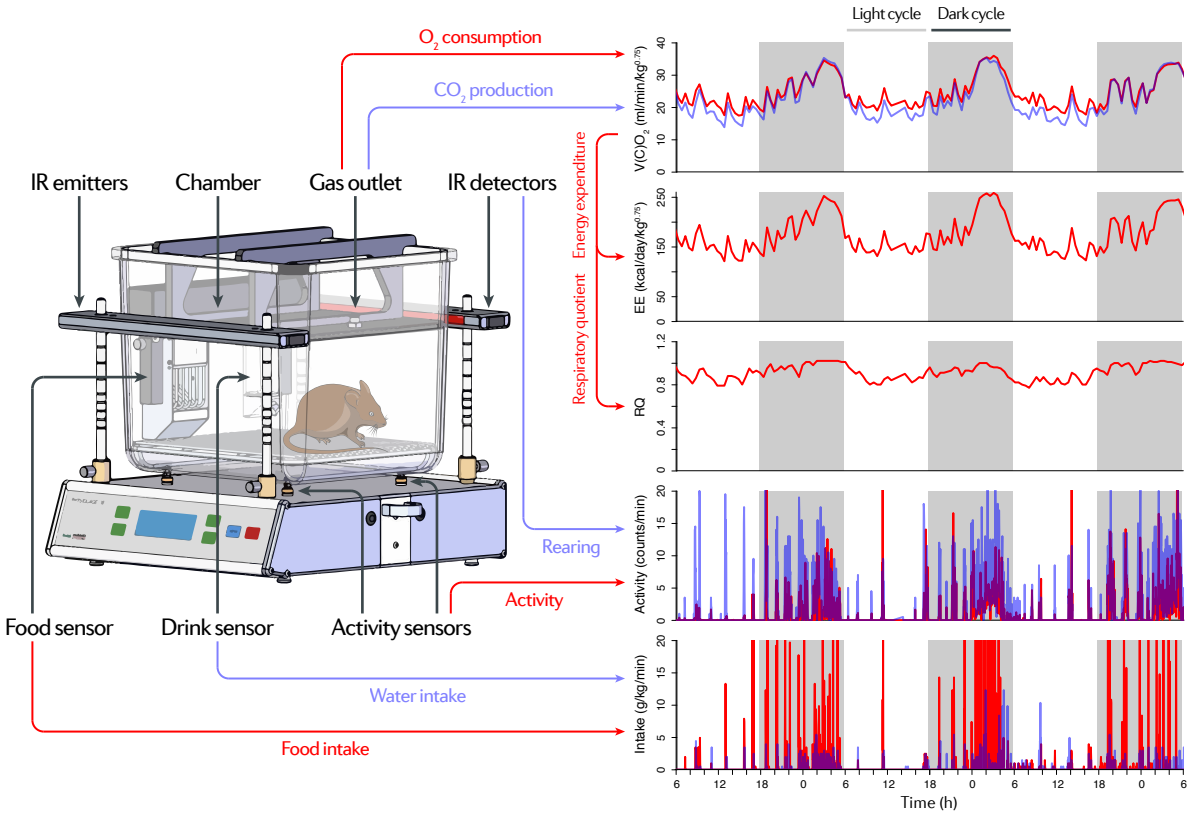

Figure 5: Metabolic chamber experiments
Mice were placed individually in metabolic chambers to evaluate gas exchange, food and water intake, as well as locomotor activity during three days. EE and the respiratory quotient (RQ) were estimated from these observations.

determined to analyze ventricle relative size. Whole-body fat spectrum was analyzed using the Mestrenova program (Mestrlab Research). Measurements of the area under the curve and peak height of fat referred to water peak were taken to quantify body fat. Whole body images were analyzed using Fiji-ImageJ software. Fat was segmented from each slice to obtain the fat volume. Fat mass was estimated by the product between fat volume and fat density (0.923 g/cm^3) (Hill et al., 2007).

3.1.7 Metabolic Chamber Experiments

Metabolic parameters, as well as locomotor activity, eating and drinking patterns were assessed using the indirect calorimetry system OxyletPro Physiocage (Panlab, Harvard Apparatus) (Fig. 5). Mice kept on standard rodent chow were housed individually in chambers and kept on a 12:12 h light-dark cycle. Constant airflow (250 ml/min) was drawn through each chamber to maintain atmospheric O_2 and CO_2 concentrations. After 72 h of acclimation, animals were monitored

during 72 h by a blinded operator, using METABOLISM 3.0 software (Panlab, Harvard Apparatus) and following the manufacturer's instructions. Data were exported and analyzed using custom R scripts that 1) rearrange and consolidate the output data in a single spreadsheet; 2) include information about light-dark cycles, torpor bouts, events; and 3) plot the different parameters by individual, experiment or chamber.

O_2 consumption (VO_2) and CO_2 production (VCO_2) were calculated considering the air flow entering the cage (F), and the O_2 and CO_2 concentrations inside ($[O_2]_i$, $[CO_2]_i$) and outside ($[O_2]_e$, $[CO_2]_e$) the cage. RQ, also known as respiratory exchange ratio (RER), was obtained dividing VCO_2 by VO_2 and EE was estimated using the Lusk equation (Lusk, 1909). VO_2, VCO_2 and EE may be normalized by body weight (W) to account for differences in animal size. Since the relationship between metabolism and body weight is not linear, an allometric exponent (k) of 0.75 may be added to the equations; although body weight could be included as a covariate in the statistical model instead (Tschöp et al., 2011).

$$
\begin{aligned}
VO_2\ (ml/min) &= \quad F\left([O_2]_e - [O_2]_i\ \frac{1-[O_2]_e-[CO_2]_e}{1-[O_2]_i-[CO_2]_i}\right)\\
VCO_2\ (ml/min) &= -F\left([CO_2]_e - [CO_2]_i\ \frac{1-[O_2]_e-[CO_2]_e}{1-[O_2]_i-[CO_2]_i}\right)\\
RQ &= VCO_2\ /\ VO_2\\
EE\ (kcal/day) &= \frac{1.44\ kcal\ min}{1\ cal\ day}\ (3.815\ VO_2 + 1.232\ VCO_2)\\
V(C)O_2n\ (ml/min/kg^k) &= \frac{V(C)O_2}{W^k}\ ;\ EEn\ (kcal/day/kg^k) = \frac{EE}{W^k}
\end{aligned}
$$

Locomotor activity (physical work or exertion) was measured by a transducer platform located under the cage, and rearing (standing up to explore, eat or drink) was detected by infrared sensor bars featuring 11 infrared beams. Food and drink consumption was calculated with high precision through weight changes in the dispensers detected by load cells. Food and drink consumption may be normalized by body weight.

3.1.8 Tolerance to Challenge Tests

For the acute cold stress experiments, mice were individualized and kept for 6 h at 4 °C. Rectal and brown adipose tissue (BAT) temperatures were measured before the exposure to cold (time 0) and every hour until the end of the experiment. Rectal temperature was determined by rectal

probe (RET-3) and thermometer (Microtherma 2T, ThermoWorks). BAT-adjacent interscapular temperature was quantified by thermographic images using a FLIR T430sc Infrared Camera (FLIR Systems) and analyzed through FLIR R&D Software (FLIR Systems). BAT relative temperature was calculated by subtracting rectal temperature from BAT temperature.

Acute cold stress experiments were also performed on mice bearing ECG transmitters (TA11ETA-F10, Data Sciences International). ECG recording was performed on single-caged conscious mice with the HD-X11 PhysioTel Implantable Telemetry System (Data Sciences International). Baseline ECGs, body temperature and physical activity were measured for 5 min in resting conditions followed by 300 min at 4 °C. For heat shock experiments, mice were introduced in a Thermacage (Datesand) station at 40 °C for 60 min instead.

For glucose tolerance test (GTT), overnight fasted mice received an intraperitoneal injection of glucose (1 g/kg of body weight, Sigma-Aldrich). In insulin tolerance test (ITT) studies, 1 h fasted mice received an intraperitoneal injection of insulin (0.75 IU/kg, Lilly). Blood glucose levels were determined by a Contour Next One Smart Meter (Contour Next) at 0, 15, 30, 60, 90, and 120 min post injection using blood from the tail vein (Matesanz et al., 2017).

3.2 Cell Biology and Histology Methods

3.2.1 Blood Analysis

Animals were fasted overnight before blood was extracted directly from the mandibular sinus (live mice) or from the heart and renal artery (euthanized mice). For biochemical analysis, blood samples were collected in plastic tubes and incubated at room temperature for 1 to 2 h to allow clotting and obtain serum. Alternatively, plasma was obtained by collecting the blood in Microvette 100 ethylenediaminetetraacetic acid (EDTA) tubes (Sarstedt). Serum or plasma samples were centrifuged at 1200g for 15 min and the supernatant was stored at –80 °C. Biochemical variables were analyzed using a Dimension RxL Max Integrated Chemistry System (Siemens Healthineers). All protocols were performed according to manufacturer's instructions.

3.2.2 Histopathological Analysis

Mouse organs were collected after euthanasia in a CO_2 chamber, examined, washed in 0.9% saline, divided in portions (if required) and fixed in 4% paraformaldehyde (PFA) in phosphate-

buffered saline (PBS). Samples were dehydrated to xylol through an ethanol series and embedded in paraffin. Serial 4 μm sections were made from the paraffin blocks at different levels using a microtome (Leica). Sections were mounted on Superfrost slides (Fisher Scientific), deparaffinised in xylol, rehydrated and washed in distilled water. Next, sections were stained with hematoxylin and eosin (H&E), Masson trichrome or Periodic acid–Schiff (PAS) using a ST5020 Multistainer (Leica). Stained sections were scanned with a NanoZoomer-XR Digital slide scanner (Hamamatsu), and images were analyzed using NDP.view2 (Hamamatsu) and Fiji-ImageJ software in a blinded fashion.

For adipose tissue evaluation, portions of BAT and perigonadal and inguinal white adipose tissue (WAT) fat pads were processed as described above. Large intestine mucosa (and muscular) mean thickness were estimated by dividing the mucosal (or muscular) area between its external perimeter. PAS intensity was normalized by mucosal area.

3.2.3 Cell Culture and *in vitro* Adipogenesis

Inguinal (subcutaneous) WAT (iWAT) and perigonadal (visceral) WAT (pWAT) pads were excised from mice euthanized by CO_2 inhalation. Tissues were washed in Krebs-Henseleit (KH) buffer (115 mM NaCl, 25 mM $NaHCO_3$, 4.6 mM KCl, 1.2 mM KH_2PO_4, 2.5 mM $CaCl_2$, 1.2 mM $MgSO_4$, 0.01 mM EDTA, 2 g/l glucose), minced and digested in 2 mg/ml collagenase I (Sigma-Aldrich) in KH buffer for 1 h at 37 °C. Digestion was stopped with KH buffer supplemented with 20% inactivated fetal bovine serum (FBS) (Invitrogen). After centrifugation, supernatants were removed to obtain the stromal vascular fraction, which was resuspended and filtered through 4 μm cell strainers (Becton Dickinson) in KH buffer supplemented with 2% FBS. Cells were then resuspended in 10% dimethyl sulfoxide (DMSO) (Sigma-Aldrich) in FBS and frozen at -80 °C until further use.

Cells were plated in Dulbecco's Modified Eagle Medium Nutrient Mixture F-12 (DMEM/F12) (Gibco) containing 50% FBS, 100 U/ml penicillin and 100 μg/ml streptomycin (Life Technologies). The culture was maintained in DMEM/F12 with 10% FBS, penicillin and streptomycin at 37 °C and 5% CO_2. Cells were observed daily using an inverted phase contrast microscope and split at a ratio of 1:3 using standard methods of trypsinization.

For adipogenic differentiation, cultures were incubated for seven days in DMEM/F12 containing 10% FBS, 0.5 μM 1-methyl-3 isobutylxanthine, 1 μM dexamethasone, 10 μg/ml insulin and 100 μM indomethacin (Oldenburg et al., 2017). To visualize lipid droplets, cells were fixed with

4% PFA and stained with Oil-Red O (ORO). The reagents were kindly provided by the group of Philippe Collas (University of Oslo).

3.3 Molecular Biology Methods

The basic molecular biology techniques employed in this work, including agarose or polyacrylamide gel electrophoresis, which are not detailed below, were performed following manufacturer's instructions or standard protocols.

3.3.1 DNA Genotyping

Genotyping of the different mouse strains for this project was performed to detect the presence of the *Lmna*^{LCS}, *Lmna*^{G609G}, *αMHC-Cre* and *aP2-Cre* alleles. DNA was extracted after alkaline lysis from biopsies of mouse tails. Polymerase chain reaction (PCR) were carried out with the primers listed in table 2 and following the protocols detailed in table 3.

Table 2: Primers used for genotyping in this project

Locus	Primer sequence (5' - 3')		Amplicon size (bp)	
	Forward	Reverse	WT	Mutant
αMHC-Cre	ATGACAGACAGATCCCTCCTATCTCC	CTCATCACTCGTTGCATCGAC	-	350
Lmna$^{LCS/G609G}$	AAGGGGCTGGGAGGACAGAG	AGTAGAAGGTGGCGCGAAGG AGCATGCAATAGGGTGGAAGGA	100	340 (LCS) 240 (G609G)
aP2-Cre	TTACTGACCGTACACCAAATTTGCCTGC CTTGGGCTGCCAGAATTTCTC	CCTGGCAGCGATCGCTATTTTCCATGAGTG TTACAGTCGGCCAGGCTGAC	350	450

3.3.2 RNA Preparation and Quantitative RT-qPCR

Mice were euthanized in a CO_2 chamber and tissues were collected, snap-frozen in liquid nitrogen and preserved at -80 °C until further use. Frozen samples were homogenized using a pestle and mortar, and later by TissueLyser (Qiagen). Alternatively, cells were collected from cell-culture plates or flasks, frozen or directly used for RNA extraction. RNA was extracted with QIAzol reagent (Qiagen) and processed through alcohol precipitation according to the manufacturer's instructions. RNA pellets were then washed in cold 75% ethanol and resuspended in nuclease-free water. Samples from WAT were further purified with the RNeasy Plus Mini kit (Qiagen).

Table 3: Genotyping protocols used in this project

Step	*αMHC-Cre*			*Lmna*$^{LCS/G609G}$			*aP2-Cre*		
	T (°C)	Time (s)	Cycles	T (°C)	Time (s)	Cycles	T (°C)	Time (s)	Cycles
Initial denaturation	95	300	1	94	300	1	95	300	1
Denaturation	95	30		94	30		94	30	
Annealing	56	30	10	62	30	28	60	30	35
Extension	72	40		72	45		72	60	
Denaturation	95	40							
Annealing	62	30	10						
Extension	72	40							
Final extension	72	300	1	72	300	1	72	300	1
End	12	-	1	12	-	1	12	-	1

The samples were quantified and evaluated for purity (260/280 and 260/230 ratios) with a NanoDrop ND-1000 spectrophotometer (Thermo Fisher Scientific). Complementary DNA was synthesized using 1-2 µg of total RNA using the High Capacity cDNA Reverse Transcription Kit (Applied Biosystems) following the manufacturer's instructions.

Reverse transcription - quantitative PCR (RT-qPCR) was carried out in triplicate for each sample using Power SYBR Green PCR Master Mix (Applied Biosystems) in a CFX384 Touch Real-Time PCR Detection System (Bio-Rad Laboratories) with the following protocol: denaturation at 95 °C for 10 min; 40 amplification cycles of denaturation (95 °C, 15 s), annealing (61 °C, 30 s) and extension (72 °C, 45 s); final extension at 72 °C for 5 min and melt curve (65 to 95 °C with a 0.5 °C increment, for 5 s). Oligonucleotides for amplification were acquired from Sigma-Aldrich and are listed in table 4. Relative messenger RNA (mRNA) expression was normalized to two appropriate housekeeping genes (internal controls) measured in each sample.

3.3.3 Protein Extraction and Western-blot Analysis

Cells were collected from cell-culture plates or flasks, frozen at -80 °C until further use or directly lysed in radioimmunoprecipitation assay (RIPA) buffer (50 mM Tris-HCl at pH 7.5, 150 mM NaCl, 1% Triton X-100, 0.1% sodium dodecyl sulfate (SDS), 2 mM EDTA, 0.5% sodium deoxicholate) supplemented with 1 mM dithiothreitol (DTT), Complete protease inhibitors (Roche) and PhosSTOP phosphatase inhibitors (Sigma-Aldrich). Alternatively, mice were euthanized in a CO_2 chamber and tissues were collected, snap-frozen in liquid nitrogen and preserved at -80 °C until further use. Tissue samples were homogenized in supplemented RIPA buffer by TissueLyser (Qiagen) and sonicated with a Sonopuls Ultrasonic Homogenizer HD 2070 (Bandelin) or with a

Table 4: Primers used for RT-qPCR in this project

Locus	Forward primer		Reverse primer		Amplicon
	Sequence (5'-3')	Tm (°C)	Sequence (5'-3')	Tm (°C)	size (bp)
Adipoq	TCCTGCCCAGTCATGCCGAA	73.7	TGCCTGCCATCCAACCTGCA	74.7	102
Ccl2	CAAGATGATCCCAATGAGTAG	59.1	TTGGTGACAAAAACTACAGC	58.4	87
Cebpa	CCAAGAAGTCGGTGGACAAG	65	TTGTTTGGCTTTATCTCGGC	64.3	95
Cebpb	ACGACTTCCTCTCCGACCTCT	65.8	CGAGGCTCACGTAACCGTAGT	65.6	84
Cidea	GCCGTGTTAAGGAATCTGCTG	66	TGCTCTTCTGTATCGCCCAGT	66.4	113
Cox5b	GCTGCATCTGTGAAGAGGACAAC	67.5	CAGCTTGTAATGGGTTCCACAGT	66.3	98
Cycs	GCAAGCATAAGACTGGACCAAA	65.4	TTGTTGGCATCTGTGTAAGAGAATC	65.4	88
Fabp4	ACACCGAGATTTCCTTCAAACTG	65.5	CCATCTAGGGTTATGATGCTCTTCA	66.3	88
Il6	TAGTCCTTCCTACCCCAATTTCC	65.2	TTGGTCCTTAGCCACTCCTTC	64.7	76
Lep	CTTTGGTCCTATCTGTCTTATG	57.5	TCTTGGACAAACTCAGAATG	58.4	190
Pgc1a	CCCTGCCATTGTTAAGACC	62.4	TGCTGCTGTTCCTGTTTTC	62.2	161
Ppara	GCGTACGGCAATGGCTTTAT	66.1	GAACGGCTTCCTCAGGTTCTT	66	57
Pparg	GTGCCAGTTTCGATCCGTAGA	66.6	GGCCAGCATCGTGTAGATGA	66.6	142
Pparg2	CTGATGCACTGCCTATGAGC	64.1	GCTGATTCCGAAGTTGGTGG	67.1	86
Prdm16	CAGCACGGTGAAGCCATTC	67.3	GCGTGCATCCGCTTGTG	68.6	87
Prdm3	AACAAAACCTGGAGAGTGAGAG	61.7	AATGCCTTGGGACACTGATC	64.3	160
Retn	CAGAAGGCACAGCAGTCTTGA	66.1	CTGTCCAGTCTATCCTTGCACAC	65.2	108
Tnfa	ACGGCATGGATCTCAAAGAC	64.5	AGATAGCAAATCGGCTGACG	64.5	138
Ucp1	GGGTCAAGATCTTCTCAGCCGGA	71.7	TTGCCTCTGAATGCCCGCAG	73	281
Arbp	ACTGAGATTCGGGATATGCTGT	64	TCCTAGACCAGTGTTCTGAGCTG	65.1	108
Hprt	AGGCCAGACTTTGTTGGATTT	64	GGCTTTGTATTTGGCTTTTCC	63.7	132
Tbp	CCCCTTGTACCCTTCACCAAT	66.1	GAAGCTGCGGTACAATTCCAG	66	89
Ywhaz	GATCCCCAATGCTTCGCAAC	69.1	GAGAAGTTGAGGGCCAGACC	65.5	210

Primer sequences and melting temperatures (Tm), and expected amplicon size for each locus. The last four were used as internal controls for experiments involving WAT (*Arbp* and *Tbp*) and BAT (*Hprt* and *Ywhaz*).

Bioruptor Sonication System (Diagenode) coupled to a Neslab RTE 7 Circulating Chiller (Thermo Fisher Scientific). For tissues such as liver or kidney, lysis was performed in 50 mM Tris-HCl at pH 8.8 supplemented with 2% SDS, 8 M urea and 2 M thiourea. After centrifugation, protein extracts from cells or tissues were collected and protein concentration was evaluated by the Bradford method (Bradford, 1976).

Equal amounts of proteins were loaded into SDS-polyacrylamide gels. After electrophoresis, gels were electrotransferred onto nitrocellulose membranes (Bio-Rad Laboratories) or Immobilon-FL polyvinylidene fluoride membranes (Millipore), blocked with 5% nonfat dry milk in tris-buffered saline with Tween 20 (TBS-T) buffer (20 mM Tris-HCl at pH 7.4, 150 mM NaCl, and 0.05% Tween 20), and incubated overnight at 4 °C with the corresponding primary antibodies. After 3

washes with TBS-T, membranes were incubated for 1 h at room temperature with the appropriate secondary antibody conjugated with horseradish peroxidase (HRP) (Santa Cruz Biotechnology) diluted in 5% nonfat dry milk in TBS-T. When specified in the commercial instructions, blocking and dilution of antibodies was performed in TBS-T with 5% bovine serum albumin (BSA) (Sigma-Aldrich). Membranes were then washed and developed with Luminata Forte chemiluminescent HRP substrate (Millipore) in a ImageQuant LAS 4000 mini (GE Healthcare).

The antibodies against lamin A/C (SC-6215 and SC-376248) and α-tubulin (SC-8035) were obtained from Santa Cruz Biotechnology; and against GAPDH (MAB374), from Millipore. The antibodies used to detect caveolin 1 (BD Biosciencess, 610407) and FABP4 (Cell Signaling, 2120) were provided by the group of Philippe Collas (University of Oslo).

3.4 Proteomics Methods

3.4.1 Sample Preparation for Proteomics

High-throughput shotgun proteomic experiments were performed on hearts from 16 male mice: four 4-month-old and four 20-month-old wild-type animals, as well as four 4-month-old heterozygous and four 4-month-old homozygous progeric animals (Fig. 6). Mice were euthanized in a CO_2 chamber and 0.9% saline-perfused hearts were collected, snap-frozen in liquid nitrogen, pulverized by pestle and mortar, and preserved at -80 °C until further use. Protein extracts were obtained from homogenized tissue using ceramic beads (MagNa Lyser Green Beads apparatus, Roche) in lysis buffer (1.5% SDS, 1 mM EDTA, 50 mM Tris-HCl at pH 8.5) supplemented with 50 mM iodacetamide (Sigma-Aldrich) in order to block reduced cysteine residues (Martínez-Acedo et al., 2012). Protein concentration in extracts was determined by the RC/DC Protein Assay (Bio-Rad Laboratories) and two samples from each experimental condition were pooled, ensuring equal contributions from each biological replicate.

Samples were subjected to tryptic digestion using filter-aided sample preparation (FASP) technology (Expedeon) according to the previously published method (Wiśniewski et al., 2009), which was adapted for oxidized cysteine labeling and renamed filter-aided stable isotope labeling of oxidized cysteines (FASILOX). Briefly, 100 μg of protein extracts were diluted in Urea Sample Solution (USS, 8 M urea in 100 mM Tris-HCl at pH 8.5) and loaded on filters. After centrifugation and a washing step with USS, cysteine residues were reduced with 50 mM DTT (GE Healthcare) in preparation buffer (50 mM HEPES, 1 mM EDTA at pH 7.5) for 1 h at room temperature. Next,

the samples were centrifuged, washed with preparation buffer and subsequently alkylated with 50 mM s-methyl thiomethanesulfonate (MMTS) (Thermo Fisher Scientific) in preparation buffer for 1 h at room temperature. Later, filters were washed 3 times with USS and 3 times with ABC Buffer (50 mM NH4HCO3 at pH 8.8). Proteins were digested using sequencing grade trypsin (Promega) in 1:40 trypsin: sample mass ratio.

Eluted and cleaned-up peptides were subjected to isobaric tag for relative and absolute quantitation (iTRAQ) 8-plex labeling (AB Sciex) according to the manufacturer's protocol, combined, and desalted on Waters Oasis HLB C18 cartridges (Waters Corp). Labeled peptides were separated into 8 fractions using Waters Oasis MCX cartridges (Waters Corp) and graded concentrations of ammonium formate (pH 3.0) (AF3) in acetonitrile (ACN). Briefly, desalted and dried peptides were taken up in 1 ml of 5 mM AF3 containing 25% (v/v) ACN. The MCX cartridge was equilibrated by slowly passing 1 ml of 1:1 methanol: water across the cartridge, followed by 3 ml of 5 mM AF3 containing 25% (v/v) ACN. Samples were applied on the cartridge and was washed with AF3, 25% (v/v) ACN. Bound peptides were eluted into 8 fractions with freshly prepared buffer: 1) 500 mM AF3, 25% (v/v) ACN; 2) 1 M AF3, 25% (v/v) ACN; 3) 1.5 M AF3, 25% (v/v) ACN; 4) 500 mM AF3, 25% (v/v) ACN, 1 M potassium chloride (KCl); 5) 1.25 M AF3, 37,5% (v/v) ACN; 6) 1.25 M AF3, 37,5% (v/v) ACN; 7) 1 M AF3, 50% (v/v) ACN; and 8) 1 M AF3, 50% (v/v) ACN. Obtained fractions were purified and desalted with the MiniSpin Column Kit (The Nest Group), dried, and stored at -20 °C until further use.

3.4.2 Mass Spectrometry Acquisition

The tryptic peptide mixtures were subjected to nanoscale liquid chromatography (LC) coupled to tandem mass spectrometry (MS/MS) (Fig. 6). High-resolution analysis was performed on a EASY-nLC 1000 liquid chromatograph (Thermo Fisher Scientific) coupled to an Orbitrap Fusion (Thermo Fisher Scientific) mass spectrometer. Peptides were suspended in 0.1% formic acid, loaded onto a C18 RP nano-precolumn (Acclaim PepMap100, 75 μm internal diameter, 3 μm particle size and 2 cm length, Thermo Fisher Scientific), and separated on an analytical C18 nano-column (EASY-Spray column PepMap RSLC C18, 75 μm internal diameter, 3 μm particle size and 50 cm length, Thermo Fisher Scientific) in a continuous gradient: 8-27% B for 240 min, 31-100% B for 2 min, 100% B for 7 min, 100-2% B for 2 min and 2% B for 30 min (where A is 0.1% formic acid in HPLC-grade water and B is 90% ACN, 0.1% formic acid in HPLC-grade water).

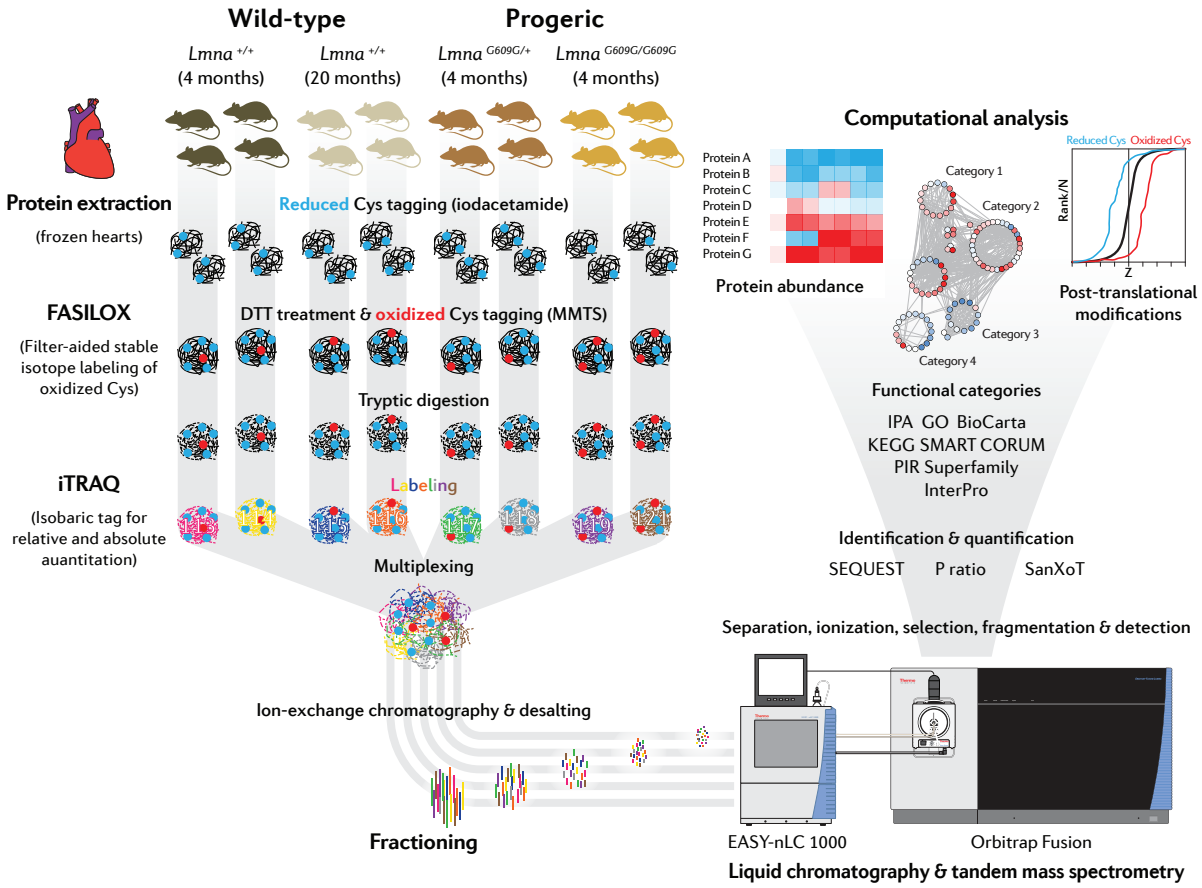

Figure 6: Proteomics methodology
Sample preparation (protein extraction, FASILOX, iTRAQ, fractioning), mass spectrometry acquisition and computational analysis. Cys: cysteine

Spectra were acquired using full ion-scan mode over the mass-to-charge (m/z) range 400-1500 and 120000 Full Width at Half Maximum Fourier transform resolution, at the automatic gain control target setting of 2 x 10^5 with the maximum injection time of 50 ms. Data-dependent acquisition speed mode was performed at 5 x 10^4 automatic gain control and 120 ms injection time, with 1 Da isolation window and 45 s dynamic exclusion. High collision energy dissociation induced fragmentation was set to 33% normalized collision energy. MS/MS scan resolution was set to 15000 Full Width at Half Maximum and the first mass in fragmentation spectrum range was fixed at 100 m/z.

3.4.3 Computational Analysis

Proteins were identified in the raw files using the SEQUEST HT algorithm integrated in Proteome Discoverer 2.1 (Thermo Fisher Scientific) (Fig. 6). MS/MS scans were matched against the mouse proteome supplemented with pig trypsin and human keratin proteins database (UniProtKB 2016-07 Release). For database searching, parameters were selected as follows: trypsin digestion with

maximum 2 missed cleavage allowed, precursor mass tolerance of 800 ppm, and a fragment mass tolerance of 0.02 ppm. The N-terminal and lysine iTRAQ 8-plex modifications were chosen as fixed modifications, whereas methionine oxidation, cysteine carbamidomethylation, and cysteine methylthiolation were chosen as variable modifications. The same MS/MS spectra collections were searched against inverted databases constructed from the same target databases. SEQUEST results were analyzed by the probability ratio method (Martínez-Bartolomé et al., 2008). False discovery rate (FDR) was calculated for peptides identified in the inverted database search results using the refined method (Bonzon-Kulichenko et al., 2015; Navarro and Vázquez, 2009). Quantitative information was extracted from iTRAQ reporter intensities of the MS/MS spectra (García-Marqués et al., 2016).

For comparative analysis of protein abundance changes, we applied the SanXoT software package (Trevisan-Herraz et al., 2018), designed for the statistical analysis if high-throughput, quantitative proteomics experiments and based on the Weighted Scan-Peptide-Protein (WSPP) statistical model (Navarro et al., 2014). As input, WSPP uses a list of quantifications in the form of $\log_2$-ratios (each condition versus the mean of the control 4-month-old wild-type mice) with their statistical weights. From these, WSPP generates the standardized forms of the original variables by computing the quantitative values expressed in units of standard deviation around the means (Zq). A list of candidate proteins with altered expression was elaborated according to the following criteria: protein is quantified with more than one unique peptide, abundance change is greater than 2 standard deviations ($|Zq| > 2$) in at least one comparison, abundance change is validated in preliminary experiments. Additionally, two of these criteria had to be met: abundance change has FDR < 0.05 in at least one comparison, is validated in replicate comparisons, is confirmed by accessory comparisons, is validated in a meta-analysis including protein and RNA expression data sets of progeria and aging samples (Dobson et al., 2003; Csoka et al., 2004; Zahn et al., 2007; Scaffidi and Misteli, 2008; Osorio et al., 2011; Liu et al., 2011; Wang et al., 2012; Rivera-Torres et al., 2013; McCord et al., 2013; Fernandez-Sanz et al., 2014; Fernandez et al., 2014; Mateos et al., 2015).

For the protein functional analysis, we used the Systems Biology Triangle (SBT) model, which estimates functional category averages (Zc) from protein values by performing the protein-to-category integration, as described (García-Marqués et al., 2016). The protein category database was consolidated by including resources from Ingenuity Pathway Analysis (IPA) (Qiagen), CORUM (Helmholtz Zentrum Muñchen) and DAVID (Leidos Biomedical Research) (Gene Ontology - GO, KEGG Pathway, BioCarta, InterPro, PIR SuperFamily, SMART). STRING (ELIXIR Core Data Resources) was used for analyzing protein interaction networks.

3.5 Statistical and Visualization Methods

Experimental conditions were randomized and comparisons in animal studies were made between age-matched groups including male and female mice. No statistical method was used to predetermine sample size.

Statistical analysis of the results was performed by custom R scripts that 1) assess the factors to be considered in each test, including both fixed and random effects; 2) evaluate normality and apply natural-logarithm transformations if convenient; 3) estimate statistical differences between each group applying a suitable model (logistic, linear or generalized linear) with fixed or mixed effects; 4) extract confidence intervals and p-values. Significant differences were considered when $p < 0.05$.

The following factors were considered as fixed effects: condition (genotype, age group or treatment), age, sex, HR (ECG, tolerance tests), body temperature (ECG, tolerance tests), weight (metabolic cages, MRI, echocardiography), tibia length (echocardiography), time (ECG, metabolic cages, tolerance tests) and cycle (metabolic cages). Subject or sample replicates (HR and blood pressure, RT-qPCR), date of measurement and section or region of interest (histopathology) were included in the models as random effects.

Proteomic networks interpretation was carried out with Cytoscape (The Cytoscape Consortium). R scripts used for statistical analysis were used for data visualization. Results were represented in beeswarm-boxplots or scatter plots with linear or LOESS curve fitting. Survival analysis was performed by using the Kaplan-Meier method and statistical differences were analyzed with Log-rank (Mantel-Cox) test.

4 Results

4.1 Cardiometabolic Disease in Progeric and Normally Aged Mice

The first objective of this Doctoral Thesis was to characterize cardiometabolic alterations present in mouse models of premature and normal aging. For this, we selected 20-month-old wild-type mice with a C57BL/6 genetic background as standard for normal aging, given that their median survival is 28 months (Flurkey et al., 2007).

Among the available murine models of HGPS, the *Lmna*^{G609G} knock-in strain carries the mutation present in HGPS patients - therefore accumulates progerin in the nuclear envelope - and recapitulates most of the clinical manifestations of this rare disease, such as growth impairment, bone abnormalities, lipodystrophy and arteriosclerosis (Osorio et al., 2011; Villa-Bellosta et al., 2013; Balmus et al., 2018; Hamczyk et al., 2018b; Del Campo et al., 2019) (Fig. 2). These animals also have shortened lifespan - mean survival is around 5 months and 12 months for homozygous and heterozygous progeric mice, respectively. We included both 4-month-old *Lmna*$^{G609G/G609G}$ and *Lmna*$^{G609G/wt}$ animals in order to assess progerin dose effects; and 4-month-old ("young") wild-type animals were used as controls. The studies comprised both male and female animals in balanced proportions to avoid gender-biased results.

To tackle the cardiometabolic phenotypical alterations in these models, we first performed ECG experiments. Previous studies showed cardiac electrical abnormalities in the *Lmna*^{G609G} strain (Osorio et al., 2011). However, we proposed a deeper characterization, comparing homozygous and heterozygous progeric animals with old and young wild-type mice (Fig. 7). We also assessed HR in a non-invasive tail-cuff device in conscious animals, to avoid anesthetic interference. The results showed that both old and *Lmna*$^{G609G/G609G}$ mice present reduced HR, prolonged PR, QT, QT_{90} and QT_e intervals in comparison to heterozygous and young wild-type animals (Fig. 7). The alterations are more severe in homozygous progeric mice, which also show T-wave flattening and retardation, manifested by a gap between the J and T waves. These observations are consistent with bradycardia and electrical conduction and repolarization abnormalities, previously described

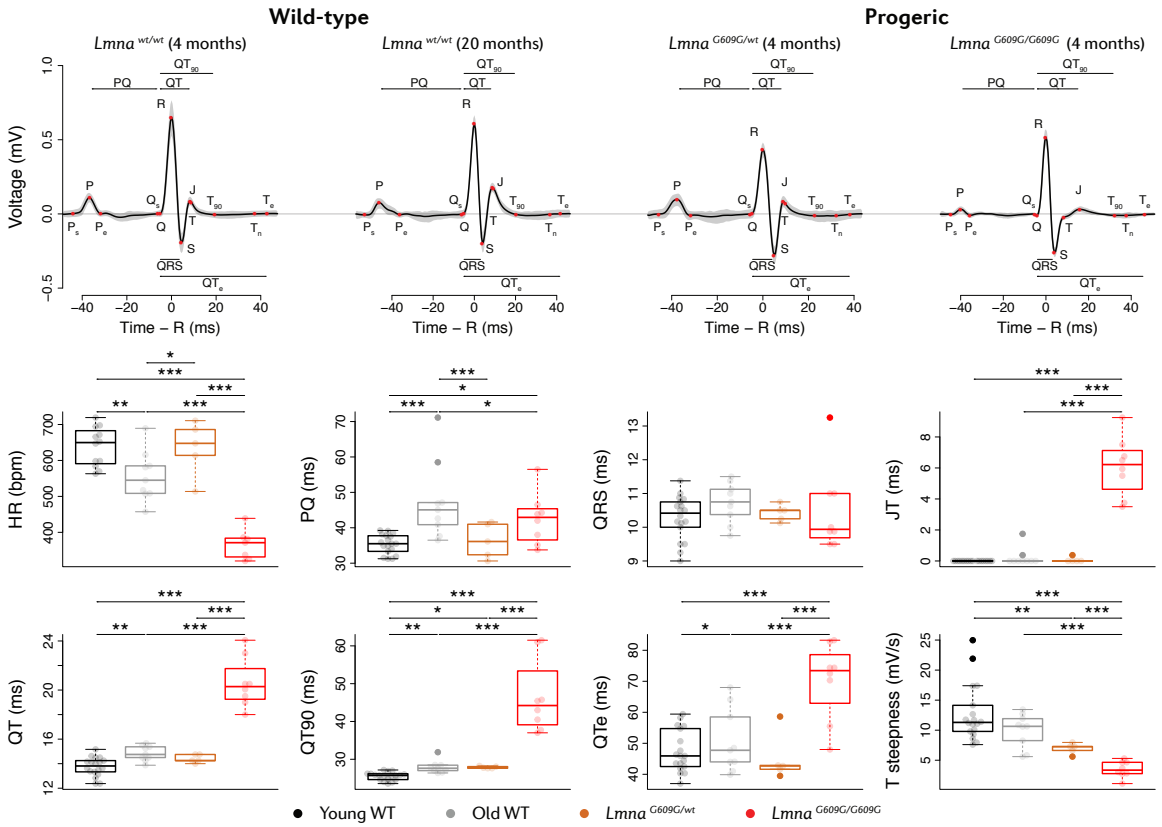

Figure 7: Bradycardia and repolarization abnormalities in progeric and old mice
HR measurement and ECGs of 4-month-old *Lmna*$^{G609G/G609G}$ (n = 8) and *Lmna*$^{G609G/wt}$ progeric mice (n = 5) compared to age-matched (n = 18) and 20-month-old wild-type animals (n = 9). Measurements were performed at least 3 times within a month. * P<0.05, ** P<0.01, *** P<0.001.

for HGPS patients and progeric *Zmpste24*-deficient mice (Rivera-Torres et al., 2016). 4-month-old *Lmna*$^{G609G/wt}$ animals showed normal ECGs, except for a mild but significant reduction in the T-wave steepness in relation to the controls. QRS complex duration was normal in all groups.

We next performed MRI to study cardiac function and body mass composition (Fig. 8). NMR spectral analysis revealed that 20-month-old mice weight more and have increased adiposity in relation to 4-month-old mice (Fig. 8B). In contrast, *Lmna*$^{G609G/G609G}$ are smaller and leaner when compared to the other groups (Fig. 8B). This indicates that mice become obese during normal aging, whereas progeric mice develop cachexia, like HGPS patients (Hennekam, 2006; Merideth et al., 2008).

Systolic function is preserved in all groups, as both LV and RV EF are normal (Fig. 8C). Interestingly, CO is reduced in homozygous progeric mice. This could be a consequence of bradycardia (Fig. 7), although HR was leveled during the experiment through anesthetic dose modulation to ensure optimal image acquisition. Furthermore, SV is also reduced in these animals. Nevertheless, these differences in CO and SV are abrogated when considering body weight as a covariate in the

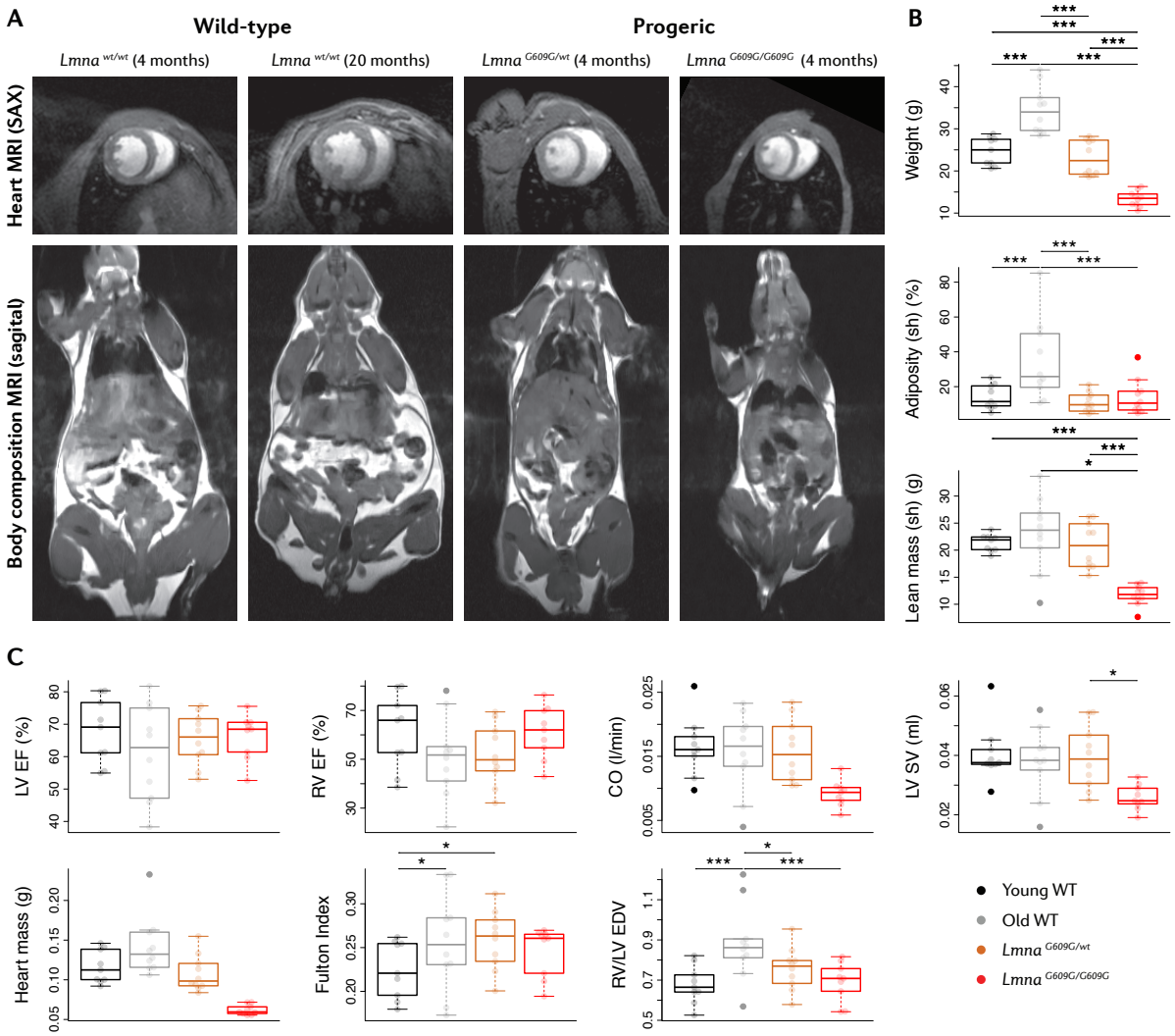

Figure 8: Altered cardiac function and body composition in progeric and old mice
MRI of 4-month-old $Lmna^{G609G/G609G}$ and $Lmna^{G609G/wt}$ progeric mice compared to age-matched and 20-month-old wild-type animals (n = 10 per group). A) Representative images of the heart ventricles in SAX view (blood in white) and sagital whole body cross sections (fat in white). B) NMR spectral analysis of body composition. C) Cardiac function parameters derived from MRI. Body weight was considered as a covariate in the statistical analysis of lean mass, CO, SV and heart mass. * P<0.05, ** P<0.01, *** P<0.001.

statistical model (Fig. 8C). In a different regard, old mice have an increased Fulton index and RV to LV EDV ratio in relation to young mice, as well as a modest non-significant reduction of the RV EF, which evidences their enlarged RV (Fig. 8C).

In order to identify metabolic anomalies in the normal and premature aging models, we subjected mice to an array of biochemical serum analysis and to metabolic tolerance tests (Fig. 9). $Lmna^{G609G/G609G}$ progeric mice are hypoglycemic in both fasting (GTT) and non-fasting (ITT) conditions, and show increased glucose tolerance during an intra-peritoneal GTT (Fig. 9A). $Lmna^{G609G/wt}$ and old animals also show reduced glucose levels in non-fasting conditions in

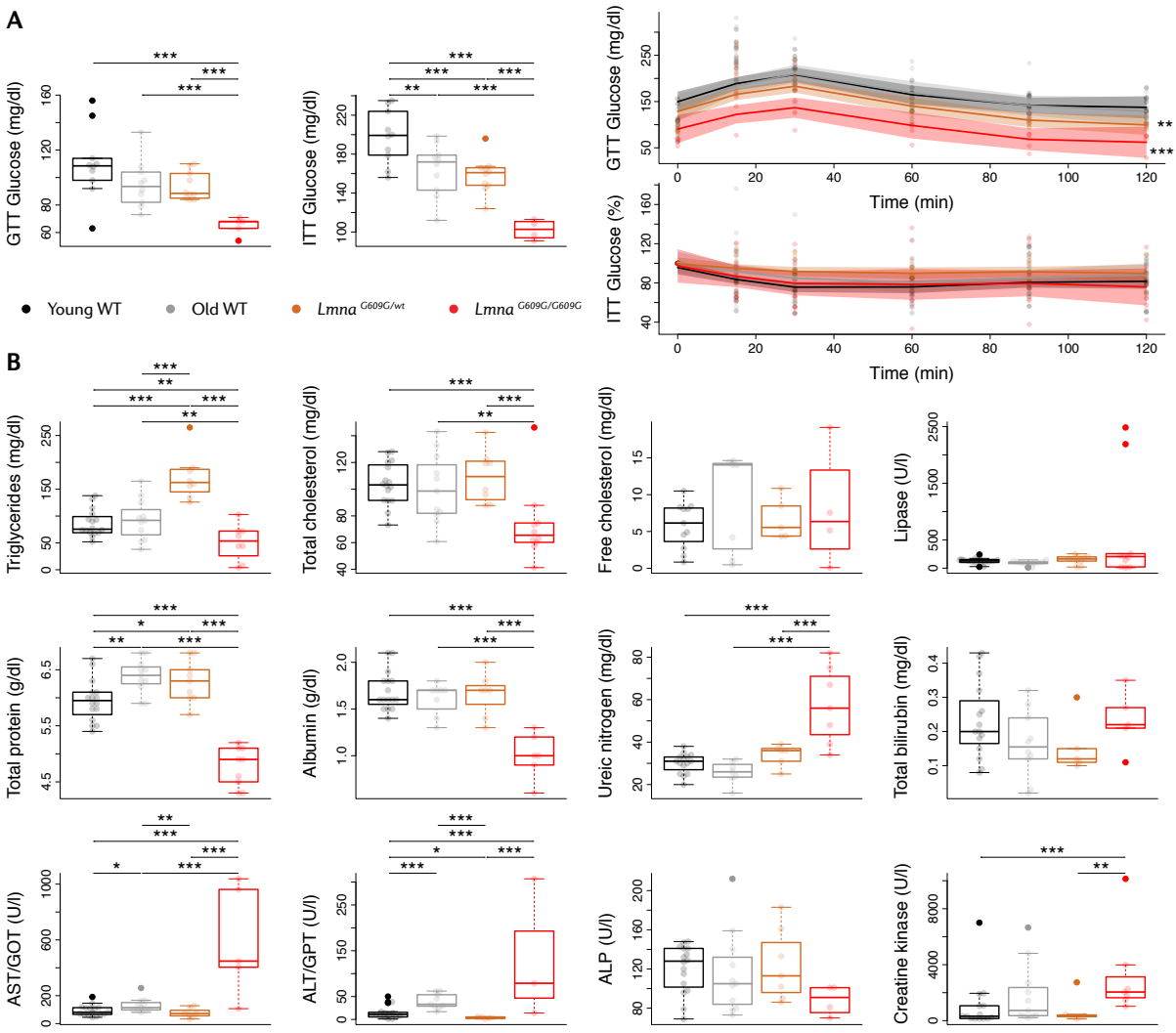

Figure 9: Metabolic systemic alterations in progeric and old mice
A) GTT and ITT of 4-month-old *Lmna*$^{G609G/G609G}$ (n = 5) and *Lmna*$^{G609G/wt}$ progeric mice (n = 10) compared to age-matched (n = 10) and 20-month-old wild-type animals (n = 10). Glucose levels are represented at time 0 after overnight fasting (2 h for the ITT) and during the course of the experiment. B) Biochemical analysis of serum metabolical parameters (n = 10-16 per group). ALP: alkaline phosphatase, AST: aspartate transaminase, GOT: oxaloacetic transaminase, ALT: alanine transaminase, GPT: glutamate pyruvate transaminase. * P<0.05, ** P<0.01, *** P<0.001.

relation to young wild-type mice, and the former present increased glucose tolerance during the GTT (Fig. 9A). None of the groups manifested insulin intolerance during an ITT (Fig. 9A).

The biochemical analysis revealed extensive alterations in the homozygous knock-in mice: reduced levels of triglycerides, total cholesterol, total protein and albumin, as well as increased levels of ureic nitrogen, transaminases and creatine kinase (Fig. 9B). Bilirubin and alkaline phosphatase levels appear normal, therefore suggesting these abnormalities are not related to liver damage but to cachexia (Fig. 8B). Surprisingly, triglyceride levels in heterozygous progeric mice are significantly higher than in the other groups; and old mice present elevated levels of the transaminases (Fig. 9B).

Collectively, these results show that both progeric *Lmna*^{G609G} and old wild-type mice develop a conspicuous cardiometabolic disease characterized by bradycardia, cardiac repolarization abnormalities, preserved systolic function, hypoglycemia and altered body composition. Furthermore, while old mice become overweight and display enlarged RV, young *Lmna*$^{G609G/wt}$ mice show very mild alterations and *Lmna*$^{G609G/G609G}$ animals present profound abnormalities and develop hypolipidemia and cachexia.

4.2 Cardiometabolic Alterations in the Aging Heart Proteome

We performed cardiac high-throughput proteomics combining FASILOX with 8-plex iTRAQ (Wiśniewski et al., 2009; Martínez-Acedo et al., 2012) with the purpose of unraveling the molecular mechanisms underlying cardiometabolic disease in progeria and aging. This pertains to the second objective of the present Doctoral Thesis: To identify proteomic changes in the mouse heart, common or specific to premature and normal aging.

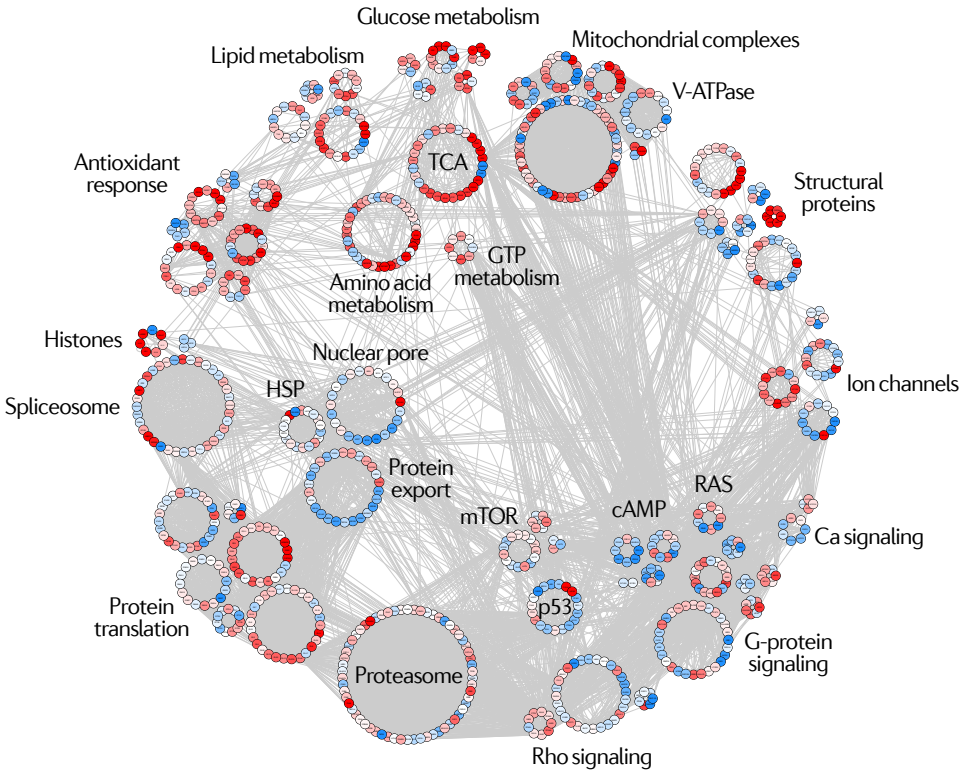

Figure 10: Systems biology overview of the aging heart proteome
Proteomic landscape showing the main categories altered in progeric and old mice. Each dot represents a protein, which is colored according to its mean abundance in the aging proteome. Blue: decreased abundance, red: increased abundance, white: no change.

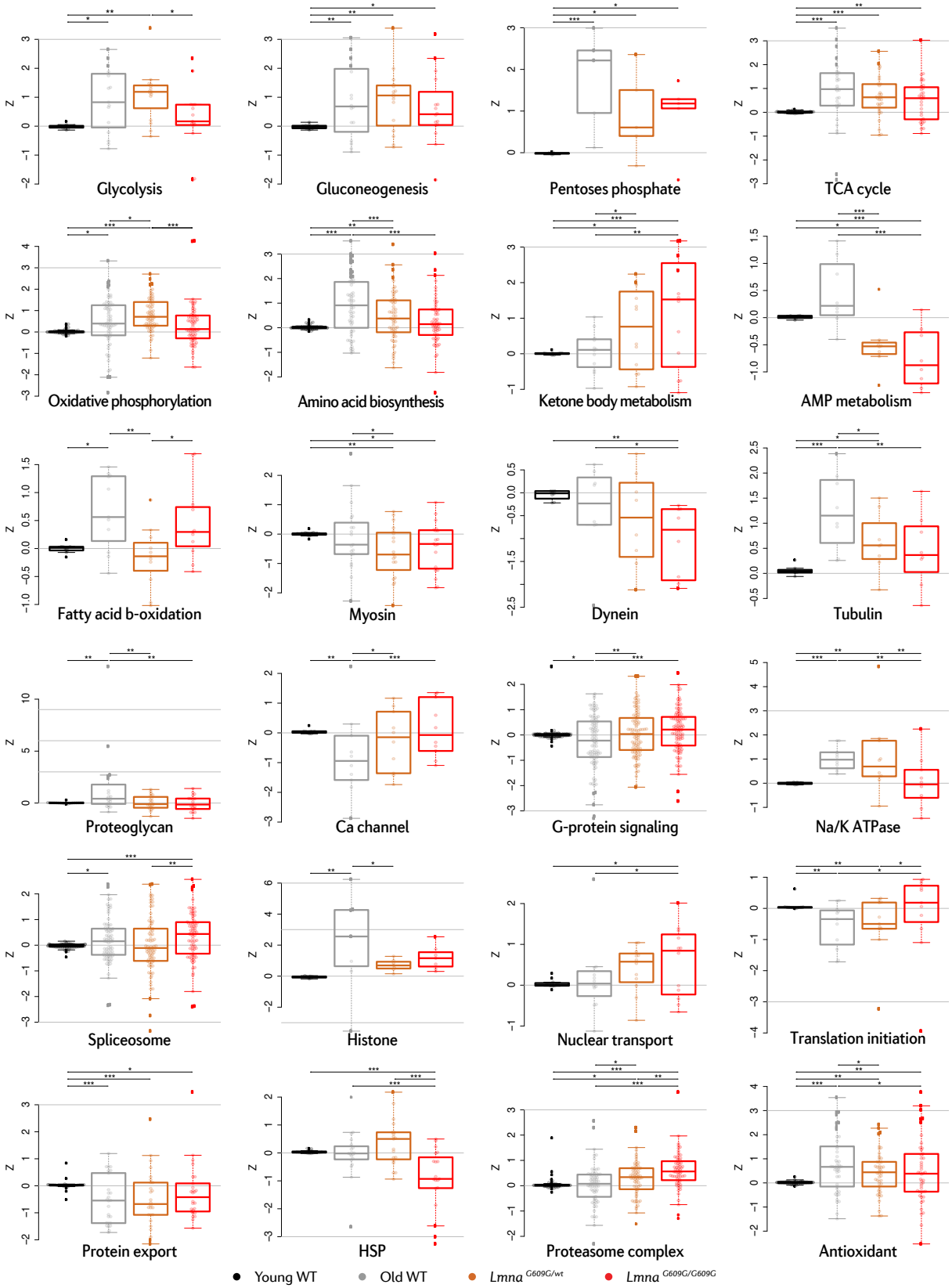

Figure 11: Main altered pathways in the aging heart proteome
Representative pathways with significant changes extracted from the systems biology analysis. Each dot represents a protein in the pathway. Z (Z score) indicates protein abundance compared to 4-month-old wild-type mice. HSP: Heat shock proteins. * P<0.05, ** P<0.01, *** P<0.001.

Following the design explained in the previous section, we analyzed changes in protein abundance in hearts from 4-month-old $Lmna^{G609G/G609G}$ and $Lmna^{G609G/wt}$ progeric mice compared to age-matched and 20-month-old wild-type animals. Due to the elevated cost of this technology, we performed the experiment only in male mice (n = 16), which led to the identification and quantitation of roughly 5000 proteins with < 1% FDR.

Systems biology computational analyses using the SanXoT software package (Trevisan-Herraz et al., 2018) revealed changes in pathways related to energy metabolism, cellular structure and signaling, gene expression and proteostasis (Fig. 10). Energy metabolism alterations are common to old, heterozygous and (to a less extent) homozygous knock-in mice (Fig. 11). These involve increased glycolysis, gluconeogenesis, pentoses phosphate synthesis, tricarboxylic acid cycle and oxidative phosphorylation. Other metabolic abnormalities comprise increased ketone body metabolism and decreased AMP metabolism in both $Lmna^{G609G}$ groups, increased amino acid biosynthesis in $Lmna^{G609G/wt}$ and old mice, and elevated fatty acid β -oxidation in $Lmna^{G609G/G609G}$ and old animals (Fig. 11).

Motor and structural protein groups are also affected in the aging heart (Fig. 11). Hence, myosins and dyneins have decreased expression in progeric knock-in mice, whereas β tubulins and proteoglycans are upregulated in old animals. Signaling pathways related to cardiac contraction, such as calcium and G-protein signaling are downregulated in old mice, while sodium and potassium channels are upregulated in both old and $Lmna^{G609G/wt}$ mice. These alterations suggest there is a remodeling of cardiac tissue in these aging models, although cardiac function seems preserved (section 4.1).

Regarding gene expression regulation during aging, spliceosome components, histones and proteins involved in nuclear export exhibit increased expression (Fig. 11). The first is common to both old and $Lmna^{G609G/G609G}$ mice, while the second seems to be specific of old animals and the third, of homozygous progeric mice. As for protein homeostasis, a reduction is seen in protein translation initiation in $Lmna^{G609G/wt}$ and old mice, in protein export in all aging groups and in heat shock proteins specifically in the $Lmna^{G609G/G609G}$ model, while proteasome complex abundance is increased in both homozygous and heterozygous animals. It is noteworthy that a compensatory antioxidant response is activated in all groups, involving the glutathione and peroxiredoxin systems (Fig. 11).

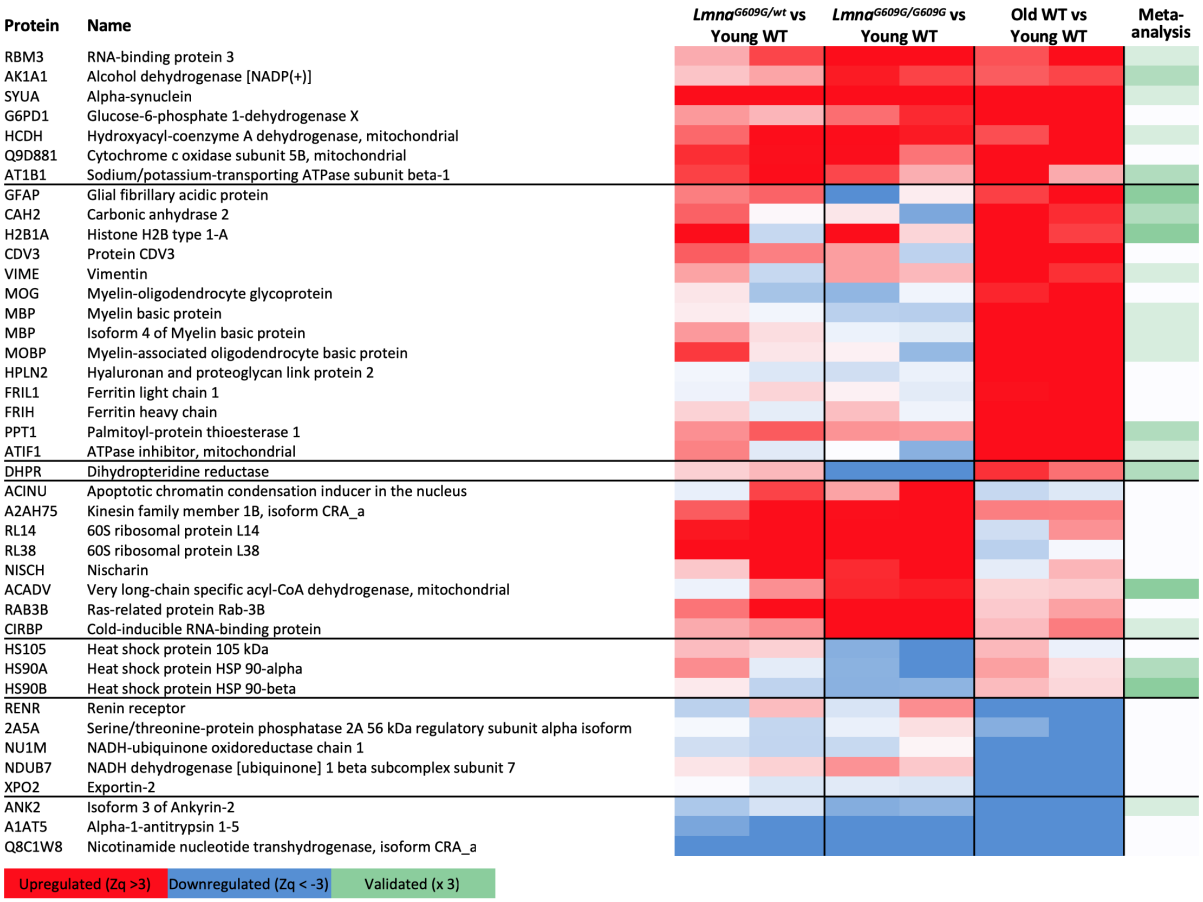

Figure 12: Changes in protein abundance in the aging heart proteome
Panel of curated protein candidates with altered expression in premature and/or normal aging models. Zq (Z score) indicates protein abundance compared to 4-month-old wild-type mice. A meta-analysis was performed to validate the results with data sets of previous aging studies (section 3.4). Cell color intensity is maximal when $|Zq| > 3$ or when validated in at least 3 data sets.

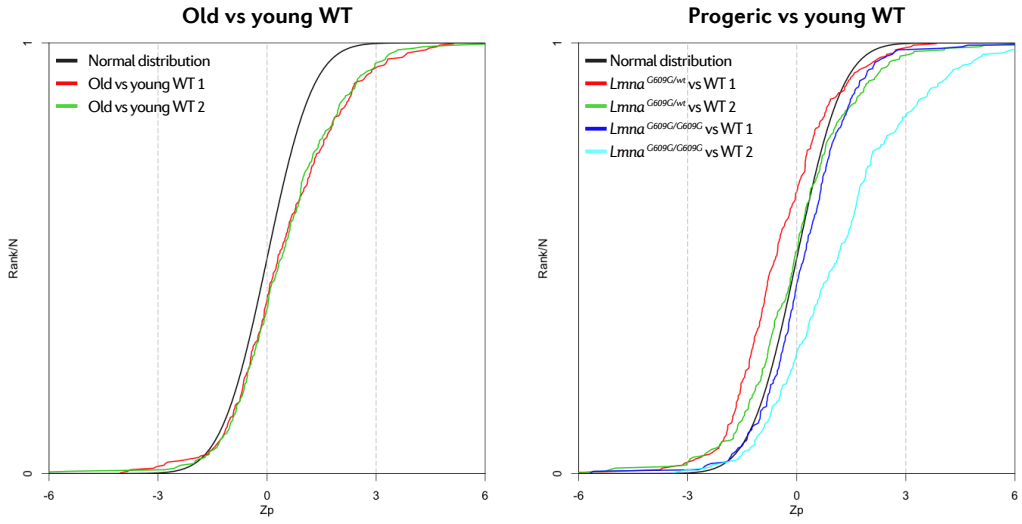

Figure 13: Increased oxidation in the aging heart proteome
Sigmoid plots showing the abundance of oxidized cysteine peptides. Zp (Z score) indicates peptide abundance compared to 4-month-old wild-type mice.

We curated a list of candidate proteins with altered expression in $Lmna^{G609G/wt}$, $Lmna^{G609G/G609G}$ and old mice (Fig. 12). Proteins with the higher changes in abundance in both progeria and normal aging are related to energy metabolism. Among the proteins with specific altered abundance in old mice, there are several myelin-related proteins, ferritins and histones and components of the mitochondrial complexes. As for those altered specifically in progeria, the most prominent are the cold and heat shock proteins, which suggest these mice may display temperature regulation abnormalities.

Finally, global oxidation of peptides bearing glycine residues is increased in both homozygous progeric mice and in old mice, being higher in the latter (Fig. 13). Oxidized peptides correspond mainly to mitochondrial and structural proteins, supporting the observations made at the category and protein levels. All these results ratify the presence of cardiometabolic disease in both premature and normal aging mouse models.

4.3 Energy Imbalance and Impaired Temperature Regulation in Progeria

Given the observed alterations in energy metabolism and cold shock proteins (Fig. 11), we sought to study temperature regulation and energy balance in progeria and aging. We thus measured body temperature of 4-month-old *Lmna*$^{G609G/G609G}$ and *Lmna*$^{G609G/wt}$ progeric mice compared to age-matched and 20-month-old wild-type animals. Mice were individually placed in metabolic

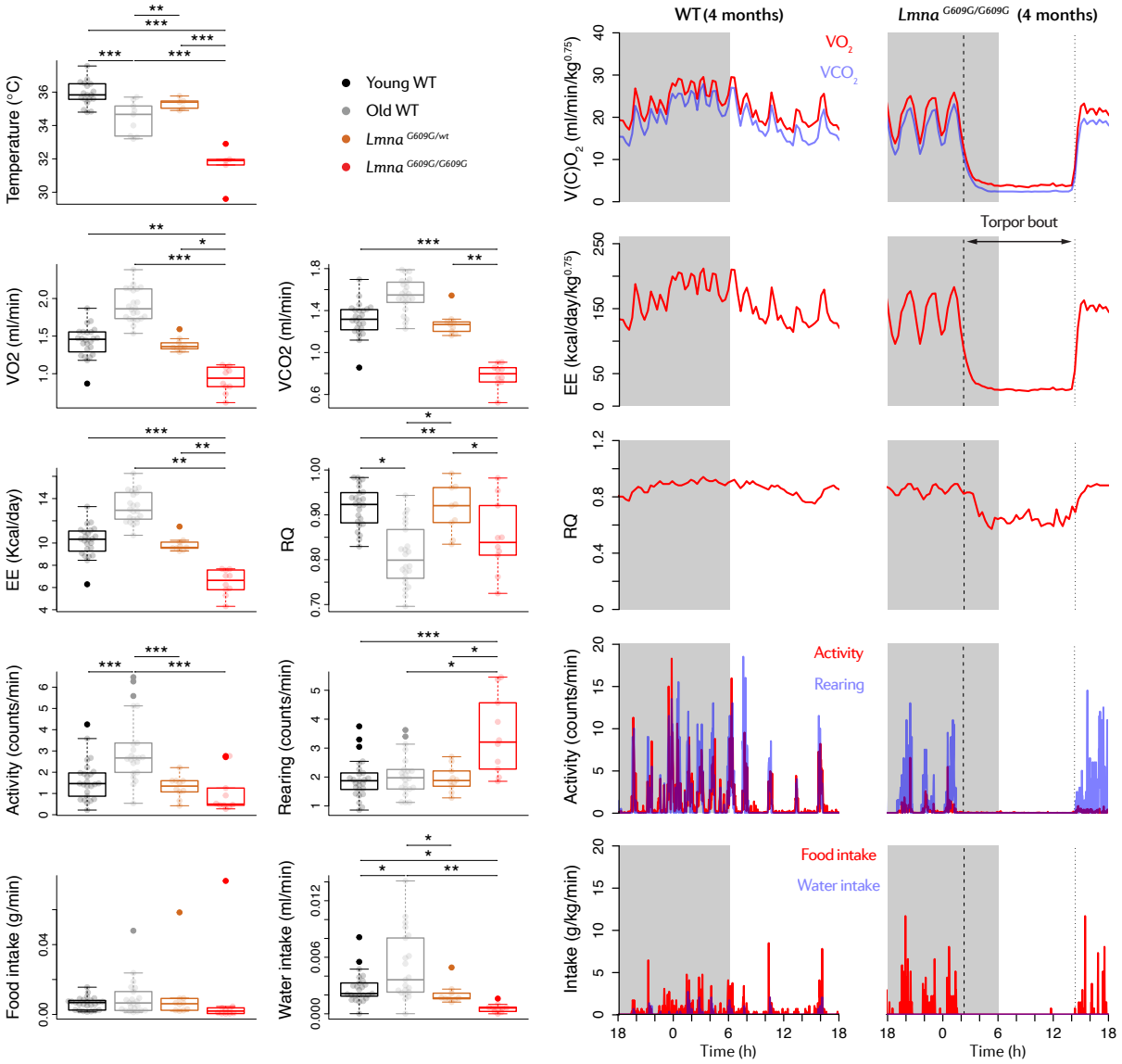

Figure 14: Hypothermia and altered EE in progeric and old mice
Body temperature measurement and metabolic chamber monitorization of 4-month-old *Lmna*$^{G609G/G609G}$ (n = 10) and *Lmna*$^{G609G/wt}$ progeric mice (n = 10) compared to age-matched (n = 25) and 20-month-old wild-type animals (n = 22). Body weight was included as a covariate in the statistical analysis of oxygen consumption (VO_2), CO_2 production (VCO_2), EE and food and water intake. * P<0.05, ** P<0.01, *** P<0.001.

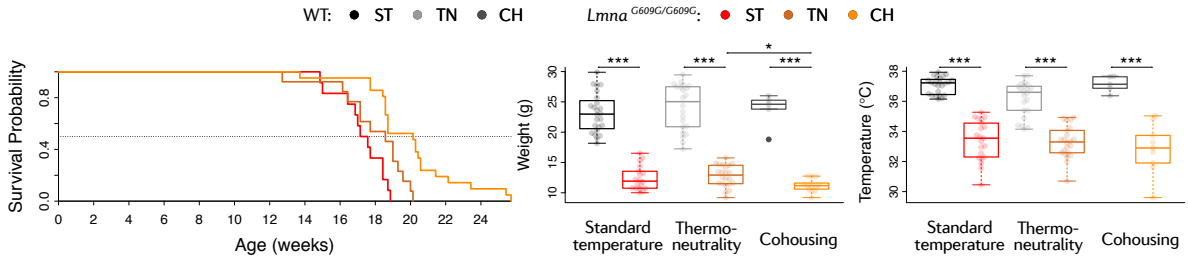

Figure 15: Higher environmental temperature prolongs lifespan in progeric mice
Longitudinal study of *Lmna*$^{G609G/G609G}$ and age-matched wild-type controls in standard temperature (ST, 22 °C and single-genotype housing) (n_{WT} = 24 & n_{G609G} = 21), thermoneutrality (TN, 28 °C and single-genotype housing) (n_{WT} = n_{G609G} = 22) or cohousing (CH, 22 °C and joint-genotype housing) (n_{WT} = 5 & n_{G609G} = 41). * P<0.05, ** P<0.01, *** P<0.001.

chambers for oximetry, activity and intake monitorization during 36 h. Compared with young wild-type and heterozygous knock-in animals, old wild-type and (more eminently) homozygous progeric mice are hypothermic and present a lower RQ (Fig. 14).

Furthermore, oxygen consumption, carbon dioxide production and EE is reduced in *Lmna*$^{G609G/G609G}$ animals, even when accounting for body weight differences by including it as a covariate in the statistical model (Fig. 14). Additionally, old wild-type mice showed increased ambulation (physical activity) and water intake, whereas homozygous progeric mice displayed increased rearing but decreased water intake as compared to controls. There were no significant differences in food intake between the different groups (Fig. 14).

Surprisingly, besides observing circadian oscillation between the active dark phase and the resting light phase (mice are nocturnal animals), we found that *Lmna*$^{G609G/G609G}$ mice enter daily torpor bouts that last several hours (Fig. 14). During these periods, basal metabolic rate decreases up to 90 % in order to preserve energy in small mammals with compromised metabolism, when nutrients are scarce or when environmental temperature is too low (Brown and Staples, 2010; Oelkrug et al., 2011).

In mice housed at typical laboratory temperatures (20 °C – 22 °C), about 30% of resting EE is devoted to thermoregulation, and thus variations in BAT activity can have profound effects on systemic energy balance (Cannon and Nedergaard, 2010). In order to alleviate this expense, we resorted to either house *Lmna*$^{G609G/G609G}$ mice at a temperature close to their thermoneutral zone (28 °C) or to cohouse these animals with age-matched wild-type mice, so that progeric mice would share body heat with healthy normothermic individuals. As a result, life expectancy was increased in both conditions in relation to progeric mice housed at standard temperature and single-genotype housing (Fig. 15). However, body temperature and weight were not rescued,

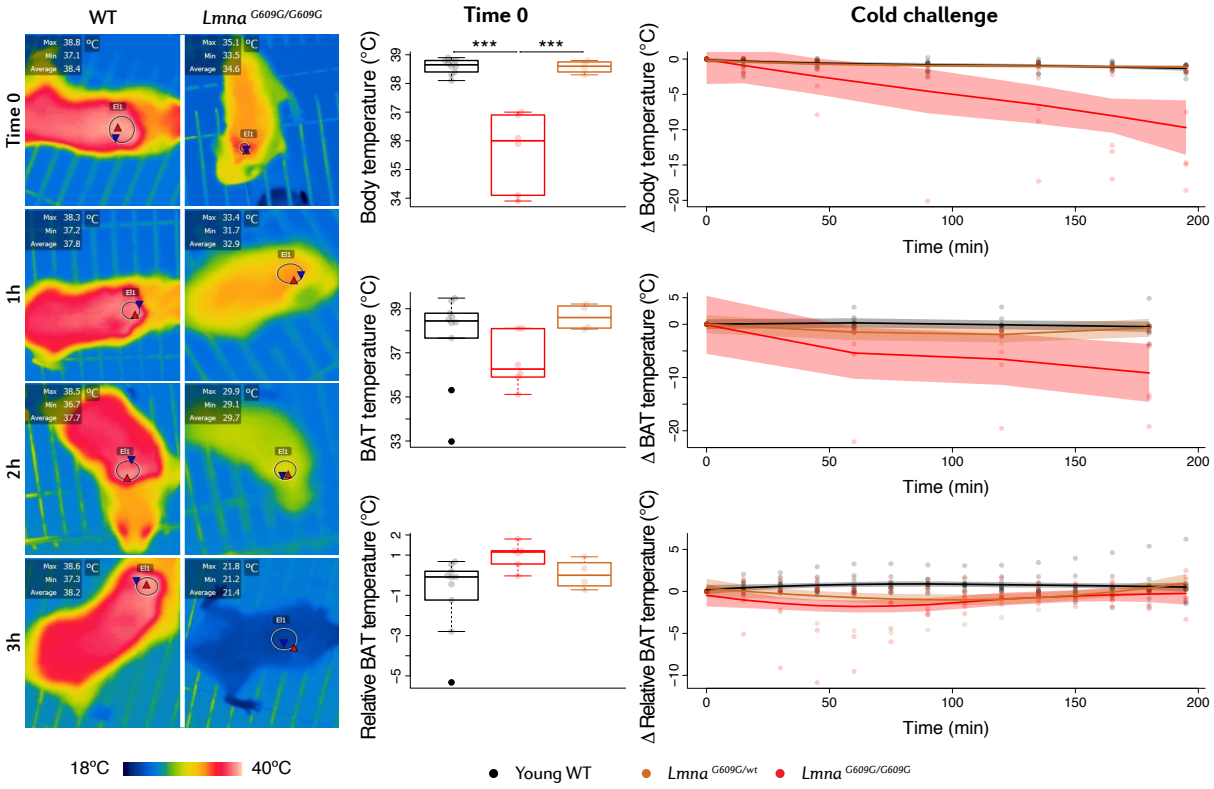

Figure 16: Altered temperature regulation in *Lmna*$^{G609G/G609G}$ mice upon cold challenge
Homozygous (n = 6) and heterozygous *Lmna*^{G609G} mice (n = 4), and age-matched wild-type controls (n = 10) where exposed to an acute cold challenge (4 °C) for 3 h. Body temperature was measured with a rectal probe, and BAT temperature was determined by thermography. Relative BAT temperature was calculated by spline interpolation as the difference between BAT and body temperature. * P<0.05, ** P<0.01, *** P<0.001.

indicating that ambient temperature only accounts for a small part of the energy imbalance observed in these animals.

To assess whether progeric mice have compromised thermoregulation or have simply adapted to minimize EE on temperature maintenance we subjected *Lmna*^{G609G} mice and age-matched wild-type controls to acute cold stress (4 °C, 3 h) (Fig. 16). Initial body temperature was lower in homozygous progeric mice in relation to wild-type and heterozygous animals, while no significant differences were observed in interscapular BAT temperature, the major organ involved in nonshivering thermogenesis. Relative BAT temperature was modestly elevated in *Lmna*$^{G609G/G609G}$ mice, suggesting a basal activation of the organ. During the course of the experiment, body and BAT and temperatures decreased in all groups, but at a faster rate in *Lmna*$^{G609G/G609G}$ mice. Conversely, relative BAT temperature increased with time in all groups, although at a slower rate in homozygous progeric mice. Taken together, these results indicate that BAT thermogenesis is active in progeric mice, but insufficient to overcome heat loss during cold exposure.

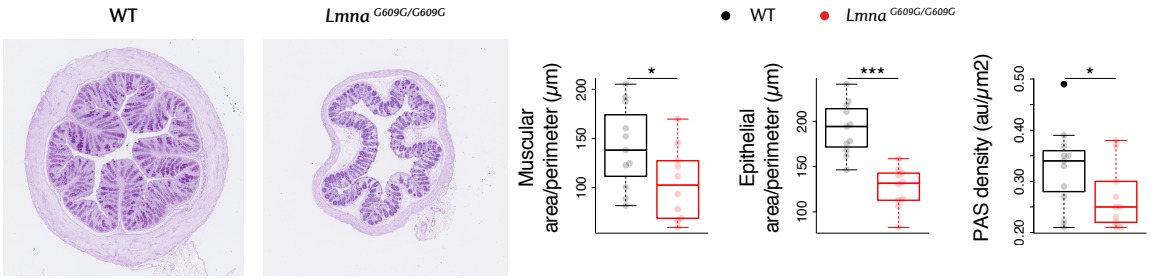

Figure 17: Reduced intestinal absorption in *Lmna*$^{G609G/G609G}$ mice
Histopathological analysis of homozygous *Lmna*^{G609G} mice and age-matched wild-type controls (n = 10-11 per group). PAS staining of the large intestine. * P<0.05, ** P<0.01, *** P<0.001.

Since progeric mice become cachectic (Fig. 8), their inability to thermoregulate may derive from low energy availability. Food intake seems normal (Fig. 14), but nutrient assimilation may be impaired. To test this hypothesis, we performed a histopathological analysis of large intestines and found that this organ has thinner muscular and mucosa layers, as well as a reduced amount of secretory goblet cells in *Lmna*$^{G609G/G609G}$ compared with controls (Fig. 17). These observations are consistent with intestinal malabsorption, which could lead to malnutrition and accelerate disease progression.

Aside from the reduced energy availability, thermoregulation in progeric mice may also be a consequence of impaired non-shivering thermogenesis. Hence, we examined the interscapular BAT and found no significant differences anatomical and histological appearance when comparing *Lmna*$^{G609G/G609G}$ mice and age-matched wild-type controls (Fig. 18). We next assessed the mRNA expression levels of different thermogenic, adipogenic and inflammatory genes. At 4 months of age, progeric mice show low levels of *Ucp1*, *Pgc1a*, *Pparg2*, *Cidea*, *Cebpb*, *Cycs*, *Cox5*, *Prdm16* and an increase in *Prdm3* and *Tnfa* (Fig. 18). Together, these results indicate that progeric mice have impaired BAT thermogenesis.

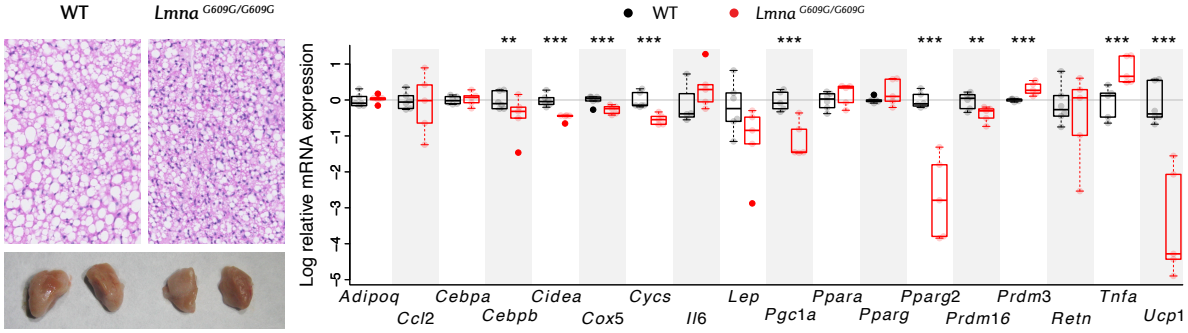

Figure 18: BAT thermogenesis is impaired in *Lmna*$^{G609G/G609G}$ mice
BAT anatomical, histopathological and RT-qPCR analysis of homozygous *Lmna*^{G609G} mice and age-matched wild-type controls (n = 5-6). * P<0.05, ** P<0.01, *** P<0.001.

4.4 Bradycardia is Promoted by Heart-Extrinsic Mechanisms in Progeric Mice

Energy imbalance and impaired thermogenesis (section 4.3) are likely to contribute systemically to the cardiometabolic disease present in progeric mice. Thus, we also sought to investigate the interplay between local and systemic mechanisms that promote cardiometabolic disease during aging. This constitutes the third objective of the present Doctoral Thesis.

We decided to focus first on the study of heart-intrinsic mechanisms. For this, we generated mice that express progerin specifically in the heart, crossing the *Lmna*^{LCS} strain with mice bearing a cardiac-specific Cre recombinase (*αMHC-Cre*). *Lmna*$^{LCS/LCS}$ mice carry a conditional HGPS allele with a floxed cassette that prevents the formation of prelamin A but allows the expression of lamin C (Fig. 2). These mice are deficient for lamin A but show no overt progeric phenotype (Osorio et al., 2011). Nevertheless, it has been reported that these animals outlive wild-type mice and have a tendency towards overweight (López-Mejía et al., 2014). Therefore, we first conducted a study that verified these observations and revealed no cardiac abnormalities in the *Lmna*^{LCS} strain (Fig. 19).

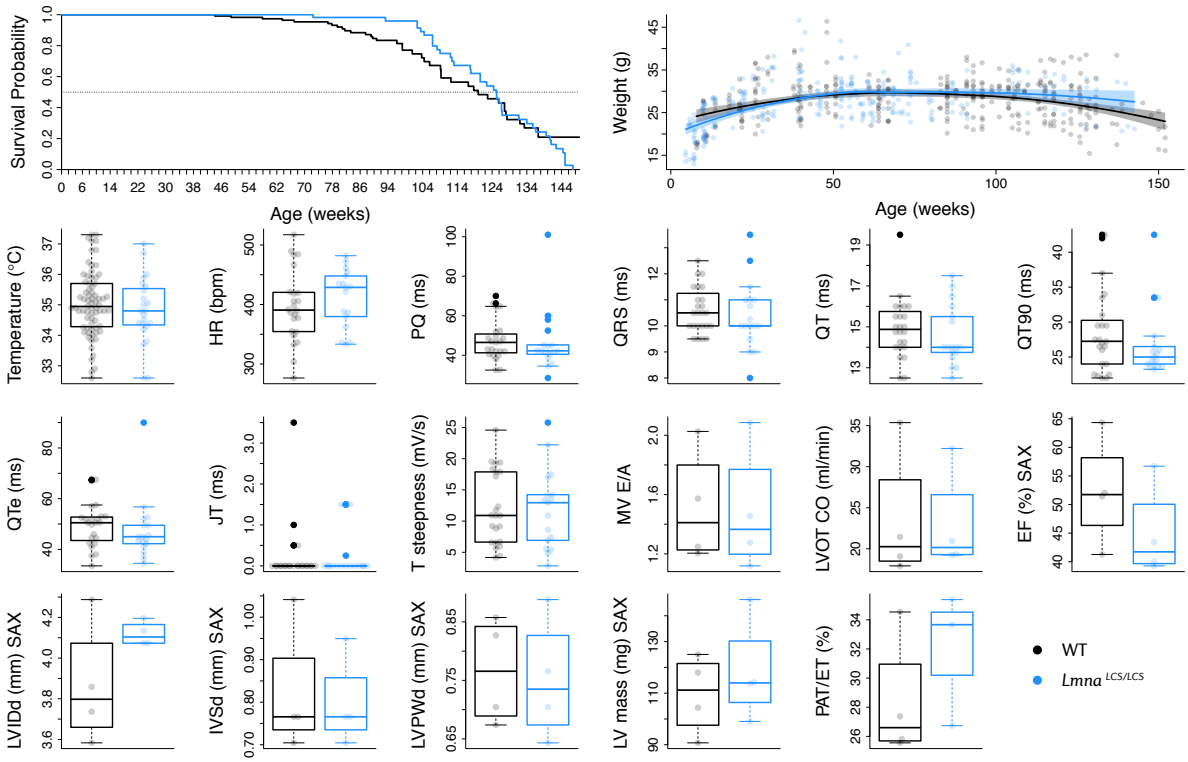

Figure 19: *Lmna*$^{LCS/LCS}$ mice show no overt progeric phenotype
Characterization of *Lmna*$^{LCS/LCS}$ mice and wild-type controls. Survival analysis (n = 134-151), weight and temperature measurement (n = 74-82), ECG experiments (n = 17-24) and echocardiographic study (n = 4 per group). * P<0.05, ** P<0.01, *** P<0.001.

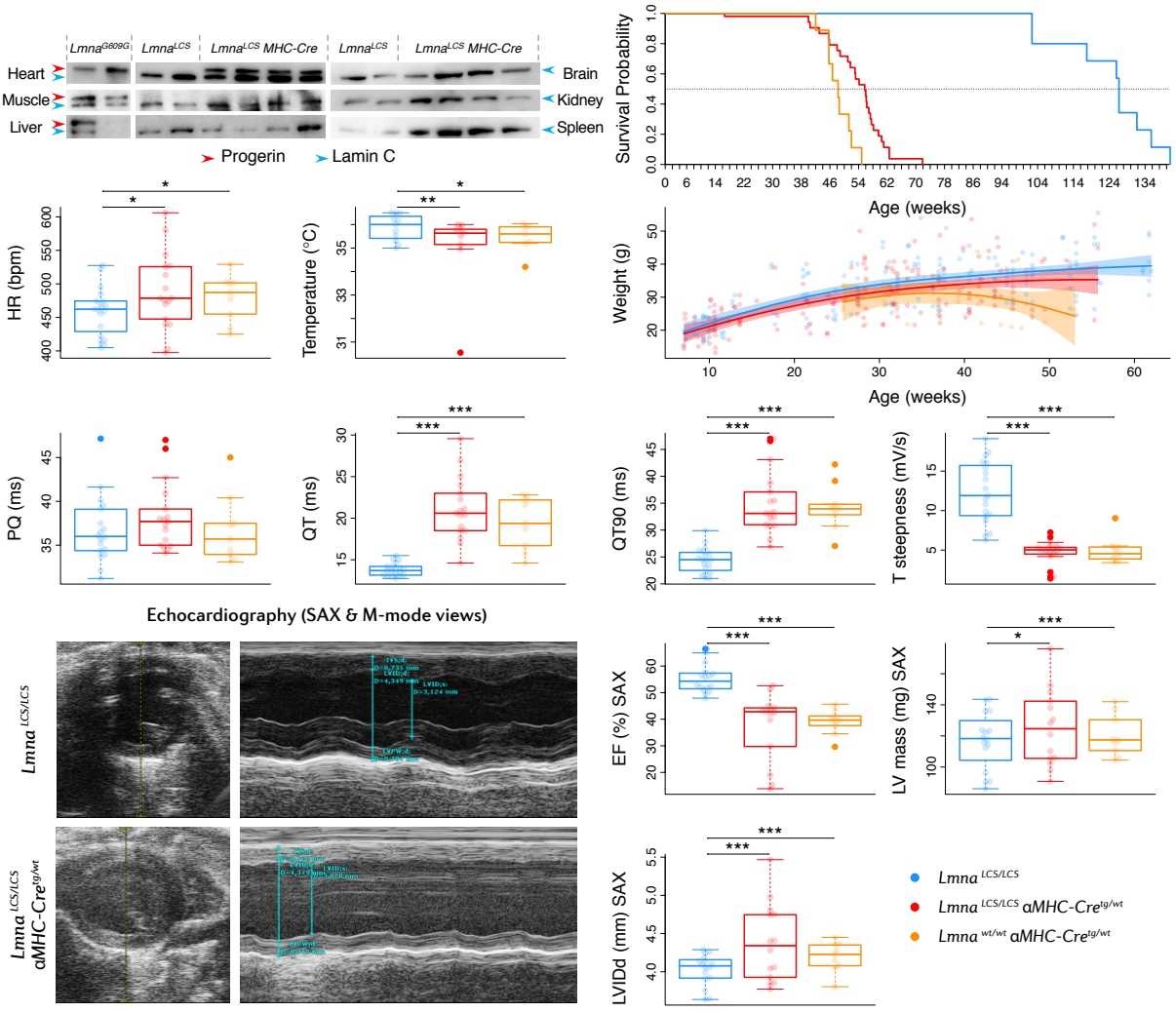

Figure 20: *Lmna*$^{LCS/LCS}$ *αMHC-Cre* mice develop dilated cardiomyopathy
Western-blot to check progerin expression in heart, brain, muscle, kidney, liver and spleen. Lamin C (lower band) and progerin (upper band) were detected with a monoclonal antibody against lamin A/C. Longitudinal study of *Lmna*$^{LCS/LCS}$ *αMHC-Cre*$^{tg/wt}$, *Lmna*$^{wt/wt}$ *αMHC-Cre*$^{tg/wt}$ and *Lmna*$^{LCS/LCS}$ controls involving survival, weight and temperature examination (n = 52, 9 & 55, respectively), ECG (n = 18, 9 & 19, respectively, in 10 time points) and echocardiography (n = 14, 9 & 16, respectively, in 6 time points). * P<0.05, ** P<0.01, *** P<0.001.

Lmna$^{LCS/LCS}$ *αMHC-Cre*$^{tg/wt}$ mice constitutively express a Cre recombinase under the alpha myosin heavy chain promoter, which allows for cardiomyocyte-specific expression of progerin. After verifying by Western-blot that progerin was indeed expressed only in cardiac tissue (Fig. 20), we conducted a longitudinal study to characterize possible cardiac alterations in these animals. To our surprise, echo and electrocardiographic analyses revealed that *Lmna*$^{LCS/LCS}$ *αMHC-Cre*$^{tg/wt}$ mice develop a very conspicuous dilated cardiomyopathy, evidenced by ventricular enlargement (increased LVIDd), QT prolongation, T-wave flattening and reduced EF and CO in relation to *Lmna*$^{LCS/LCS}$ controls (Fig. 20).

Furthermore, cardiac-specific progerin-expressing mice die prematurely at a median age of 12 months, probably as a result of heart failure derived from dilated cardiomyopathy (Fig. 20). Nonetheless, control $Lmna^{wt/wt}$ $\alpha MHC\text{-}Cre^{tg/wt}$ mice, which express Cre but no progerin, also manifest this disease and die at 12 months of age. This leads to the conclusion that the cardiac dilation in these animals is progerin-independent and linked to high and constitutive Cre expression (Buerger et al., 2006; Davis et al., 2012).

Accordingly, this model is not appropriate for the intended research, given that any effect that progerin may exert in the heart is obscured by the toxicity driven by long-term expression (or activity) of the Cre recombinase. However, it is noteworthy that HR appears increased in $Lmna^{LCS/LCS}$ $\alpha MHC\text{-}Cre^{tg/wt}$ mice (Fig. 20), which suggests that bradycardia in progeric mice is caused by heart-extrinsic mechanisms.

In order to explore this possibility, we opted for a thorough cardiometabolic characterization of aged $Lmna^{G609G/wt}$ mice. Heterozygous progeric mice show no significant cardiometabolic abnormalities nor thermoregulaton impairment at 4 months of age (sections 4.1 and 4.3), but already present profound proteomic anomalies in multiple pathways (section 4.2). As they age, these animals develop many of the alterations observed in homozygous progeric mice and die at approximately 12 months of age (Osorio et al., 2011; Villa-Bellosta et al., 2013). As the disease progresses at a slower rate in heterozygous mice, we would expect some phenotypical differences in relation to homozygous knock-in animals. For instance, $Lmna^{G609G/wt}$ mice grow normally until adulthood (which allows for experiments where body size is limiting) and are fertile (crucial for colony maintenance).

To elucidate the cardiometabolic phenotype of old $Lmna^{G609G/wt}$ mice, we resorted to ECG and echocardiography and found similar alterations as in 5-month-old homozygous progeric mice (Fig. 7). Indeed, 12-month-old heterozygous knock-in animals display bradycardia as compared to 12-month-old wild-type mice, and exhibit prolonged QT, QT_{90}, JT gap and T-wave flattening (Fig. 21A). EF and TAPSE are preserved, suggesting normal systolic function in both LV and RV (respectively). Moreover, we found no evidence of diastolic dysfunction (evidenced by the MV E/A ratio) nor pulmonary hypertension (indirectly measured by PAT/ET) (Fig. 21B).

Metabolic chamber experiments on heterozygous mice of different ages and age-matched wild-type controls revealed no significant changes in gas exchange, EE, RQ or intake, although rearing is increased in progeric mice (Fig. 21C). Interestingly, old heterozygous knock-in mice become lipodystrophic (reduced weight) and hypothermic, resorting to daily torpor when approaching the

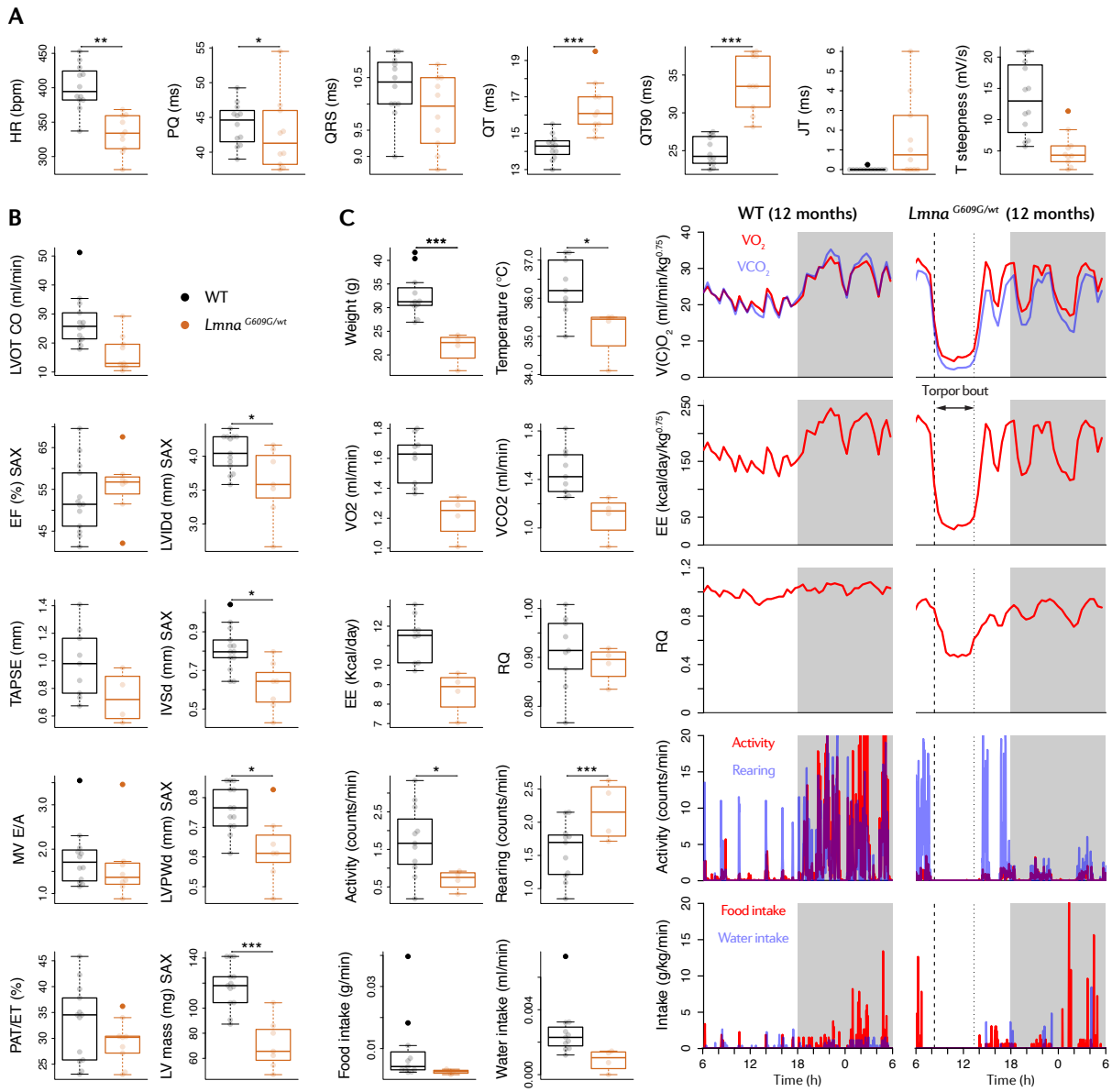

Figure 21: Cardiometabolic disease in old *Lmna*$^{G609G/wt}$ mice
Characterization of 12-month-old *Lmna*$^{G609G/wt}$ and age-matched wild-type mice. A) Electrocardiographic experiments (n = 10-12). B) echocardiographic studies (n = 9-13). C) Weight and temperature measurement, along with metabolic chamber experiments (n = 4-11). Body weight was included as a covariate in the statistical analysis of CO, VO_2, VCO_2, EE and food and water intake. * P<0.05, ** P<0.01, *** P<0.001.

life expectancy threshold (Fig. 21C). This confirms the thermoregulation impairment displayed by *Lmna*$^{G609G/G609G}$ mice (section 4.3).

The next step was to perform telemetric ECG experiments on conscious *Lmna*$^{G609G/wt}$ mice using implantable ECG transmitters that incorporate a thermometer. Circadian monitorization revealed bradycardia, hypothermia and torpor bouts in the progeric animals, which involved a 70-80% reduction in HR and a 10 °C drop in body temperature (Fig. 22A). Given the similarity

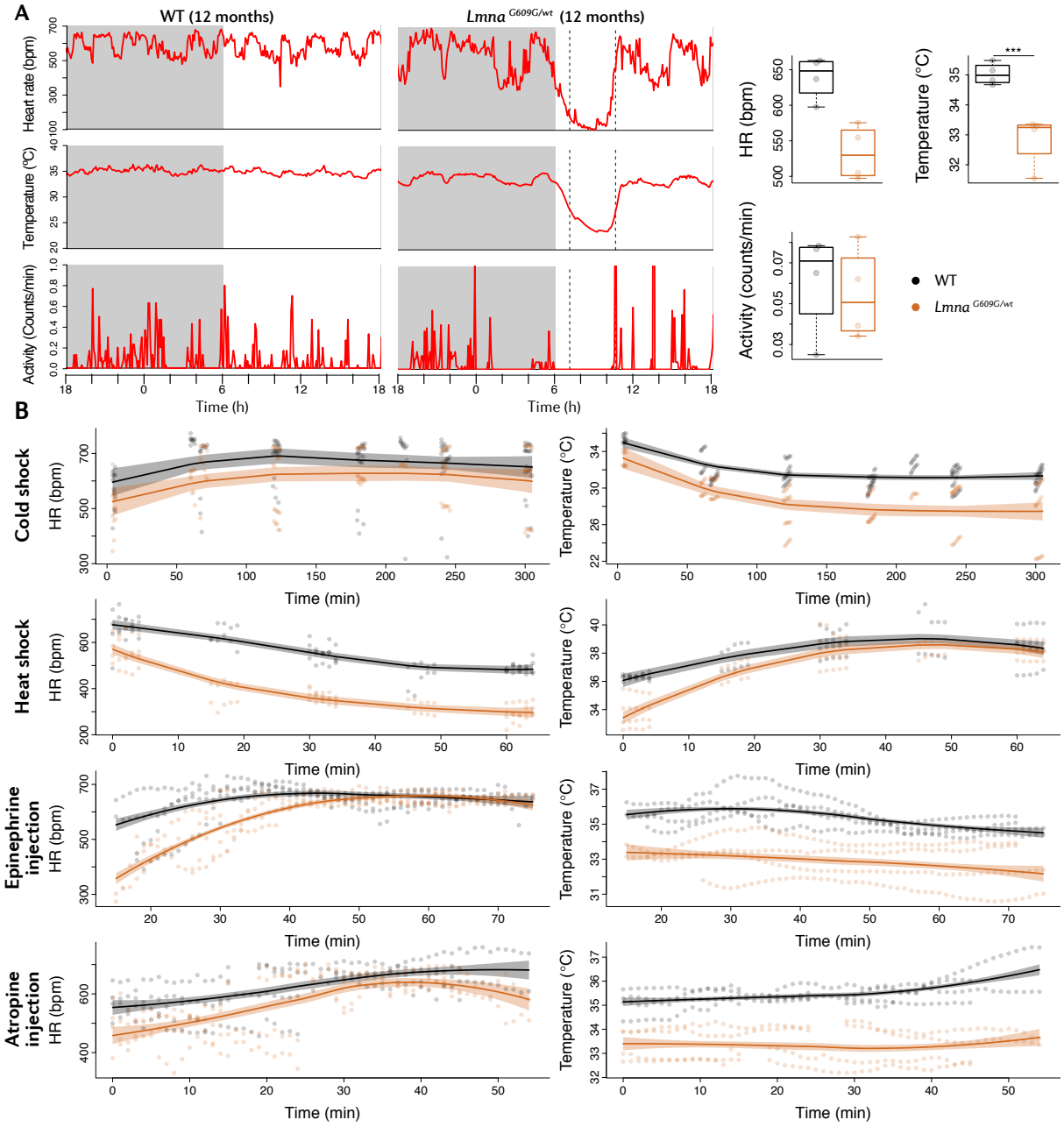

Figure 22: Bradycardia is related to hypothermia in progeric mice
Telemetric ECG study involving 12-month-old *Lmna*$^{G609G/wt}$ and age-matched wild-type mice (n = 4 per group). A) 60 h-circadian experiment. B) Tolerance to challenge tests including cold and heat shock, as well as response to epinephrine or atropine injection. * P<0.05, ** P<0.01, *** P<0.001.

between the HR and temperature curves, we studied the relation between these two parameters. Interestingly, when body temperature was included as a covariate in the statistical analysis, there were no significant differences in HR, whereas when HR was considered a factor, differences in body temperature prevailed. This supports the hypothesis that bradycardia is a consequence of hypothermia.

To ratify this, telemeter-implanted mice were subjected to a series of tolerance to challenge tests. During cold shock, the animals were placed at 4 °C for 5 h. As expected given the results

obtained for *Lmna*$^{G609G/G609G}$ mice (section 4.3), body temperature dropped with time in all groups, at a faster rate in progeric mice (Fig. 22B). Conversely, the activation of the shivering and non-shivering thermogenic systems cause HR to rise, abrogating the differences between progeric and wild-type animals. When mice were exposed to a 60 min heat shock at 40 °C, we observed a reversed situation: body temperature increased abrogating differences between genotypes and HR decreased, but at a similar rate in both groups (Fig. 22B). These results suggest that HR regulation is not impaired in progeria, as it responds normally to changes in ambient and body temperature.

Finally, to test HR regulation independently of body temperature, we challenged telemeter-implanted mice with either epinephrine, which activates the sympathetic nervous system, or atropine, a parasympathetic nervous system inhibitor. After the injections, both drugs raised the HR of progeric and wild-type mice abrogating the basal differences between both groups (Fig. 22B). Collectively, these results support that HR regulation is not impaired in progeria and that the observed bradycardia is a response to heart-extrinsic signals.

4.5 Lipodystrophy in Progeria is Mediated by Systemic Factors

WAT is a key regulator of energy balance in the organism, and WAT lipolysis is essential to maintain body temperature (Shin et al., 2017). For this reason, we next focused on the characterization of this tissue in progeric mice, to better understand the interplay between the local and systemic environments in age-related cardiometabolic disease.

At 2 months of age, *Lmna*$^{G609G/G609G}$ mice show normal adiposity compared to age-matched wild-type controls. Nevertheless, these animals develop lipodystrophy, losing most WAT with disease progression (Fig. 23). At the molecular level, an exhaustive mRNA expression analysis revealed profound alterations in genes of 4-month-old progeric animals (Fig. 23). Most adipogenic genes were downregulated, including *Cebpa*, *Fabp4* and *Pparg*, as well as genes related to thermogenic processes such as *Ucp1* or *Prdm16*. Adipokines as *Adipoq*, *Lep*, *Retn* and *Ccl2* were also downregulated in progeria, whereas *Il6* appeared upregulated. Mitochondria were also affected, since *Cycs* and *Cox5b* had reduced expression and *Pgc1a* was upregulated already in 2-month-old *Lmna*$^{G609G/G609G}$ animals (Fig. 23).

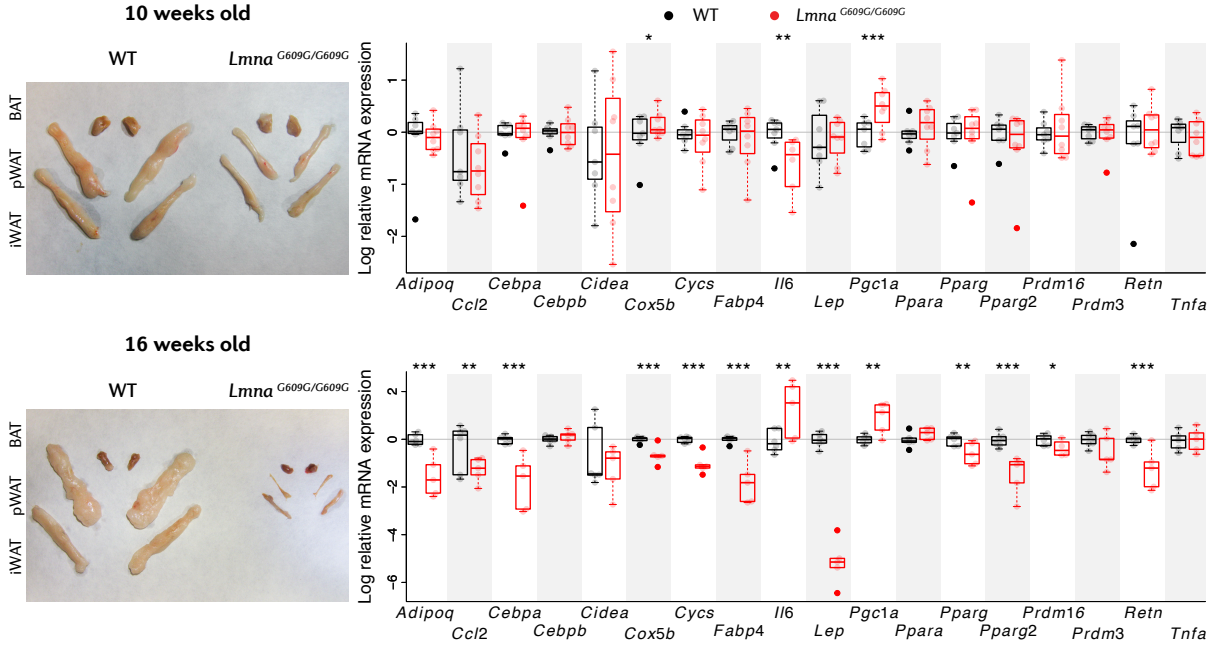

Figure 23: Lipodystrophy in *Lmna*$^{G609G/G609G}$ mice
Anatomical and molecular evaluation of lipodystrophy in progeric mice in relation to wild-type controls. mRNA expression analysis of pWAT is summarized in the table (red: upregulated in progeria, blue: downregulated). The mice used were 10 and 16 weeks old ($\tilde{2}$ and 4 months) (n = 5-8 per group and age).

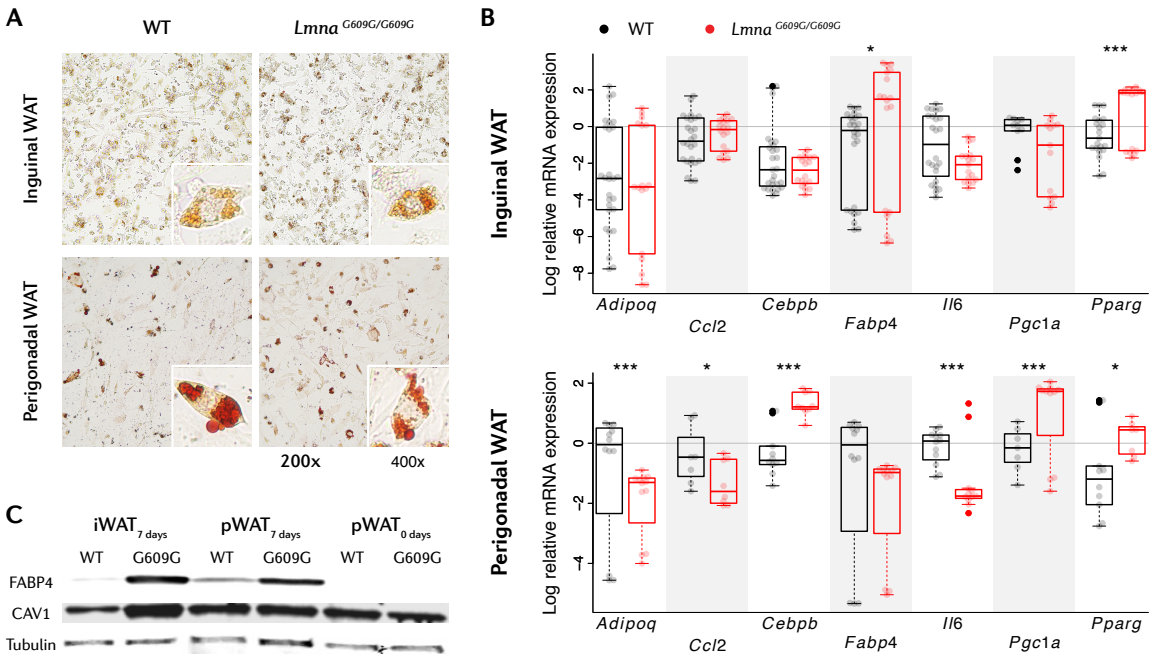

Figure 24: Altered *in vitro* adipogenesis in $Lmna^{G609G/G609G}$ mice
A) *In vitro* 7-day adipocyte differentiation protocol applied to pWAT or iWAT adipocyte progenitor cells from 3-month-old progeric mice and age-matched wild-type controls (n = 2-3 4-mouse pools). A) ORO staining of cultured cells. B) mRNA expression profile of adipogenic markers. C) Protein expression evaluation by Western-blot. CAV1: cavolin 1. * P<0.05, ** P<0.01, *** P<0.001.

Given the profound alterations found in progeric adipose tissue, we next sought to investigate cell-intrinsic mechanisms that could lead to impaired adipogenesis in progeria. *In vitro* differentiation studies with perigonadal and inguinal adipocyte progenitor cells from 3-month-old $Lmna^{G609G/G609G}$ mice revealed adipogenesis was indeed altered in these animals. Whereas no abnormalities were observed in the cultures by ORO staining (Fig. 24A), we found changes at the molecular level during the 7-day differentiation protocol by RT-qPCR and Western-blot. *Pparg* and *Fabp4* (and FABP4) were upregulated in progeric cells from both tissues, as well as *Cebpb* in pWAT and caveolin 1 in iWAT, suggesting differentiation was accelerated in $Lmna^{G609G/G609G}$ preadipocytes (Fig. 24B, C). *Adipoq*, *Ccl2* and *Il6* were downregulated in differentiating pWAT progeric cells, as observed in whole tissue (Fig. 23), and *Pgc1a* was consistently upregulated (Fig. 24B).

Following these experiments, to address the relevance of cell-intrinsic versus systemic mechanisms in progeria-related lipodystrophy, we generated mice that express progerin specifically in the adipose tissue by crossing $Lmna^{LCS/LCS}$ mice, which express lamin C but lack lamin A (Fig. 19), with $aP2\text{-}Cre^{tg/wt}$ mice. After corroborating by Western-blot that progerin expression was specific to iWAT and pWAT, as well as to BAT (Fig. 25A), we conducted a longitudinal study in a cohort including male and female mice. We found no significant differences in body weight and temperature between $Lmna^{LCS/LCS}$ $aP2\text{-}Cre^{tg/wt}$ mice and the $Lmna^{LCS/LCS}$ $aP2\text{-}Cre^{wt/wt}$

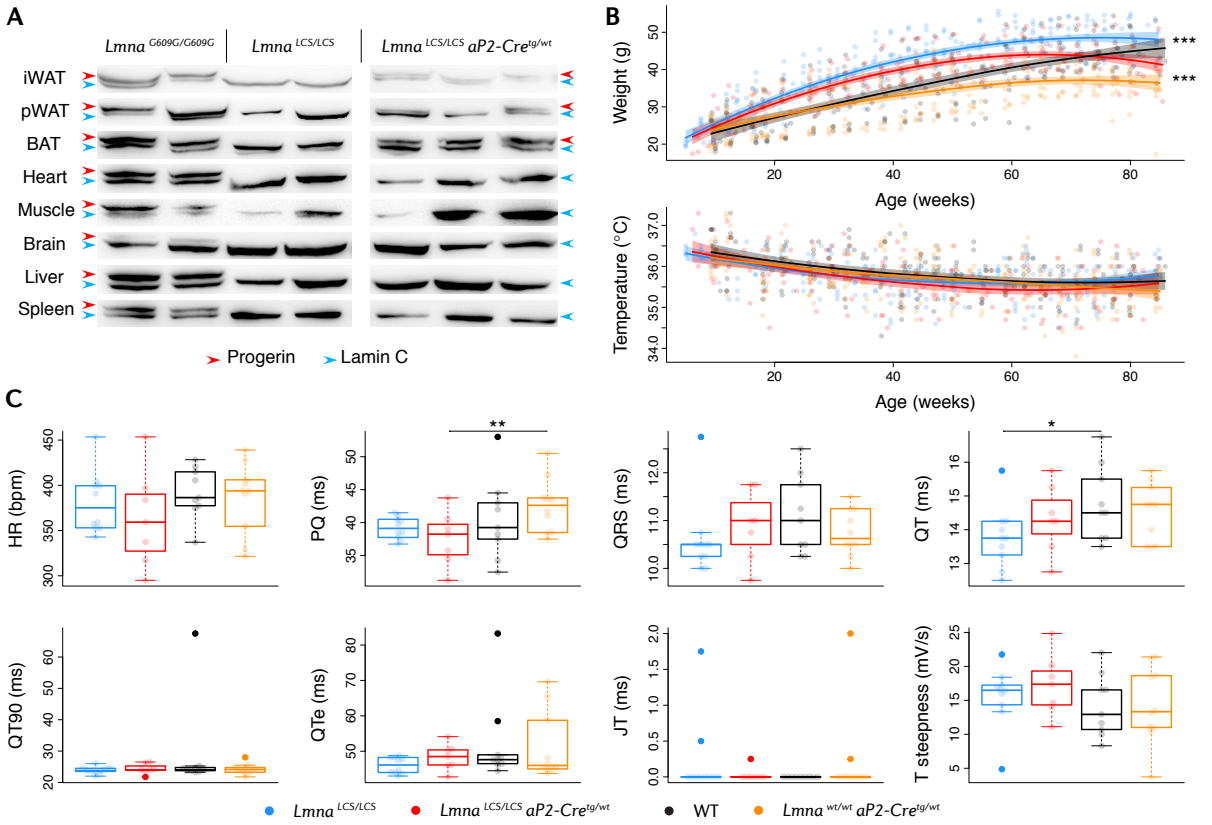

Figure 25: *Lmna*$^{LCS/LCS}$ *aP2-Cre*$^{tg/wt}$ mice show no overt cardiometabolic phenotype
A) Western-blot to check progerin expression in iWAT, pWAT, BAT, heart, muscle, brain, liver and spleen. Lamin C (lower band) and progerin (upper band) were detected with a monoclonal antibody against lamin A/C. B) Longitudinal study of *Lmna*$^{LCS/LCS}$ *aP2-Cre*$^{tg/wt}$ mice and age-matched controls (n = 7-10 per group). C) ECG experiments of *Lmna*$^{LCS/LCS}$ *aP2-Cre*$^{tg/wt}$ animals and age-matched controls at 7 and 10 months of age (n = 7-10 per group). * P<0.05, ** P<0.01, *** P<0.001.

controls (from hereon referred to as *Lmna*$^{LCS/LCS}$), although animals carrying the *LCS* allele had increased body weight in relation to wild-type mice and *Lmna*$^{wt/wt}$ *aP2-Cre*$^{tg/wt}$ controls (Fig. 25B). Moreover, as expected, no electrocardiologic abnormalities were detected in any of the groups (Fig. 25C) and life expectancy was normal up to 18 months of age (data not shown).

Aiming at identifying possible metabolic alterations in adipose-specific progerin-expressing mice, we conducted biochemical plasma analysis of mice at different ages (Fig. 26). The most remarkable result was that *Lmna*$^{LCS/LCS}$ *aP2-Cre*$^{tg/wt}$ mice (adipose tissue-specific progerin expression) show reduced levels of plasma triglycerides, in relation to the control groups. Interestingly, *Lmna*$^{LCS/LCS}$ mice not bearing the Cre recombinase present alterations in multiple lipid metabolism markers, including lower triglyceride, cholesterol and non-esterified fatty acids (NEFA) plasma levels (Fig. 26).

We then subjected *Lmna*$^{LCS/LCS}$ *aP2-Cre*$^{tg/wt}$ mice to a cold challenge, to test whether temperature regulation was impaired in these animals as in progeric mice (section 4.3) with ubiqui-

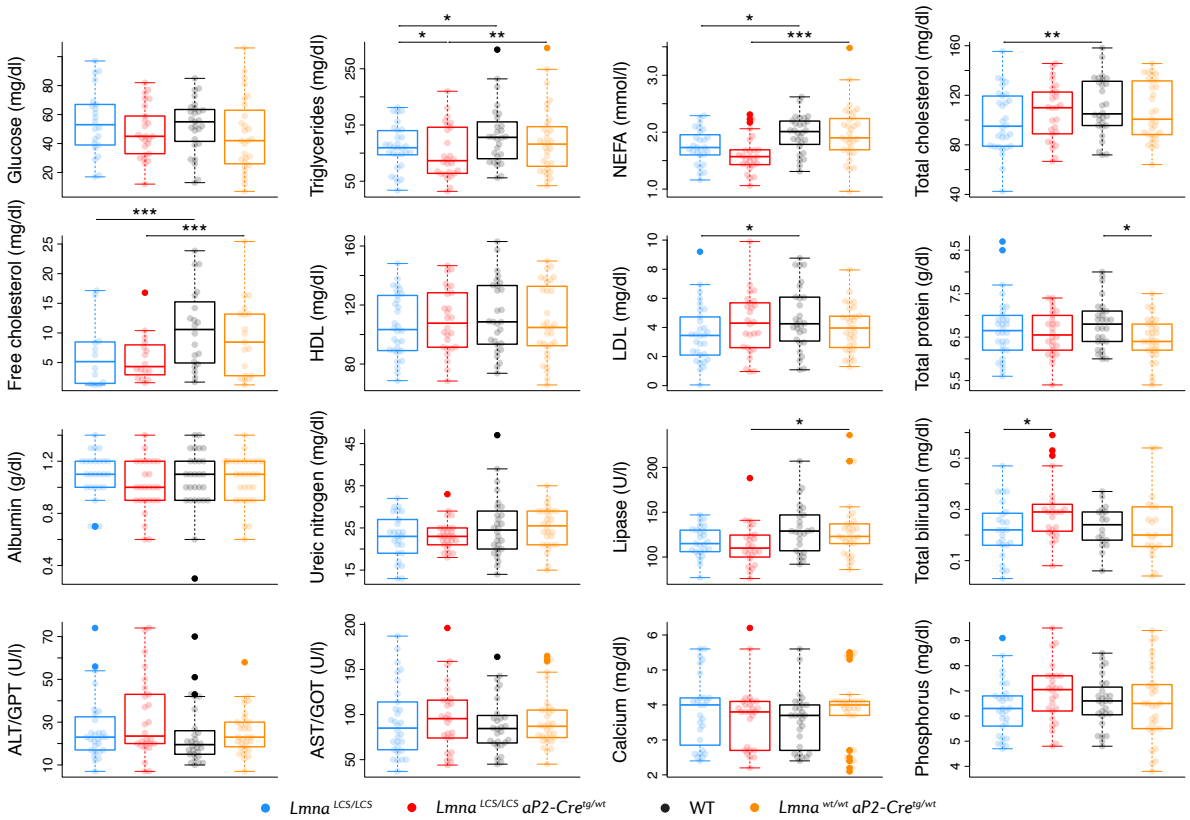

Figure 26: *Lmna*$^{LCS/LCS}$ *aP2-Cre*$^{tg/wt}$ mice present reduced levels of plasma triglycerides
Biochemical plasma analysis of metabolic markers in *Lmna*$^{LCS/LCS}$ *aP2-Cre*$^{tg/wt}$ 5, 7 and 12-month-old animals and age-matched controls. Age was included as a covariate in the statistical analysis (n = 26-31 per group). * P<0.05, ** P<0.01, *** P<0.001.

tous progerin expression. No differences were observed between *Lmna*$^{LCS/LCS}$ *aP2-Cre*$^{tg/wt}$ and *Lmna*$^{LCS/LCS}$ mice, but both groups with *LCS* background had decreased initial body and BAT temperature and showed resistance to cold shock in relation to lamin A/C wild-type mice (Fig. 27A). Furthermore, in metabolic chamber experiments, *Lmna*$^{LCS/LCS}$ mice had decreased EE (Fig. 27B). This could explain why mice lacking lamin A are prone to overweight (López-Mejía et al., 2014).

Taken together, the results of the *in vitro* adipogenesis experiments and the adipose-specific progerin expression study indicate that lipodystrophy in progeric mice is promoted by systemic mechanisms.

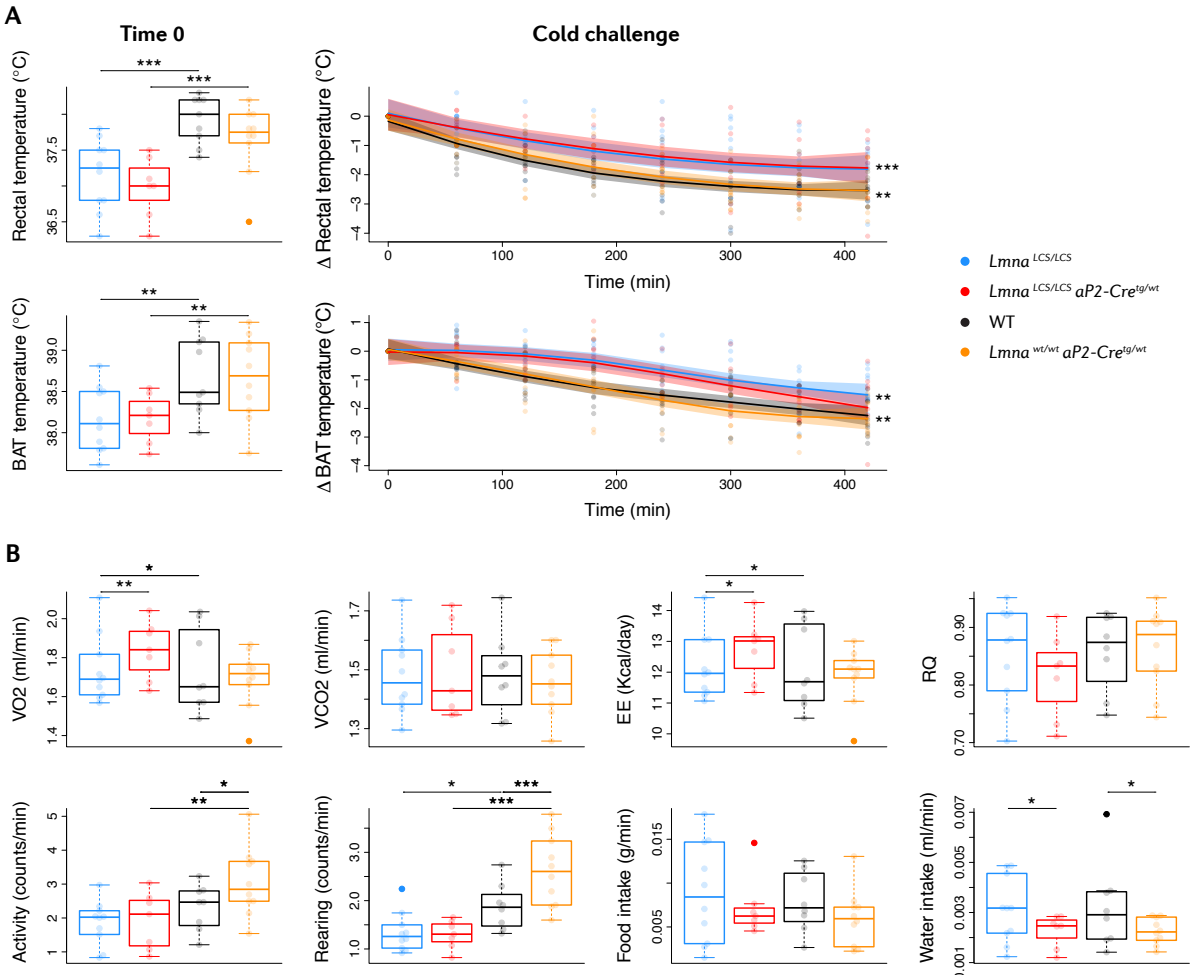

Figure 27: Normal energy metabolism in *Lmna*$^{LCS/LCS}$ *aP2-Cre*$^{tg/wt}$ mice
A) *Lmna*$^{LCS/LCS}$ *aP2-Cre*$^{tg/wt}$ mice and age-matched controls (n = 7-10 per group) were exposed to a 7 h cold challenge (4 °C). Body and BAT temperatures were measured every hour with a rectal probe and a thermographic camera (respectively). B) Metabolic chamber study of the same animals at 7 and 12 months of age (n = 7-10 per group). * P<0.05, ** P<0.01, *** P<0.001.

5

Discussion

The world population is aging (Christensen et al., 2009). Since aging is the main risk factor for the development of cardiometabolic disorders (Savji et al., 2013; Kennedy et al., 2014), these diseases are on the rise and have become a global financial and health concern (Dunbar et al., 2018). It is therefore of utmost importance to elucidate the mechanisms driving age-related cardiometabolic diseases to help develop more effective preventive and therapeutic strategies to promote healthier aging.

Our current understanding of the molecular mechanisms underlying aging - collected under the hallmarks of aging (López-Otín et al., 2013) - has been possible in part thanks to the study of progeroid syndromes, and particularly, of HGPS. This disease is characterized by premature aging and cardiometabolic disorders. Interestingly, age-related comorbidities such as cancer or neurodegeneration are absent in progeria, and environmental risk factors (smoking, sedentarism, environmental toxicants, unhealthy diet, etc.) have a minimal implication in disease progression (Gordon et al., 2014b). Furthermore, HGPS recapitulates all the hallmarks of aging (Carrero et al., 2016) and progerin - the mutant form of lamin A that causes HGPS - is produced at low levels in normally aging individuals (Scaffidi, 2006; McClintock et al., 2007; Rodriguez et al., 2009). Isolated from comorbidities and environmental risk factors, the study of HGPS therefore provides an opportunity to elucidate the molecular mechanisms that drive cardiometabolic diseases during aging. Consequently, animal models of HGPS constitute a unique tool for this purpose and to develop rejuvenation strategies.

In this Doctoral Thesis we first sought to characterize the cardiometabolic alterations present in the $Lmna^{G609G}$ progeria mouse model in juxtaposition to 20-month-old wild-type mice. Our studies were primarily directed at cardiac and metabolic disorders, as recent projects from our laboratories focused on the progeria-associated vascular pathology (Hamczyk et al., 2018b; Del Campo et al., 2019). The $Lmna^{G609G}$ knock-in strain carries the equivalent of the mutation present in HGPS patients - therefore accumulates progerin in the nuclear envelope - and recapitulates most of the clinical manifestations of this rare disease, including growth impairment, bone abnormalities, lipodystrophy, arteriosclerosis and premature death (Osorio et al., 2011; Villa-Bellosta et al., 2013; Balmus et al., 2018; Hamczyk et al., 2018b; Del Campo et al., 2019) (Fig.

2). Previous studies show that these animals also present bradycardia and cardiac electrical abnormalities (Osorio et al., 2011). In our work, we have confirmed these observations. Both old wild-type and *Lmna*$^{G609G/G609G}$ mice present prolonged PR and QT intervals, as well as T-wave flattening in comparison to young heterozygous *Lmna*$^{G609G/wt}$ and young wild-type animals. Young *Lmna*$^{G609G/wt}$ mice show normal ECGs, except for a mild but significant reduction in the T-wave steepness compared to the controls. Nevertheless, with the passage of time, these animals present the same alterations as homozygous progeric and old mice. These findings are consistent with electrical conduction and repolarization abnormalities potentially leading to arrhythmias, which have been previously described for 30-month-old wild-type mice, progeroid *Zmpste24*-deficient mice and HGPS patients (Signore et al., 2015; Rivera-Torres et al., 2016).

The primary cause of death in HGPS is heart failure with preserved EF (Gordon et al., 2018a). This could be provoked by a combination of diastolic dysfunction, LV hypertrophy, cardiac valve dysfunction and interstitial myocardial fibrosis, all of which have been reported for HGPS patients (Nair et al., 2004; Hennekam, 2006; Merideth et al., 2008; Hanumanthappa et al., 2011; Prakash et al., 2018) and are typical in the elderly (Lakatta, 2003; Biernacka and Frangogiannis, 2011; Horn, 2015; Wong et al., 2016). Besides the aforementioned electrical alterations, our work did not yield any result suggesting that progeric or old mice may die of heart failure. Systolic function is preserved in both progeric and old mice, as in human HGPS patients and aged individuals, but there was no indication of LV hypertrophy in our mouse models, as heart mass is not elevated in any of the groups (accounting for body weight). In fact, old mice exhibit an increased Fulton Index and RV to LV EDV ratio compared with young mice, which evidences they have enlarged RV. Furthermore, progeric mice may have thinner ventricular walls, since old *Lmna*$^{G609G/wt}$ mice show thinner IVSd and LVPWd. We have not addressed cardiac fibrosis directly due to technical difficulties, but collagens were not dysregulated in the proteomics study (section 4.2) and interstitial fibrosis is absent in progeric *Zmpste24*-deficient mice (Signore et al., 2015; Rivera-Torres et al., 2016). Finally, although we did not analyze diastolic function or valve regurgitation in the MRI study, we found no differences in the MV E/A ratio by echocardiography in *Lmna*$^{G609G/wt}$ mice compared with controls, and there was no MV or aortic valve regurgitation detected (data not shown). Collectively, these findings illustrate similarities and dissimilarities when comparing cardiac alterations during normal and premature aging, as well as between mouse models and patients.

To deepen into the mechanisms underlying cardiac aging, we performed high throughput proteomics on hearts from 4-month-old *Lmna*$^{G609G/G609G}$ and *Lmna*$^{G609G/wt}$ progeric mice compared to age-matched and 20-month-old wild-type animals. We identified around 5000 proteins at 1% FDR, surpassing the amount described in previous studies for the aging proteome (Walther

and Mann, 2011). Systems biology computational analyses revealed predominantly changes in pathways related to energy metabolism, cellular structure and signaling, gene expression and proteostasis. Furthermore, global oxidation is increased in hearts aged both prematurely and physiologically despite the upregulation of antioxidant response proteins including the glutathione and peroxiredoxin systems. These results are consistent with oxidative stress, previously reported in the aging heart proteome (Dai et al., 2008; Richardson et al., 2008; Grant et al., 2009; Fernandez-Sanz et al., 2014; Dai et al., 2014).

We also observed energy metabolism alterations during cardiac aging, involving increased glucose and fatty acid catabolism, as well as the upregulation of oxidative phosphorylation components, which could indicate mitochondrial dysfunction and energy imbalance. These alterations have been already described for HGPS cells and animal models (Rivera-Torres et al., 2013), as well as for the normally aged heart (Fernandez-Sanz et al., 2014; Dai et al., 2014). Interestingly, ketone body metabolism may also be increased in prematurely and normally aged hearts, constituting a pro-survival mechanism as ketone body supplementation prolongs healthspan in old mice (Newman et al., 2017). Different motor and structural protein groups are also affected in the aging heart, as well as signaling pathways involved in cardiac contraction as calcium signaling. Although our pathophysiological studies showed that cardiac function is preserved in both progeric and normally aged mice, these molecular alterations could potentially lead to contractile dysfunction and failure in the aging heart (Richardson et al., 2008; Grant et al., 2009; Fernandez-Sanz et al., 2014; Kaushik et al., 2015).

Regarding gene expression regulation, aging is associated with a progressive loss of histones (Sen et al., 2016), which are paradoxically increased in our study. One possible explanation for this apparent discrepancy is that age-related histone loss is tightly linked to cell division, which is absent in mature cardiomyocytes. Increased histone expression during aging may be an overcompensating mechanism in this tissue. Similarly, protein translation is increased in progeria cells (Buchwalter and Hetzer, 2017), whereas our results and previous proteomic studies indicate that translation initiation may be reduced in old and progeric mice (Rivera-Torres et al., 2013). Lowering the abundance of translation initiation proteins could constitute a mechanism to compensate the global age-associated increase in protein translation. Finally, it is noteworthy in our finding that loss of proteostasis involving the proteasome and heat shock protein systems may play a key role in the progeric aging. While the downregulation of heat shock proteins could lead to an accumulation of unfolded proteins and to an impaired response to stress signals such as oxidative stress, the upregulation of the proteasome complex would increase protein clearance aiming to compensate the toxic effects that accumulating dysfunctional proteins elicit in the cell. Globally, the dysregulation of gene expression and protein homeostasis mechanisms as well as

the activation of compensatory systems, increases the energy requirements of cardiac cells during aging, which may aggravate the effect of the metabolic alterations detected in this tissue.

Body composition changes during aging, with a reduction in bone (osteopenia) and muscle mass (sarcopenia), as well as a redistribution of fat from subcutaneous to visceral depots, thus eliciting central obesity and peripheral lipodystrophy (Tchkonia et al., 2013; Batsis and Villareal, 2018). These changes are associated with increased risk for other cardiometabolic disorders, as diabetes, hypertension, atherosclerosis or dyslipidemia (Shuster et al., 2012). All of the above, except for obesity, are present in HGPS patients, although dyslipidemia or (pre)diabetes are not highly prevalent (Gordon et al., 2005; Merideth et al., 2008; Gerhard-Herman et al., 2012; Gordon et al., 2018b). Consistent with these observations, we found that old wild-type mice become obese, whereas progeric mice develop cachexia and lipodystrophy, evidenced as loss of lean mass and adiposity, and by reduced protein and increased creatine kinase and transaminase serum levels. Previous studies had already analyzed lipodystrophy in different progeroid models (Pendás et al., 2002; Osorio et al., 2011; López-Mejía et al., 2014; Kreienkamp et al., 2018). Pendás et al. 2002 and Osorio et al. 2011 reported loss of body weight and of the subcutaneous adipose layer in *Zmpste24*-deficient and $Lmna^{G609G}$ mice, respectively. Moreover, in the López-Mejía 2014 and Kreienkamp 2018 publications, there is a deeper characterization of $Lmna^{G609G/wt}$ and $Lmna^{G609G/G609G}$ mice, respectively, which exhibit reduced adiposity by imaging techniques and decreased adipocyte size in different fat depots.

Reduced HDL levels in blood is a common feature in HGPS patients, but it is rarely associated with increased plasma levels of LDL or triglycerides (Gordon et al., 2005; Merideth et al., 2008; Gerhard-Herman et al., 2012; Gordon et al., 2018b). Interestingly, $Lmna^{G609G/G609G}$ mice show low levels of serum cholesterol and triglycerides. Similarly, while insulin levels are high and some patients display hyperglycemia or low glucose tolerance (Gordon et al., 2005; Merideth et al., 2008; Gerhard-Herman et al., 2012; Gordon et al., 2018b), progeric mice present hypoglycemia, hypoinsulinemia and high glucose tolerance (Fig. 9A) (Osorio et al., 2011; López-Mejía et al., 2014). We found No alterations in old mice, except low glucose levels in non-fasting conditions. These dissimilarities between patients and murine models are not surprising, as they have been described as interspecific differences between humans and mice (Yin et al., 2012).

Obesity or lipodystrophy may result from an imbalance between food intake and energy expenditure (Michalakis et al., 2013). During aging, EE is significantly reduced, as well as appetite and intestinal absorption, although food intake is not markedly compromised (Speakman and Westerterp, 2010; Volkert and Sieber, 2011; Morley, 2013). In our work, we did not observe altered EE nor changes in food intake in old wild-type mice, which present a lower RQ compared

with young controls. These findings suggest increased fatty acid oxidation in relation to glucose oxidation (Martin et al., 2006). *Lmna*$^{G609G/G609G}$ also display lower RQ and normal food intake, as well as reduced EE, whereas *Lmna*$^{G609G/wt}$ animals show no abnormalities in the oximetry measurements. These observations agree with a recent study (Kreienkamp et al., 2018), but may seem contradictory to previous studies reporting increased EE in this knock-in model (López-Mejía et al., 2014; Bárcena et al., 2018). It is noteworthy that in the López-Mejía 2014 and Bárcena et al. 2018 publications, oximetry measurements were normalized dividing each one by body weight, whereas in Kreienkamp et al. 2018 and in our project, body weight was included as a covariate in the statistical model. Given that metabolic rate is not linearly proportional to body size and that progeric mice are cachectic, the former approach results in an overcorrection and may lead to opposite conclusions (Tschöp et al., 2011). Although there are no comprehensive EE studies in HGPS patients, it has been reported that progeric children have normal calorie intake (Merideth et al., 2008), while progeria patient cells and animal models present mitochondrial dysfunction (Rivera-Torres et al., 2013). This could promote energy imbalance, as ATP production is inefficient, and agrees with the deregulated oxidative phosphorylation and increased global oxidation observed in our cardiac proteomics study.

Remarkably, both homozygous and old heterozygous progeric mice manifest hypothermia and daily torpor bouts, encompassing a striking decrease in EE, body temperature, HR and activity. These observations are specific to the murine models, not only due to a lack of reports of hypothermia in human patients, but because these comprise pro-survival energy-saving strategies specific to certain mammalian species (Brown and Staples, 2010; Oelkrug et al., 2011). Torpor is a state of hypometabolism in which core temperature drops under 32 °C and there is markedly reduced activity for several hours (Geiser and Stawski, 2011; Geiser et al., 2014). This adaptive response is termed hibernation when the torpid state lasts several days or months (Ruf and Geiser, 2015). Torpor is induced when animals are subjected to cold temperatures or nutrient deprivation, and can be artificially triggered with the administration of 2-deoxy-D-glucose, which blocks cellular uptake of glucose (Bechtold et al., 2012), hydrogen sulfide, which inhibits oxidative phosphorylation (Blackstone, 2005), or pyruvate, which modulates adenosine and GABA signaling (Soto et al., 2018).

Progeric mice show normal food intake, but water intake is significantly reduced, and abnormalities in the intestinal wall of these animals suggest nutrient malabsorption. Moreover, their cachectic phenotype, hypoglycemia and hypolipidemia denote signs of malnutrition, which could aggravate disease progression and the appearance of torpor bouts. Otherwise, this hypometabolic state could be induced through exposure to low environmental temperatures. In this regard, mice are typically housed at 20 °C – 22 °C, way below their thermoneutral zone (> 28 °C), so about

30% of resting EE in these animals is devoted to thermoregulation (Cannon and Nedergaard, 2010). We observed increased life expectancy in progeric mice when environmental temperature was raised to thermoneutrality or when these animals were housed with healthy normothermic individuals. Nonetheless, body weight and temperature were not rescued in these conditions, indicating that ambient temperature is not a major cause for the energy imbalance.

In this line, we hypothesized thermoregulation was impaired in progeric mice. Indeed, we found these animals were unable to maintain body temperature when subjected to a cold challenge. Moreover, our transcriptional analysis, revealed downregulation of key thermogenic and adipogenic genes, and *Tnfa*-mediated inflammation in the BAT of $Lmna^{G609G/G609G}$ mice. These results indicate impaired non-shivering thermogenesis in progeria. Nevertheless, BAT is still functional, as it shows basal activation and this organ is crucial for arousal from torpor (Oelkrug et al., 2011).

Our work also involves the characterization of $Lmna^{LCS/LCS}$ mice, which are deficient for lamin A but express lamin C (Fig. 2) (Osorio et al., 2011). Interestingly, the cardiometabolic phenotype of these animals is very different from that of progeric $Lmna^{G609G/G609G}$ mice. While progeric mice present shortened lifespan and develop cachexia, cardiac electrical abnormalities and cold intolerance, LCS mice live longer than wild-type controls, become overweight (López-Mejía et al., 2014), show no cardiac alterations and are cold resistant (Fig. 19, 25B, 25C and 27A). Furthermore, in concert with the aforementioned observations, we found that $Lmna^{LCS/LCS}$ mice have low plasma levels of triglyceride, cholesterol and free fatty acids, and present reduced EE despite normal food intake. These results indicate that LCS mice present energy imbalance, and that lamin C and progerin may play opposite roles on energy metabolism, as previously proposed (López-Mejía et al., 2014).

$Lmna^{LCS/LCS}$ mice carry a conditional HGPS allele with a floxed cassette that prevents the formation of progerin (Osorio et al., 2011). Therefore, these animals may be crossed with different Cre-expressing strains to generate mice with tissue-specific progerin expression. In recent projects, we used this strategy to study how vascular smooth muscle cells, endothelial cells and macrophages affect atherosclerosis and vascular stiffness progression in progeric mice (Hamczyk et al., 2018b; Del Campo et al., 2019). In the present Doctoral Thesis, we were interested in studying the interplay between the local and systemic environments in age-related cardiometabolic disease. Hence, we generated mice that express progerin specifically in cardiomyocytes or in adipose tissue. We observed that the former, which express a Cre recombinase under the alpha myosin heavy chain promoter ($\alpha MHC\text{-}Cre^{tg/wt}$), develop systolic dysfunction and a very conspicuous dilated cardiomyopathy that led to premature death by heart failure. This

pathology - very different from the disease in HGPS patients - was also present in Cre-positive non-progerin-expressing wild-type animals, and therefore linked to a high and constitutive Cre expression (Buerger et al., 2006; Davis et al., 2012). Consequently, this model was excluded from further experiments, as the toxicity of Cre would obscure any effect that progerin may exert in the heart. Future studies using other cardiac-specific Cre transgenic mice are warranted to assess the role of progerin expression in the heart, such as the tamoxifen-induced $\alpha MHC\text{-}Cre^{tg/wt}$ model (Davis et al., 2012).

One of the intended uses for the above-mentioned model was to study HR regulation during aging. While HR at rest is not modified during aging in humans, heart rhythm alterations arise in response to physical exercise (Brubaker and Kitzman, 2011). Moreover, aging reduces the intrinsic pacemaker activity of the sinoatrial node due to fibrosis and electrical conduction alterations (Moghtadaei et al., 2016), and defective autonomous nervous regulation emerges in relation to increased plasma levels of catecholamines and decreased β-adrenergic sensitivity (Lakatta, 2003). Our results revealed development of bradycardia in homozygous and heterozygous knock-in progeric mice, as well as in old wild-type animals. A reduction of HR was also identified in *Zmpste24*-deficient mice, but there are conflicting results in the literature regarding its presence in HGPS patients (Rivera-Torres et al., 2016; Prakash et al., 2018). Rivera-Torres et al. 2016 reported a non-statistically significant decrease in HR between the first and last follow-up in a cohort of 15 HGPS individuals. Conversely, Prakash et al. 2018 presented results that suggest HR was elevated for age in a cohort of 27 patients, although the Z score did not vary with age. These apparent inconsistencies between the studies may be due to substantial differences in median age at the time of evaluation - 11.8 [1.8 - 19.4] years in Rivera et al. 2014 versus 5.6 [2.1 - 17.5] years in Prakash et al. 2018 - with the older cohort being predicted to exhibit a greater burden of cardiovascular pathology.

Notwithstanding the discrepancy in the field, HR alterations - similarly to thermoregulation impairment - may be specific to murine models. Interestingly we found that HR may be increased in $Lmna^{LCS/LCS}$ $\alpha MHC\text{-}Cre^{tg/wt}$ mice, suggesting that bradycardia in progeric mice is caused by heart-extrinsic mechanisms. This hypothesis was supported by telemetry experiments with $Lmna^{G609G/wt}$ mice, since heart rhythm differences between groups were abrogated when body temperature was included as a covariate in the statistical model. Bradycardia may therefore be a consequence of hypothermia and the energy homeostasis dysregulation. Accordingly, HR responded normally when progeric mice were subjected to either heat or cold shock. Furthermore, when progeric mice were injected with sympathetic system activators or parasympathetic tone inhibitors, HR rose and the differences between genotypes were abrogated. Collectively, these

results support that HR regulation is not impaired in progeria and that the observed bradycardia might be a response to heart-extrinsic signals specific to murine models.

WAT is a key regulator of energy balance in the organism, and WAT lipolysis is essential to maintain body temperature (Shin et al., 2017). We found that *Lmna*$^{G609G/G609G}$ mice become cachectic and lipodystrophic, losing most adipose mass, a feature also present in HGPS patients (Merideth et al., 2008). Hence, understanding the molecular mechanisms that drive progerin-induced lipodystrophy could derive in a therapeutic strategy. Our studies revealed downregulation of several adipogenic genes in progeric mouse pWAT, including *Cebpa*, *Fabp4* and *Pparg*, indicating a repression of the *in vivo* adipocyte differentiation. Conversely, when adipogenesis was induced *in vitro* in mouse preadipocytes, *Pparg*, *Fabp4*, *Cebpb* and caveolin 1 were upregulated in progeric cells. These results suggest that preadipocytes may differentiate faster in progeria when taken out of the systemic environment. Adipokines as *Adipoq*, *Lep*, *Retn* and *Ccl2* were also downregulated in progeric mouse pWAT, whereas the pro-inflammatory cytokine *Il6* appeared upregulated. Consistent results were observed in the *in vitro* studies and in progeroid or normally aging individuals (Capell et al., 2007; Michalakis et al., 2013). Remarkably, we observed upregulation of the master metabolic regulator *Pgc1a* in both perigonadal differentiating preadipocytes and whole tissue. This may seem contradictory to our results in BAT - were this coactivator is downregulated - and to the fact that *Pgc1a* levels decrease during aging (López-Otín et al., 2016). Nevertheless, previous studies detected upregulated *Pgc1a* in WAT from *Lmna*$^{G609G/wt}$ animals (López-Mejía et al., 2014). Furthermore, it is noteworthy that *Pgc1a* plays tissue-specific roles, as it promotes thermogenesis in BAT - which is impaired in progeric mice - (Corrales et al., 2018) or gluconeogenesis and beta oxidation in *Zmpste24*-deficient mouse livers (Mariño et al., 2008).

Adipogenic differentiation in progeria has been investigated *in vitro* by several authors in recent years. Although some failed to see any alteration (Zhang et al., 2011; López-Mejía et al., 2014), others have reported impaired differentiation, mediated by a downregulation of *Cebpa* or *Pparg* (Scaffidi and Misteli, 2008; Xiong et al., 2013; Revêchon et al., 2017). The variability between studies might be due to the use of different progeria models (mesenchymal stem cells, iPSCs, embryoid bodies, mouse preadipocytes...), the duration of the differentiation protocol or even the mechanical properties of the culture plate matrix. In order to overcome the limitations of *in vitro* studies, we sought to study *in vivo* cell-intrinsic mechanisms of adipocytes in progeria. Hence, we characterized the model with adipose tissue-specific expression of progerin (*Lmna*$^{LCS/LCS}$ *aP2-Cre*$^{tg/wt}$ mice). Surprisingly - with the exception of hypotriglyceridemia - we found no overt progeroid phenotype, as weight, body temperature, ECGs, serum markers, cold response and energy intake and expenditure were comparable in *Lmna*$^{LCS/LCS}$ *aP2-Cre*$^{tg/wt}$ mice and age-

matched controls. Taken together, these results indicate for the first time that lipodystrophy in progeric mice is promoted by systemic mechanisms.

According to our results, the *Lmna*$^{G609G/G609G}$ progeria mouse appears an appropriate model to study cardiometabolic disease in aging as it recapitulates many features present not only in normally aged mice but also in HGPS patients and in the elderly. These include cardiac electrical conduction and repolarization abnormalities, preserved systolic function, cachexia, lipodystrophy or oxidative stress. Nevertheless, these animals present impaired thermoregulation - a mechanism especially important in small mammals and easily compromised due to energy imbalance - and may develop malnutrition-related disorders. Therefore, caution should be taken when working with this mouse model, as these alterations accelerate disease progression and may promote the appearance of bradycardia and confounding cardiometabolic abnormalities. An alternative would be to perform our studies on the heterozygous *Lmna*$^{G609G/wt}$ mouse, which develops milder alterations later in life. Moreover, to better understand the interplay between the local and systemic environments, we could resort to design a mouse model of progeria that allows for tissue-specific reversion of progerin expression. From a translational point of view and aiming to develop new treatments for HGPS, it would be most instructive to generate new non-murine animal models of progeria - using rabbits or pigs as host species - in which to validate our studies.

Most of the therapeutical interventions associated with enhanced survival in progeria models also lead to delayed weight loss and increased fat content. These include inhibition of progerin farnesylation (Varela et al., 2008), hormonal supplementation (Mariño et al., 2010), blocking of aberrant splicing (Osorio et al., 2011), epigenetic reprogramming (Ocampo et al., 2016), targeting genome instability (Balmus et al., 2018), metabolic interventions (Bárcena et al., 2018) or reverting the HGPS mutation (Santiago-Fernández et al., 2019; Beyret et al., 2019). Therefore, restoration of adipose tissue may be crucial in the treatment of HGPS patients and of those with lipodystrophy. We propose rescuing *Pparg* with thiazolidinediones (TZDs) as a possible new approach, since these pharmacological agonists also improve insulin resistance and exert anti-inflammatory effects on a systemic level, which is potentially important in the treatment of obesity, diabetes and to prevent aging (Corrales et al., 2018).

In summary, in this Doctoral Thesis we have focused on identifying mechanisms that drive cardiometabolic disease in premature and physiological aging. First, we have characterized the cardiometabolic phenotype of progerin expressing mice in juxtaposition to wild-type old mice and found bradycardia and cardiac conduction and repolarization abnormalities in both models. Regarding metabolism, wild-type mice become obese during aging, while progeric mice

develop cachexia and lipodystrophy. Next, our high-throughput proteomics study in heart tissue revealed increased global oxidation and deregulated energy metabolism, proteostasis, splicing and pathways involved in cardiac muscle contraction in both premature and normal aging models. These results led us to discover decreased EE and impaired thermogenesis as a feature of progeric *Lmna*$^{G609G/G609G}$ mice.

We next studied the interplay between the local and systemic environments in age-related cardiometabolic disease. For that, we generated heart and adipose tissue-specific progerin-expressing mice by crossing *Lmna*$^{LCS/LCS}$ (which present no cardiac alterations but altered energy metabolism) with *αMHC-Cre*$^{tg/wt}$ and *aP2-Cre*$^{tg/wt}$ animals, respectively. The first model was discarded, because long-term Cre expression led to dilated cardiomyopathy and premature death by heart failure in the absence of progerin expression. However, using *Lmna*$^{G609G/wt}$ mice - which develop a late cardiometabolic disease - and a telemetry system, we found that bradycardia in progeria is promoted by heart-extrinsic mechanisms. Similarly, lipodystrophy in these animals is mediated by systemic factors, since adipose-specific progerin expressing mice show no overt phenotype, and *in vitro* adipogenesis is altered in *Lmna*$^{G609G/G609G}$ preadipocytes.

Collectively, our work has focused on better understanding the etiology of cardiometabolic disease during aging. Furthermore, our results highlight the relevance of employing mouse models for the study of the molecular and cellular mechanisms underlying age-related human diseases. We have comprehensively characterized different available mouse models of aging, identifying both the advantages they offer as well as their pitfalls. This work may serve to establish the basis for new treatments against progeria and for the development of new strategies to promote healthier aging in the general population.

6

Conclusions

In this Doctoral Thesis, we have identified mechanisms that promote age-related cardiometabolic disease through the characterization and juxtaposition of mouse models of premature and physiological aging and by studying the interplay between the local and systemic environments. The main conclusions derived from this research are:

1. Progeric *Lmna*$^{G609G/G609G}$ mice and normally aged wild-type mice present bradycardia, preserved systolic function, as well as cardiac electrical conduction and repolarization abnormalities involving PR and QT interval prolongation and T-wave flattening.

2. While wild-type mice become obese with aging, progeric mice develop cachexia and lipodystrophy, evidenced by reduced lean mass and adiposity, hypoglycemia, hypolipidemia, hypoproteinemia and the downregulation of adipogenic, adipokine and mitochondrial genes in WAT.

3. High-throughput proteomics revealed oxidative stress and deregulated energy metabolism, splicing, proteostasis and cardiac contraction pathways in both prematurely and normally aged mouse hearts.

4. *Lmna*$^{G609G/G609G}$ mice display energy imbalance and impaired thermoregulation, as evidenced by decreased EE, hypothermia, daily torpor bouts, cold shock intolerance, and downregulation of thermogenic and adipogenic genes in BAT. Increasing ambient temperature prolongs lifespan in these animals.

5. Heterozygous progeric *Lmna*$^{G609G/wt}$ mice develop late cardiometabolic alterations equivalent to those found in homozygous progeric animals.

6. *Lmna*$^{LCS/LCS}$ mice, that express lamin C and lack lamin A, show no cardiac alterations but exhibit altered energy metabolism as assessed by increased body weight, resistance to cold shock, reduced levels of serum lipids and decreased EE.

7. The $\alpha MHC\text{-}Cre^{tg/wt}$ mouse model is not suitable for aging studies, as the long-term expression of the Cre recombinase in cardiomyocytes leads to dilated cardiomyopathy and premature death by heart failure.

8. Bradycardia in progeric mice is promoted by heart-extrinsic mechanisms, as this feature is absent in cardiac-specific progerin-expressing mice and statistical differences in HR are abrogated when $Lmna^{G609G/wt}$ mice are challenged with extreme temperatures or autonomic nervous system modulators.

9. Lipodystrophy in progeric mice is mediated by systemic factors, despite *in vitro* adipogenesis being altered in $Lmna^{G609G/G609G}$ mouse preadipocytes, since mice with progerin expression restricted to adipose tissue show no overt phenotypic alterations.

Conclusiones

En esta Tesis Doctoral hemos identificado mecanismos que promueven la enfermedad cardiometabólica asociada a la edad mediante la caracterización y comparación de modelos murinos de envejecimiento prematuro y fisiológico, así como estudiando la interacción entre los ambientes local y sistémico. Las principales conclusiones que se derivan de este trabajo son:

1. Los ratones progéricos *Lmna*$^{G609G/G609G}$ y ratones silvestres envejecidos presentan bradicardia, función sistólica preservada y alteraciones eléctricas de conducción y repolarización que incluyen la prolonganción de los intervalos PR y QT y el aplanamiento de la onda T.

2. Mientras que los ratones silvestres desarrollan sobrepeso durante el envejecimiento, los ratones progéricos desarrollan caquexia y lipodistrofia evidenciadas por una reducción en la masa magra y grasa, hipoglucemia, hipolipidemia, hipoproteinemia, y la inhibición de la expresión de genes de adipogénesis, mitocondriales y de adipoquinas en el tejido adiposo.

3. Mediante proteómica cuantitativa se identificó estrés oxidativo y una desregulación del metabolismo energético y en rutas de proteostasis y de contracción muscular en el corazón de ratones viejos y progéricos.

4. Los ratones *Lmna*$^{G609G/G609G}$ presentan alteraciones en la regulación energética y térmica, manifestadas por un gasto energético reducido, hipotermia, ciclos de torpor, intolerancia al choque por frío, e inhibición de genes termogénicos y adipogénicos en el tejido adiposo pardo. La supervivencia de estos animales aumenta al elevar la temperatura ambiental.

5. Los ratones *Lmna*$^{G609G/wt}$ progéricos desarrollan alteraciones cardiometabólicas tardías similares a aquéllas identificadas en sus homólogos homozigotos.

6. Los ratones *Lmna*$^{LCS/LCS}$, que expresan lamina C pero no lamina A, no muestran alteraciones cardiacas, pero presentan alteraciones en el metabolismo energético evidenciadas por sobrepeso, resistencia al choque por frío, hipolipidemia y gasto energético reducido.

7. El modelo $\alpha MHC\text{-}Cre^{tg/wt}$ no es adecuado para estudios de envejecimiento, pues la expresión prolongada de la recombinasa Cre en cardiomiocitos provoca cardiomiopatía dilatada y muerte prematura por insuficiencia cardiaca.

8. La bradicardia en ratones progéricos está provocada por mecanismos ajenos al corazón, pues no se observa en animales que expresan progerina específicamente en el corazón y las diferencias estadísticas en frecuencia cardiaca desaparecen cuando se someten ratones $Lmna^{G609G/wt}$ a choque térmico o son tratados con moduladores del sistema nervioso autónomo.

9. Aunque la adipogénesis *in vitro* está alterada en preadipocitos de ratones $Lmna^{G609G/G609G}$, la lipodistrofia en animales progéricos está mediada por factores sistémicos, ya que la expresión de progerina restingida a tejido adiposo en ratones no provoca alteraciones fenotípicas.

Bibliography

Adler, A. S., S. Sinha, T. L. A. Kawahara, et al. (2007). Motif module map reveals enforcement of aging by continual NF-kappaB activity. *Genes & Development*. 21 (24): 3244–3257 (cit. on p. 8).

Agah, R., P. A. Frenkel, B. A. French, et al. (1997). Gene recombination in postmitotic cells. Targeted expression of Cre recombinase provokes cardiac-restricted, site-specific rearrangement in adult ventricular muscle in vivo. *Journal of Clinical Investigation*. 100 (1): 169–179 (cit. on p. 24).

Alenghat, F. J. (2016). The prevalence of atherosclerosis in those with inflammatory connective tissue disease by race, age, and traditional risk factors. *Scientific reports*. 6 (1): 20303 (cit. on p. 4).

Andrés, V. and J. M. Gonzalez-Granado (2009). Role of A-type lamins in signaling, transcription, and chromatin organization. *The Journal of Cell Biology*. 187 (7): 945–957 (cit. on p. 12).

Armanios, M. and E. H. Blackburn (2012). The telomere syndromes. *Nature Reviews Genetics*. 13 (10): 693–704 (cit. on p. 7).

Baixauli, F., C. López-Otín, and M. Mittelbrunn (2014). Exosomes and autophagy: coordinated mechanisms for the maintenance of cellular fitness. *Frontiers in Immunology*. 5: 403 (cit. on p. 7).

Baker, D. J., T. Wijshake, T. Tchkonia, et al. (2011). Clearance of p16Ink4a-positive senescent cells delays ageing-associated disorders. *Nature*. 479 (7372): 232–236 (cit. on p. 8).

Baker, D. J., M. M. Dawlaty, T. Wijshake, et al. (2013). Increased expression of BubR1 protects against aneuploidy and cancer and extends healthy lifespan. *Nature Cell Biology*. 15 (1): 96–102 (cit. on pp. 6, 8).

Balmus, G., D. Larrieu, A. C. Barros, et al. (2018). Targeting of NAT10 enhances healthspan in a mouse model of human accelerated aging syndrome. *Nature Communications*. 9 (1): 1700 (cit. on pp. 14, 15, 43, 67, 75).

Bapat, S. P., J. Myoung Suh, S. Fang, et al. (2015). Depletion of fat-resident T reg cells prevents age-associated insulin resistance. *Nature*. 528 (7580): 137–141 (cit. on p. 10).

Bárcena, C., P. M. Quirós, S. Durand, et al. (2018). Methionine restriction extends lifespan in progeroid mice and alters lipid and bile acid metabolism. *Cell reports*. 24 (9): 2392–2403 (cit. on pp. 15, 71, 75).

Batsis, J. A. and D. T. Villareal (2018). Sarcopenic obesity in older adults: aetiology, epidemiology and treatment strategies. Tech. rep. 9: 513–537 (cit. on pp. 4, 70).

Bechtold, D. A., A. Sidibe, B. R. Saer, et al. (2012). A role for the melatonin-related receptor GPR50 in leptin signaling, adaptive thermogenesis, and torpor. *Current Biology*. 22 (1): 70–77 (cit. on p. 71).

Bergo, M. O., B. Gavino, J. Ross, et al. (2002). Zmpste24 deficiency in mice causes spontaneous bone fractures, muscle weakness, and a prelamin A processing defect. *Proceedings of the National Academy of Sciences of the United States of America*. 99 (20): 13049–13054 (cit. on p. 14).

Beyret, E., H.-K. Liao, M. Yamamoto, et al. (2019). Single-dose CRISPR–Cas9 therapy extends lifespan of mice with Hutchinson–Gilford progeria syndrome. *Nature Medicine*.: 1 (cit. on pp. 15, 75).

Biernacka, A. and N. G. Frangogiannis (2011). Aging and cardiac fibrosis. *Aging and Disease*. 2 (2): 158–173 (cit. on pp. 2, 3, 68).

Bitto, A., T. K. Ito, V. V. Pineda, et al. (2016). Transient rapamycin treatment can increase lifespan and healthspan in middle-aged mice. *eLife*. 5 (August): e16351 (cit. on p. 11).

Blackburn, E. H., C. W. Greider, and J. W. Szostak (2006). Telomeres and telomerase: the path from maize, Tetrahymena and yeast to human cancer and aging. *Nature Medicine*. 12 (10): 1133–1138 (cit. on p. 7).

Blackstone, E. (2005). H2S induces a suspended animation-like state in mice. *Science*. 308 (5721): 518–518 (cit. on p. 71).

Blasco, M. A., H.-W. Lee, M. P. Hande, et al. (1997). Telomere shortening and tumor formation by mouse cells lacking telomerase RNA. *Cell*. 91 (1): 25–34 (cit. on p. 7).

Bonzon-Kulichenko, E., F. García-Marqués, M. Trevisan-Herraz, and J. Vázquez (2015). Revisiting Peptide Identification by High-Accuracy Mass Spectrometry: Problems Associated with the Use of Narrow Mass Precursor Windows. *Journal of Proteome Research*. 14 (2): 700–710 (cit. on p. 40).

Boukens, B. J., M. G. Hoogendijk, A. O. Verkerk, et al. (2013). Early repolarization in mice causes overestimation of ventricular activation time by the QRS duration. *Cardiovascular Research*. 97 (1): 182–191 (cit. on p. 26).

Boukens, B. J., M. R. Rivaud, S. Rentschler, and R. Coronel (2014). Misinterpretation of the mouse ECG: 'musing the waves of Mus musculus'. *The Journal of Physiology*. 592 (21): 4613–4626 (cit. on p. 26).

Bradford, M. M. (1976). A rapid and sensitive method for the quantitation of microgram quantities of protein utilizing the principle of protein-dye binding. *Analytical Biochemistry*. 72 (1-2): 248–254 (cit. on p. 36).

Brown, J. C. L. and J. F. Staples (2010). Mitochondrial metabolism during fasting-induced daily torpor in mice. *Biochimica et Biophysica Acta - Bioenergetics*. 1797 (4): 476–486 (cit. on pp. 53, 71).

Brubaker, P. H. and D. W. Kitzman (2011). Chronotropic incompetence: causes, consequences, and management. *Circulation*. 123 (9): 1010–1020 (cit. on pp. 3, 73).

Buchwalter, A. and M. W. Hetzer (2017). Nucleolar expansion and elevated protein translation in premature aging. *Nature Communications*. 8 (1): 328 (cit. on pp. 16, 69).

Buerger, A., O. Rozhitskaya, M. C. Sherwood, et al. (2006). Dilated cardiomyopathy resulting from high-level myocardial expression of Cre-recombinase. *Journal of Cardiac Failure*. 12 (5): 392–398 (cit. on pp. 58, 73).

Burtner, C. R. and B. K. Kennedy (2010). Progeria syndromes and ageing: what is the connection? *Nature Reviews Molecular Cell Biology*. 11 (8): 567–578 (cit. on pp. 6, 11, 16).

Cabanillas, R., J. Cadiñanos, J. A. Villameytide, et al. (2011). Néstor-Guillermo progeria syndrome: A novel premature aging condition with early onset and chronic development caused by BANF1 mutations. *American Journal of Medical Genetics Part A*. 155 (11): 2617–2625 (cit. on p. 11).

Camozzi, D., C. Capanni, V. Cenni, et al. (2014). Diverse lamin-dependent mechanisms interact to control chromatin dynamics. *Nucleus*. 5 (5): 427–440 (cit. on p. 16).

Cannon, B. and J. Nedergaard (2010). Metabolic consequences of the presence or absence of the thermogenic capacity of brown adipose tissue in mice (and probably in humans). *International Journal of Obesity*. 34 (S1): S7–S16 (cit. on pp. 53, 72).

Cao, K., J. J. Graziotto, C. D. Blair, et al. (2011). Rapamycin reverses cellular phenotypes and enhances mutant protein clearance in Hutchinson-Gilford progeria syndrome cells. *Science Translational Medicine*. 3 (89): 89ra58 (cit. on pp. 15, 16).

Capell, B. C., F. S. Collins, and E. G. Nabel (2007). Mechanisms of cardiovascular disease in accelerated aging syndromes (cit. on p. 74).

Capell, B. C., M. Olive, M. R. Erdos, et al. (2008). A farnesyltransferase inhibitor prevents both the onset and late progression of cardiovascular disease in a progeria mouse model. *Proceedings of the National Academy of Sciences of the United States of America*. 105 (41): 15902–15907 (cit. on p. 15).

Carrero, D., C. Soria-Valles, and C. López-Otín (2016). Hallmarks of progeroid syndromes: lessons from mice and reprogrammed cells. *Disease Models & Mechanisms*. 9 (7): 719–735 (cit. on pp. 11, 16, 67).

Caso, G., M. A. McNurlan, I. Mileva, et al. (2013). Peripheral fat loss and decline in adipogenesis in older humans. *Metabolism: Clinical and Experimental*. 62 (3): 337–340 (cit. on p. 4).

Cenni, V., M. R. D'Apice, P. Garagnani, et al. (2018). Mandibuloacral dysplasia: A premature ageing disease with aspects of physiological ageing. *Ageing Research Reviews*. 42: 1–13 (cit. on p. 11).

Chait, A. and I. Goldberg (2017). Treatment of dyslipidemia in diabetes: recent advances and remaining questions. *Current diabetes reports*. 17 (11): 112 (cit. on p. 5).

Chia, C. W., J. M. Egan, and L. Ferrucci (2018). Age-related changes in glucose metabolism, hyperglycemia, and cardiovascular risk. *Circulation Research*. 123 (7): 886–904 (cit. on p. 1).

Christensen, K., G. Doblhammer, R. Rau, and J. W. Vaupel (2009). Ageing populations: the challenges ahead. *The Lancet*. 374 (9696): 1196–1208 (cit. on pp. 1, 67).

Clark-Matott, J., A. Saleem, Y. Dai, et al. (2015). Metabolomic analysis of exercise effects in the POLG mitochondrial DNA mutator mouse brain. *Neurobiology of Aging*. 36 (11): 2972–2983 (cit. on p. 11).

Collado, M., M. A. Blasco, and M. Serrano (2007). Cellular senescence in cancer and aging. *Cell*. 130 (2): 223–233 (cit. on p. 8).

Conboy, I. M. and T. A. Rando (2012). Heterochronic parabiosis for the study of the effects of aging on stem cells and their niches. *Cell Cycle*. 11 (12): 2260–2267 (cit. on p. 8).

Conboy, I. M., M. J. Conboy, A. J. Wagers, et al. (2005). Rejuvenation of aged progenitor cells by exposure to a young systemic environment. *Nature*. 433 (7027): 760–764 (cit. on pp. 9, 10).

Corrales, P., A. Vidal-Puig, and G. Medina-Gómez (2018). PPARs and metabolic disorders associated with challenged adipose tissue plasticity. *International Journal of Molecular Sciences*. 19 (7): 2124 (cit. on pp. 74, 75).

Cox, L. M., S. Yamanishi, J. Sohn, et al. (2014). Altering the intestinal microbiota during a critical developmental window has lasting metabolic consequences. *Cell*. 158 (4): 705–721 (cit. on p. 11).

Csoka, A. B., S. B. English, C. P. Simkevich, et al. (2004). Genome-scale expression profiling of Hutchinson-Gilford progeria syndrome reveals widespread transcriptional misregulation leading to mesodermal/mesenchymal defects and accelarated atherosclerosis. *Aging Cell*. 3 (4): 235–243 (cit. on p. 40).

D'Agostino, R. B., R. S. Vasan, M. J. Pencina, et al. (2008). General cardiovascular risk profile for use in primary care: The Framingham heart study. *Circulation*. 117 (6): 743–753 (cit. on p. 5).

Dai, D.-F., T. Chen, S. C. Johnson, H. Szeto, and P. S. Rabinovitch (2012). Cardiac aging: from molecular mechanisms to significance in human health and disease. *Antioxidants & Redox Signaling*. 16 (12): 1492–1526 (cit. on p. 2).

Dai, D.-F., P. P. Karunadharma, Y. A. Chiao, et al. (2014). Altered proteome turnover and remodeling by short-term caloric restriction or rapamycin rejuvenate the aging heart. *Aging Cell*. 13 (3): 529–539 (cit. on p. 69).

Dai, Q., G. P. Escobar, K. W. Hakala, et al. (2008). The left ventricle proteome differentiates middle-aged and old left ventricles in mice. *Journal of Proteome Research*. 7 (2): 756–765 (cit. on p. 69).

Davis, J., M. Maillet, J. M. Miano, and J. D. Molkentin (2012). Lost in transgenesis: a user's guide for genetically manipulating the mouse in cardiac research. *Circulation Research*. 111 (6): 761–777 (cit. on pp. 58, 73).

De la Rosa, J., J. M. P. Freije, R. Cabanillas, et al. (2013). Prelamin A causes progeria through cell-extrinsic mechanisms and prevents cancer invasion. *Nature Communications*. 4 (1): 2268 (cit. on p. 18).

De Sandre-Giovannoli, A., R. Bernard, P. Cau, et al. (2003). Lamin A truncation in Hutchinson-Gilford progeria. *Science (New York, N.Y.)* 300 (5628): 2055 (cit. on p. 12).

Decker, M. L., E. Chavez, I. Vulto, and P. M. Lansdorp (2009). Telomere length in Hutchinson-Gilford Progeria Syndrome. *Mechanisms of Ageing and Development*. 130 (6): 377–383 (cit. on p. 16).

Del Campo, L., A. Sánchez-López, M. Salaices, et al. (2019). Vascular smooth muscle cell-specific progerin expression in a mouse model of Hutchinson-Gilford progeria syndrome promotes arterial stiffness. Therapeutic effect of dietary nitrite. *Aging Cell*. Accepted (cit. on pp. 15, 43, 67, 72).

Demaria, M., N. Ohtani, S. A. Youssef, et al. (2014). An essential role for senescent cells in optimal wound healing through secretion of PDGF-AA. *Developmental Cell*. 31 (6): 722–733 (cit. on p. 8).

Deursen, J. M. van (2014). The role of senescent cells in ageing. *Nature*. 509 (7501): 439–446 (cit. on p. 8).

Dietz, W. H., L. A. Baur, K. Hall, et al. (2015). Management of obesity: improvement of health-care training and systems for prevention and care. *The Lancet*. 385 (9986): 2521–2533 (cit. on p. 1).

Dittmer, T. A. and T. Misteli (2011). The lamin protein family. *Genome Biology*. 12 (5): 222 (cit. on p. 12).

Dobson, J. G., J. Fray, J. L. Leonard, and R. E. Pratt (2003). Molecular mechanisms of reduced β-adrenergic signaling in the aged heart as revealed by genomic profiling. *Physiological Genomics*. 15 (2): 142–147 (cit. on p. 40).

Dunbar, S. B., O. A. Khavjou, T. Bakas, et al. (2018). Projected costs of informal caregiving for cardiovascular disease: 2015 to 2035: a policy statement from the American Heart Association. *Circulation*. 137 (19): e558–e577 (cit. on pp. 1, 67).

Edgar, D., I. Shabalina, Y. Camara, et al. (2009). Random point mutations with major effects on protein-coding genes are the driving force behind premature aging in mtDNA mutator mice. *Cell Metabolism*. 10 (2): 131–138 (cit. on p. 8).

Efeyan, A., W. C. Comb, and D. M. Sabatini (2015). Nutrient-sensing mechanisms and pathways. *Nature*. 517 (7534): 302–310 (cit. on p. 7).

Eisenberg, T., H. Knauer, A. Schauer, et al. (2009). Induction of autophagy by spermidine promotes longevity. *Nature Cell Biology*. 11 (11): 1305–1314 (cit. on p. 7).

Eisenberg, T., S. Schroeder, A. Andryushkova, et al. (2014). Nucleocytosolic depletion of the energy metabolite acetyl-coenzyme a stimulates autophagy and prolongs lifespan. *Cell Metabolism*. 19 (3): 431–444 (cit. on p. 11).

Eng, J., R. L. McClelland, A. S. Gomes, et al. (2016). Adverse left ventricular remodeling and age assessed with cardiac mr imaging: the multi-ethnic study of atherosclerosis. *Radiology*. 278 (3): 714–722 (cit. on p. 2).

Eriksson, M., W. T. Brown, L. B. Gordon, et al. (2003). Recurrent de novo point mutations in lamin A cause Hutchinson–Gilford progeria syndrome. *Nature*. 423 (6937): 293–298 (cit. on p. 12).

Espada, J., I. Varela, I. Flores, et al. (2008). Nuclear envelope defects cause stem cell dysfunction in premature-aging mice. *The Journal of Cell Biology*. 181 (1): 27–35 (cit. on p. 17).

Fang, E. F., M. Scheibye-Knudsen, L. E. Brace, et al. (2014). Defective mitophagy in XPA via PARP-1 hyperactivation and NAD+/SIRT1 reduction. *Cell*. 157 (4): 882–896 (cit. on p. 9).

Fernandez, P., P. Scaffidi, E. Markert, et al. (2014). Transformation resistance in a premature aging disorder identifies a tumor-protective function of BRD4. *Cell Reports*. 9 (1): 248–260 (cit. on pp. 18, 40).

Fernandez-Sanz, C., M. Ruiz-Meana, E. Miro-Casas, et al. (2014). Defective sarcoplasmic reticulum–mitochondria calcium exchange in aged mouse myocardium. *Cell Death & Disease*. 5 (12): e1573–e1573 (cit. on pp. 40, 69).

Fisher, S. A. (2010). Vascular smooth muscle phenotypic diversity and function. *Physiological Genomics*. 42A (3): 169–187 (cit. on p. 4).

Flurkey, K., J. M. Currer, and D. E. Harrison (2007). Mouse models in aging research. *The Mouse in Biomedical Research*. Elsevier: 637–672 (cit. on p. 43).

Folgueras, A. R., S. Freitas-Rodríguez, G. Velasco, and C. López-Otín (2018). Mouse models to disentangle the hallmarks of human aging. *Circulation Research*. 123 (7): 905–924 (cit. on p. 16).

Fong, L. G., D. Frost, M. D. Meta, et al. (2006). A protein farnesyltransferase inhibitor ameliorates disease in a mouse model of progeria. *Science*. 311 (5767): 1621–1623 (cit. on p. 15).

Fontana, L. (2018). Interventions to promote cardiometabolic health and slow cardiovascular ageing. *Nature Reviews Cardiology*. 15 (9): 566–577 (cit. on p. 1).

Foppa, M., B. B. Duncan, and L. E. P. Rohde (2005). Echocardiography-based left ventricular mass estimation. How should we define hypertrophy? *Cardiovascular Ultrasound*. 3: 17 (cit. on p. 27).

Fraga, M. F. and M. Esteller (2007). Epigenetics and aging: the targets and the marks. *Trends in Genetics*. 23 (8): 413–418 (cit. on p. 7).

Freije, J. M. P. and C. López-Otín (2012). Reprogramming aging and progeria. *Current Opinion in Cell Biology*. 24 (6): 757–764 (cit. on p. 8).

Galluzzi, L., F. Pietrocola, B. Levine, and G. Kroemer (2014). Metabolic control of autophagy (cit. on p. 11).

García-Marqués, F., M. Trevisan-Herraz, S. Martínez-Martínez, et al. (2016). A novel systems-biology algorithm for the analysis of coordinated protein responses using quantitative proteomics. *Molecular & Cellular Proteomics*. 15 (5): 1740–1760 (cit. on p. 40).

Garinis, G. A., G. T. van der Horst, J. Vijg, and J. H. J. Hoeijmakers (2008). DNA damage and ageing: new-age ideas for an age-old problem. *Nature Cell Biology*. 10 (11): 1241–1247 (cit. on pp. 8, 9).

Geiser, F. and C. Stawski (2011). Hibernation and torpor in tropical and subtropical bats in relation to energetics, extinctions, and the evolution of endothermy. *Integrative and Comparative Biology*. Vol. 51. 3: 337–348 (cit. on p. 71).

Geiser, F., S. E. Currie, K. A. O'Shea, and S. M. Hiebert (2014). Torpor and hypothermia: reversed hysteresis of metabolic rate and body temperature. *American Journal of Physiology-Regulatory, Integrative and Comparative Physiology*. 307 (11): R1324–R1329 (cit. on p. 71).

Gerhard-Herman, M., L. B. Smoot, N. Wake, et al. (2012). Mechanisms of premature vascular aging in children with Hutchinson-Gilford progeria syndrome. *Hypertension*. 59 (1): 92–97 (cit. on pp. 19, 70).

Goldberg, E. L. and V. D. Dixit (2015). Drivers of age-related inflammation and strategies for healthspan extension (cit. on p. 10).

Gonzalez-Granado, J. M., C. Silvestre-Roig, V. Rocha-Perugini, et al. (2014). Nuclear envelope lamin-A couples actin dynamics with immunological synapse architecture and T cell activation. *Science Signaling*. 7 (322): ra37–ra37 (cit. on p. 17).

Gordon, C. M., L. B. Gordon, B. D. Snyder, et al. (2011). Hutchinson-Gilford progeria is a skeletal dysplasia. *Journal of Bone and Mineral Research*. 26 (7): 1670–1679 (cit. on p. 17).

Gordon, L. B., I. A. Harten, M. E. Patti, and A. H. Lichtenstein (2005). Reduced adiponectin and HDL cholesterol without elevated C-reactive protein: Clues to the biology of premature atherosclerosis in Hutchinson-Gilford Progeria Syndrome. *The Journal of Pediatrics*. 146 (3): 336–341 (cit. on pp. 19, 70).

Gordon, L. B., K. M. McCarten, A. Giobbie-Hurder, et al. (2007). Disease progression in Hutchinson-Gilford progeria syndrome: impact on growth and development. *Pediatrics*. 120 (4): 824–833 (cit. on p. 17).

Gordon, L. B., M. E. Kleinman, D. T. Miller, et al. (2012). Clinical trial of a farnesyltransferase inhibitor in children with Hutchinson-Gilford progeria syndrome. *Proceedings of the National Academy of Sciences of the United States of America*. 109 (41): 16666–16671 (cit. on p. 16).

Gordon, L. B., J. Massaro, R. B. D'Agostino, et al. (2014a). Impact of farnesylation inhibitors on survival in Hutchinson-Gilford progeria syndrome. *Circulation*. 130 (1): 27–34 (cit. on pp. 12, 16, 19).

Gordon, L. B., F. G. Rothman, C. López-Otín, and T. Misteli (2014b). Progeria: a paradigm for translational medicine. *Cell*. 156 (3): 400–407 (cit. on pp. 11, 12, 15, 67).

Gordon, L. B., M. E. Kleinman, J. Massaro, et al. (2016). Clinical trial of the protein farnesylation inhibitors Lonafarnib, Pravastatin, and Zoledronic Acid in Children with Hutchinson-Gilford progeria syndrome. *Circulation*. 134 (2): 114–125 (cit. on pp. 16, 19).

Gordon, L. B., H. Shappell, J. Massaro, et al. (2018a). Association of Lonafarnib treatment vs no treatment with mortality rate in patients with Hutchinson-Gilford progeria syndrome. *Journal of the American Medical Association*. 319 (16): 1687 (cit. on pp. 12, 16, 19, 68).

Gordon, L. B., S. E. Campbell, J. M. Massaro, et al. (2018b). Survey of plasma proteins in children with progeria pre-therapy and on-therapy with lonafarnib. *Pediatric Research*. 83 (5): 982–992 (cit. on pp. 16, 19, 70).

Grant, J. E., A. D. Bradshaw, J. H. Schwacke, et al. (2009). Quantification of protein expression changes in the aging left ventricle of Rattus norvegicus. *Journal of Proteome Research*. 8 (9): 4252–4263 (cit. on p. 69).

Graziotto, J. J., K. Cao, F. S. Collins, and D. Krainc (2012). Rapamycin activates autophagy in Hutchinson-Gilford progeria syndrome: Implications for normal aging and age-dependent neurodegenerative disorders (cit. on p. 15).

Green, D. R., L. Galluzzi, and G. Kroemer (2011). Mitochondria and the autophagy-inflammation-cell death axis in organismal aging. *Science (New York, N.Y.)* 333 (6046): 1109–1112 (cit. on pp. 8, 9).

Greer, M. M., M. E. Kleinman, L. B. Gordon, et al. (2018). Pubertal progression in female adolescents with progeria. *Journal of Pediatric and Adolescent Gynecology*. 31 (3): 238–241 (cit. on p. 17).

Gruenbaum, Y. and R. Foisner (2015). Lamins: nuclear intermediate filament proteins with fundamental functions in nuclear mechanics and genome regulation. *Annual Review of Biochemistry*. 84 (1): 131–164 (cit. on p. 12).

Gutiérrez-Fernández, A., C. Soria-Valles, F. G. Osorio, et al. (2015). Loss of MT1-MMP causes cell senescence and nuclear defects which can be reversed by retinoic acid. *The EMBO Journal*. 34 (14): 1875–1888 (cit. on p. 8).

Guzman-Castillo, M., S. Ahmadi-Abhari, P. Bandosz, et al. (2017). Forecasted trends in disability and life expectancy in England and Wales up to 2025: a modelling study. *The Lancet Public Health*. 2 (7): e307–e313 (cit. on p. 1).

Hamczyk, M. R., L. Del Campo, and V. Andrés (2018a). Aging in the cardiovascular system: lessons from Hutchinson-Gilford progeria syndrome. *Annual Review of Physiology*. 80 (1): 27–48 (cit. on pp. 15, 20).

Hamczyk, M. R., R. Villa-Bellosta, P. Gonzalo, et al. (2018b). Vascular smooth muscle–specific progerin expression accelerates atherosclerosis and death in a mouse model of Hutchinson-Gilford progeria syndrome. *Circulation*. 138 (3): 266–282 (cit. on pp. 14, 15, 43, 67, 72).

Hanumanthappa, N. B., G. Madhusudan, J. Mahimarangaiah, and C. N. Manjunath (2011). Hutchinson-Gilford progeria syndrome with severe calcific aortic valve stenosis. *Annals of pediatric cardiology*. 4 (2): 204–206 (cit. on pp. 19, 68).

Harrison, D. E., R. Strong, Z. D. Sharp, et al. (2009). Rapamycin fed late in life extends lifespan in genetically heterogeneous mice. *Nature*. 460 (7253): 392–395 (cit. on p. 7).

Hayflick, L. (2007). Biological aging is no longer an unsolved problem. *Annals of the New York Academy of Sciences*. 1100 (1): 1–13 (cit. on p. 5).

Hayflick, L. and P. S. Moorhead (1961). The serial cultivation of human diploid cell strains. *Experimental Cell Research*. 25 (3): 585–621 (cit. on p. 7).

He, W., Y. Barak, A. Hevener, et al. (2003). Adipose-specific peroxisome proliferator-activated receptor gamma knockout causes insulin resistance in fat and liver but not in muscle. *Proceedings of the National Academy of Sciences of the United States of America*. 100 (26): 15712–15717 (cit. on p. 24).

Heiberg, E., J. Sjögren, M. Ugander, et al. (2010). Design and validation of Segment - freely available software for cardiovascular image analysis. *BMC Medical Imaging*. 10 (1): 1 (cit. on p. 29).

Hekimi, S., J. Lapointe, and Y. Wen (2011). Taking a "good" look at free radicals in the aging process. *Trends in Cell Biology*. 21 (10): 569–576 (cit. on p. 8).

Hennekam, R. C. M. (2006). Hutchinson–Gilford progeria syndrome: Review of the phenotype. *American Journal of Medical Genetics Part A*. 140A (23): 2603–2624 (cit. on pp. 12, 17, 19, 44, 68).

Hernández-Porras, I., S. Fabbiano, A. J. Schuhmacher, et al. (2014). K-Ras V14I recapitulates Noonan syndrome in mice. *Proceedings of the National Academy of Sciences*. 111 (46): 16395–16400 (cit. on p. 29).

Hill, A. M., J. LaForgia, A. M. Coates, J. D. Buckley, and P. R. Howe (2007). Estimating abdominal adipose tissue with DXA and anthropometry. *Obesity*. 15 (2): 504–510 (cit. on p. 30).

Hoeijmakers, J. H. J. (2009). DNA damage, aging, and cancer. *New England Journal of Medicine*. 361 (15): 1475–1485 (cit. on p. 6).

Horn, M. A. (2015). Cardiac physiology of aging: extracellular considerations. *Comprehensive Physiology*. Vol. 5. 3. Hoboken, NJ, USA: John Wiley & Sons, Inc.: 1069–1121 (cit. on pp. 2, 68).

Houtkooper, R. H., E. Pirinen, and J. Auwerx (2012). Sirtuins as regulators of metabolism and healthspan. *Nature Reviews Molecular Cell Biology*. 13 (4): 225–238 (cit. on p. 7).

Hsu, P. D., E. S. Lander, and F. Zhang (2014). Development and applications of CRISPR-Cas9 for genome engineering. *Cell*. 157 (6): 1262–1278 (cit. on p. 15).

Huveneers, S., M. J.A. P. Daemen, and P. L. Hordijk (2015). Between Rho(k) and a hard place: the relation between vessel wall stiffness, endothelial contractility, and cardiovascular disease. *Circulation Research*. 116 (5): 895–908 (cit. on p. 3).

Ibrahim, M. X., V. I. Sayin, M. K. Akula, et al. (2013). Targeting isoprenylcysteine methylation ameliorates disease in a mouse model of progeria. *Science*. 340 (6138): 1330–1333 (cit. on p. 15).

Jaskelioff, M., F. L. Müller, J.-H. Paik, et al. (2011). Telomerase reactivation reverses tissue degeneration in aged telomerase-deficient mice. *Nature*. 469 (7328): 102–106 (cit. on p. 7).

Jasper, H. and D. L. Jones (2010). Metabolic regulation of stem cell behavior and implications for aging (cit. on p. 10).

Jones, O. R., A. Scheuerlein, R. Salguero-Gómez, et al. (2014). Diversity of ageing across the tree of life. *Nature*. 505 (7482): 169–173 (cit. on pp. 5, 10).

Jung, H.-J., C. Coffinier, Y. Choe, et al. (2012). Regulation of prelamin A but not lamin C by miR-9, a brain-specific microRNA. *Proceedings of the National Academy of Sciences of the United States of America*. 109 (7): E423–E431 (cit. on p. 17).

Kalinowski, A., P. N. Yaron, Z. Qin, et al. (2014). Interfacial binding and aggregation of lamin A tail domains associated with Hutchinson–Gilford progeria syndrome. *Biophysical Chemistry*. 195: 43–48 (cit. on p. 12).

Kang, C., Q. Xu, T. D. Martin, et al. (2015). The DNA damage response induces inflammation and senescence by inhibiting autophagy of GATA4. *Science*. 349 (6255): aaa5612–aaa5612 (cit. on p. 9).

Kaushik, G., A. Spenlehauer, A. O. Sessions, et al. (2015). Vinculin network–mediated cytoskeletal remodeling regulates contractile function in the aging heart. *Science Translational Medicine*. 7 (292): 292ra99 (cit. on p. 69).

Kennedy, B. K., S. L. Berger, A. Brunet, et al. (2014). Geroscience: linking aging to chronic disease. *Cell*. 159 (4): 709–713 (cit. on pp. 1, 67).

Kenyon, C. J. (2010). The genetics of ageing. *Nature*. 464 (7288): 504–512 (cit. on pp. 5, 7).

Kirkwood, T. B. L. (2005). Understanding the Odd Science of Aging. *Cell*. 120 (4): 437–447 (cit. on p. 1).

Kirkwood, T. B. L. and S. Melov (2011). On the programmed/non-programmed nature of ageing within the life history. *Current Biology*. 21 (18): R701–R707 (cit. on p. 5).

Koga, H., S. Kaushik, and A. M. Cuervo (2011). Protein homeostasis and aging: The importance of exquisite quality control. *Ageing Research Reviews*. 10 (2): 205–215 (cit. on p. 7).

Kohn, J. C., M. C. Lampi, and C. A. Reinhart-King (2015). Age-related vascular stiffening: causes and consequences. *Frontiers in Genetics*. 06: 112 (cit. on p. 3).

Kontis, V., J. E. Bennett, C. D. Mathers, et al. (2017). Future life expectancy in 35 industrialised countries: projections with a Bayesian model ensemble. *The Lancet*. 389 (10076): 1323–1335 (cit. on p. 1).

Kreienkamp, R., C. Billon, G. Bedia-Diaz, et al. (2018). Doubled lifespan and patient-like pathologies in progeria mice fed high-fat diet. *Aging Cell*.: e12852 (cit. on pp. 70, 71).

Krishnan, V., M. Z. Y. Chow, Z. Wang, et al. (2011). Histone H4 lysine 16 hypoacetylation is associated with defective DNA repair and premature senescence in Zmpste24-deficient mice. *Proceedings of the National Academy of Sciences of the United States of America*. 108 (30): 12325–12330 (cit. on p. 7).

Lagouge, M., C. Argmann, Z. Gerhart-Hines, et al. (2006). Resveratrol improves mitochondrial function and protects against metabolic disease by activating SIRT1 and PGC-1α. *Cell*. 127 (6): 1109–1122 (cit. on p. 9).

Lakatta, E. G. (2003). Arterial and cardiac aging: major shareholders in cardiovascular disease enterprises: Part III: cellular and molecular clues to heart and arterial aging. *Circulation*. 107 (3): 490–497 (cit. on pp. 2–4, 68, 73).

Lapasset, L., O. Milhavet, A. Prieur, et al. (2011). Rejuvenating senescent and centenarian human cells by reprogramming through the pluripotent state. *Genes and Development*. 25 (21): 2248–2253 (cit. on p. 10).

Lapierre, L. R. and M. Hansen (2012). Lessons from C. elegans: signaling pathways for longevity. *Trends in Endocrinology & Metabolism*. 23 (12): 637–644 (cit. on p. 7).

Lee, P. G. and J. B. Halter (2017). The pathophysiology of hyperglycemia in older adults: Clinical considerations. *Diabetes Care*. 40 (4): 444–452 (cit. on p. 5).

Lee, S.-J., Y.-S. Jung, M.-H. Yoon, et al. (2016). Interruption of progerin–lamin A/C binding ameliorates Hutchinson-Gilford progeria syndrome phenotype. *Journal of Clinical Investigation*. 126 (10): 3879–3893 (cit. on pp. 12, 14).

Levine, M. E., J. A. Suarez, S. Brandhorst, et al. (2014). Low protein intake is associated with a major reduction in IGF-1, cancer, and overall mortality in the 65 and younger but not older population. *Cell Metabolism*. 19 (3): 407–417 (cit. on p. 11).

Levy, D., K. M. Anderson, D. D. Savage, et al. (1988). Echocardiographically detected left ventricular hypertrophy: prevalence and risk factors. The Framingham Heart Study. *Annals of internal medicine*. 108 (1): 7–13 (cit. on p. 2).

Li, J., S. Lin, P. M. Vanhoutte, C. W. Woo, and A. Xu (2016). Akkermansia muciniphila protects against atherosclerosis by preventing metabolic endotoxemia-induced inflammation in Apoe-/-Mice. *Circulation*. 133 (24): 2434–2446 (cit. on p. 11).

Liao, H. K., F. Hatanaka, T. Araoka, et al. (2017). In vivo target gene activation via CRISPR/Cas9-mediated trans-epigenetic modulation. *Cell*. 171 (7): 1495–1507.e15 (cit. on p. 15).

Libby, P. and G. K. Hansson (2015). Inflammation and immunity in diseases of the arterial tree: players and layers. *Circulation Research*. 116 (2): 307–11 (cit. on p. 4).

Lima, J. A. C. (2017). The aging human heart. *Circulation: Cardiovascular Imaging*. 10 (1): e005899 (cit. on p. 2).

Liu, B., J. Wang, K. M. Chan, et al. (2005). Genomic instability in laminopathy-based premature aging. *Nature Medicine*. 11 (7): 780–785 (cit. on p. 16).

Liu, B., Z. Wang, L. Zhang, et al. (2013). Depleting the methyltransferase Suv39h1 improves DNA repair and extends lifespan in a progeria mouse model. *Nature Communications*. 4 (1): 1868 (cit. on p. 16).

Liu, G. H., B. Z. Barkho, S. Ruiz, et al. (2011). Recapitulation of premature ageing with iPSCs from Hutchinson-Gilford progeria syndrome. *Nature*. 472 (7342): 221–227 (cit. on p. 40).

Lo Cicero, A. and X. Nissan (2015). Pluripotent stem cells to model Hutchinson-Gilford progeria syndrome (HGPS): Current trends and future perspectives for drug discovery. *Ageing Research Reviews*. 24 (Pt B): 343–348 (cit. on p. 14).

Loffredo, F. S., M. L. Steinhauser, S. M. Jay, et al. (2013). Growth differentiation factor 11 is a circulating factor that reverses age-related cardiac hypertrophy. *Cell*. 153 (4): 828–39 (cit. on p. 9).

Longo, V. D. and S. Panda (2016). Fasting, circadian rhythms, and time-restricted feeding in healthy lifespan. (Cit. on p. 11).

López-Mejía, I. C., M. De Toledo, C. Chavey, et al. (2014). Antagonistic functions of LMNA isoforms in energy expenditure and lifespan. *EMBO Reports*. 15 (5): 529–539 (cit. on pp. 15, 56, 65, 70–72, 74).

López-Otín, C., M. A. Blasco, L. Partridge, M. Serrano, and G. Kroemer (2013). The hallmarks of aging. *Cell*. 153 (6): 1194–217 (cit. on pp. 5–7, 16, 67).

López-Otín, C., L. Galluzzi, J. M. P. Freije, F. Madeo, and G. Kroemer (2016). Metabolic control of longevity. *Cell*. 166 (4): 802–821 (cit. on pp. 7, 9, 10, 74).

Lord, C. J. and A. Ashworth (2012). The DNA damage response and cancer therapy. *Nature*. 481 (7381): 287–294 (cit. on p. 6).

Lusk, G. (1909). The elements of the science of nutrition. 2nd ed. Philadelphia: W. B. Saunders: 403 (cit. on p. 31).

Madeo, F., F. Pietrocola, T. Eisenberg, and G. Kroemer (2014). Caloric restriction mimetics: Towards a molecular definition (cit. on p. 11).

Madeo, F., A. Zimmermann, M. C. Maiuri, and G. Kroemer (2015). Essential role for autophagy in life span extension (cit. on p. 11).

Mariño, G., A. P. Ugalde, N. Salvador-Montoliu, et al. (2008). Premature aging in mice activates a systemic metabolic response involving autophagy induction. *Human Molecular Genetics*. 17 (14): 2196–2211 (cit. on pp. 15, 16, 74).

Mariño, G., A. P. Ugalde, A. F. Fernández, et al. (2010). Insulin-like growth factor 1 treatment extends longevity in a mouse model of human premature aging by restoring somatotroph axis function. *Proceedings of the National Academy of Sciences of the United States of America*. 107 (37): 16268–16273 (cit. on pp. 8, 16, 75).

Martin, G. M. (2005). Genetic modulation of senescent phenotypes in Homo sapiens. *Cell*. 120 (4): 523–532 (cit. on p. 17).

Martin, T. L., T. Alquier, K. Asakura, et al. (2006). Diet-induced obesity alters AMP kinase activity in hypothalamus and skeletal muscle. *Journal of Biological Chemistry*. 281 (28): 18933–18941 (cit. on p. 71).

Martínez-Acedo, P., E. Núñez, F. J. S. Gómez, et al. (2012). A novel strategy for global analysis of the dynamic thiol redox proteome. *Molecular & Cellular Proteomics*. 11 (9): 800–813 (cit. on pp. 37, 47).

Martínez-Bartolomé, S., P. Navarro, F. Martín-Maroto, et al. (2008). Properties of average score distributions of SEQUEST: the probability ratio method. *Molecular & Cellular Proteomics*. 7 (6): 1135–1145 (cit. on p. 40).

Martos, R., J. Baugh, M. Ledwidge, et al. (2007). Diastolic heart failure: evidence of increased myocardial collagen turnover linked to diastolic dysfunction. *Circulation*. 115 (7): 888–895 (cit. on p. 2).

Mateos, J., A. Landeira-Abia, J. A. Fafián-Labora, et al. (2015). iTRAQ-based analysis of progerin expression reveals mitochondrial dysfunction, reactive oxygen species accumulation and altered proteostasis. *Stem Cell Research and Therapy*. 6 (1): 119 (cit. on p. 40).

Matesanz, N., E. Bernardo, R. Acín-Pérez, et al. (2017). MKK6 controls T3-mediated browning of white adipose tissue. *Nature Communications*. 8 (1): 856 (cit. on p. 32).

Matilainen, O., P. M. Quirós, and J. Auwerx (2017). Mitochondria and epigenetics – crosstalk in homeostasis and stress. (Cit. on p. 9).

Mattison, J. A., R. J. Colman, T. M. Beasley, et al. (2017). Caloric restriction improves health and survival of rhesus monkeys. *Nature Communications*. 8: 14063 (cit. on p. 11).

McClintock, D., D. Ratner, M. Lokuge, et al. (2007). The mutant form of lamin A that causes Hutchinson-Gilford progeria is a biomarker of cellular aging in human skin. *PLoS ONE*. 2 (12). Ed. by A. Lewin: e1269 (cit. on pp. 17, 67).

McCord, R. P., A. Nazario-Toole, H. Zhang, et al. (2013). Correlated alterations in genome organization, histone methylation, and DNA-lamin A/C interactions in Hutchinson-Gilford progeria syndrome. *Genome Research*. 23 (2): 260–269 (cit. on p. 40).

Merideth, M. A., L. B. Gordon, S. Clauss, et al. (2008). Phenotype and course of Hutchinson-Gilford progeria syndrome. *New England Journal of Medicine*. 358 (6): 592–604 (cit. on pp. 12, 17, 19, 44, 68, 70, 71, 74).

Merino, M. M., C. Rhiner, J. M. Lopez-Gay, et al. (2015). Elimination of unfit cells maintains tissue health and prolongs lifespan. *Cell*. 160 (3): 461–476 (cit. on p. 10).

Michalakis, K., D. G. Goulis, A. Vazaiou, et al. (2013). Obesity in the ageing man. *Metabolism*. 62 (10): 1341–1349 (cit. on pp. 1, 4, 70, 74).

Mitchell, G. F., A. Jeron, and G. Koren (1998). Measurement of heart rate and Q-T interval in the conscious mouse. *American Journal of Physiology-Heart and Circulatory Physiology*. 274 (3): H747–H751 (cit. on p. 26).

Moghtadaei, M., H. J. Jansen, M. Mackasey, et al. (2016). The impacts of age and frailty on heart rate and sinoatrial node function. *The Journal of Physiology*. 594 (23): 7105–7126 (cit. on pp. 3, 73).

Molofsky, A. V., S. G. Slutsky, N. M. Joseph, et al. (2006). Increasing p16 INK4a expression decreases forebrain progenitors and neurogenesis during ageing. *Nature*. 443 (7110): 448–452 (cit. on p. 8).

Monahan, K. D. (2007). Effect of aging on baroreflex function in humans. *American Journal of Physiology-Regulatory, Integrative and Comparative Physiology*. 293 (1): R3–R12 (cit. on p. 3).

Moran, C. M., A. J. W. Thomson, E. Rog-Zielinska, and G. A. Gray (2013). High-resolution echocardiography in the assessment of cardiac physiology and disease in preclinical models. *Experimental Physiology*. 98 (3): 629–644 (cit. on pp. 27, 28).

Morley, J. E. (2013). Pathophysiology of the anorexia of aging (cit. on pp. 4, 70).

Morrow, G., M. Samson, S. Michaud, and R. M. Tanguay (2004). Overexpression of the small mitochondrial Hsp22 extends Drosophila life span and increases resistance to oxidative stress. *The FASEB Journal*. 18 (3): 598–599 (cit. on p. 7).

Moskalev, A. A., M. V. Shaposhnikov, E. N. Plyusnina, et al. (2013). The role of DNA damage and repair in aging through the prism of Koch-like criteria. *Ageing Research Reviews*. 12 (2): 661–684 (cit. on p. 6).

Mostoslavsky, R., K. F. Chua, D. B. Lombard, et al. (2006). Genomic instability and aging-like phenotype in the absence of mammalian SIRT6. *Cell*. 124 (2): 315–329 (cit. on p. 7).

Nair, K., P. Ramachandran, K. M. Krishnamoorthy, S. Dora, and T. J. Achuthan (2004). Hutchinson-Gilford progeria syndrome with severe calcific aortic valve stenosis and calcific mitral valve. *The Journal of Heart Valve Disease*. 13 (5): 866–869 (cit. on pp. 19, 68).

Navarro, P. and J. Vázquez (2009). A refined method to calculate false discovery rates for peptide identification using decoy databases. *Journal of Proteome Research*. 8 (4): 1792–1796 (cit. on p. 40).

Navarro, P., M. Trevisan-Herraz, E. Bonzon-Kulichenko, et al. (2014). General statistical framework for quantitative proteomics by stable isotope labeling. *Journal of Proteome Research*. 13 (3): 1234–1247 (cit. on p. 40).

Neufer, P. D., M. M. Bamman, D. M. Muoio, et al. (2015). Understanding the cellular and molecular mechanisms of physical activity-induced health benefits. (Cit. on p. 11).

Newman, J. C., A. J. Covarrubias, M. Zhao, et al. (2017). Ketogenic diet reduces midlife mortality and improves memory in aging mice. *Cell Metabolism*. 26 (3): 547–557.e8 (cit. on p. 69).

Nguyen, T. N., S. N. Hilmer, and R. G. Cumming (2013). Review of epidemiology and management of atrial fibrillation in developing countries. *International Journal of Cardiology*. 167 (6): 2412–2420 (cit. on p. 3).

Nissan, X., S. Blondel, C. L. Navarro, et al. (2012). Unique preservation of neural cells in Hutchinson-Gilford progeria syndrome is due to the expression of the neural-specific miR-9 microRNA. *Cell Reports*. 2 (1): 1–9 (cit. on p. 17).

Ocampo, A., P. Reddy, P. Martinez-Redondo, et al. (2016). In vivo amelioration of age-associated hallmarks by partial reprogramming. *Cell*. 167 (7): 1719–1733.e12 (cit. on pp. 8, 10, 15, 75).

Oelkrug, R., G. Heldmaier, and C. W. Meyer (2011). Torpor patterns, arousal rates, and temporal organization of torpor entry in wildtype and UCP1-ablated mice. *Journal of Comparative Physiology*. 181 (1): 137–145 (cit. on pp. 53, 71, 72).

Oldenburg, A. R., N. Briand, A. L. Sørensen, et al. (2017). A lipodystrophy-causing lamin A mutant alters conformation and epigenetic regulation of the anti-adipogenic MIR335 locus. *The Journal of Cell Biology*. 216 (9): 2731–2743 (cit. on p. 33).

Olive, M., I. A. Harten, R. Mitchell, et al. (2010). Cardiovascular pathology in Hutchinson-Gilford progeria: correlation with the vascular pathology of aging. *Arteriosclerosis, Thrombosis, and Vascular Biology*. 30 (11): 2301–2309 (cit. on p. 19).

Olivetti, G., G. Giordano, D. Corradi, et al. (1995). Gender differences and aging: Effects on the human heart. *Journal of the American College of Cardiology*. 26 (4): 1068–1079 (cit. on p. 2).

Ortega-Molina, A., E. Lopez-Guadamillas, J. A. Mattison, et al. (2015). Pharmacological inhibition of PI3K reduces adiposity and metabolic syndrome in obese mice and rhesus monkeys. *Cell Metabolism*. 21 (4): 558–570 (cit. on p. 11).

Osorio, F. G., I. Varela, E. Lara, et al. (2010). Nuclear envelope alterations generate an aging-like epigenetic pattern in mice deficient in Zmpste24 metalloprotease. *Aging Cell*. 9 (6): 947–957 (cit. on p. 16).

Osorio, F. G., C. L. Navarro, J. Cadiñanos, et al. (2011). Splicing-directed therapy in a new mouse model of human accelerated aging. *Science Translational Medicine*. 3 (106): 106ra107 (cit. on pp. 14, 15, 24, 40, 43, 56, 58, 67, 68, 70, 72, 75).

Osorio, F. G., C. Bárcena, C. Soria-Valles, et al. (2012). Nuclear lamina defects cause ATM-dependent NF- B activation and link accelerated aging to a systemic inflammatory response. *Genes & Development*. 26 (20): 2311–2324 (cit. on p. 17).

Pacheco, L. M., L. A. Gomez, J. Dias, et al. (2014). Progerin expression disrupts critical adult stem cell functions involved in tissue repair. *Aging*. 6 (12): 1049–1063 (cit. on p. 17).

Paneni, F., C. Diaz Cañestro, P. Libby, T. F. Lüscher, and G. G. Camici (2017). The aging cardiovascular system. *Journal of the American College of Cardiology*. 69 (15): 1952–1967 (cit. on p. 3).

Pendás, A. M., Z. Zhou, J. Cadiñanos, et al. (2002). Defective prelamin A processing and muscular and adipocyte alterations in Zmpste24 metalloproteinase-deficient mice. *Nature Genetics*. 31 (1): 94–99 (cit. on pp. 12, 14, 70).

Pereira, S., P. Bourgeois, C. L. Navarro, et al. (2008). HGPS and related premature aging disorders: From genomic identification to the first therapeutic approaches. *Mechanisms of Ageing and Development*. 129 (7-8): 449–459 (cit. on p. 11).

Peters, M. J., R. Joehanes, L. C. Pilling, et al. (2015). The transcriptional landscape of age in human peripheral blood. *Nature Communications*. 6 (1): 8570 (cit. on p. 10).

Picard, F., M. Kurtev, N. Chung, et al. (2004). Erratum: Sirt1 promotes fat mobilization in white adipocytes by repressing PPAR-γ. *Nature*. 429 (6993): 771–776 (cit. on p. 9).

Piek, A., R. A. de Boer, and H. H. W. Silljé (2016). The fibrosis-cell death axis in heart failure. *Heart Failure Reviews*. 21 (2): 199–211 (cit. on p. 2).

Pietrocola, F., J. Pol, E. Vacchelli, et al. (2016). Caloric restriction mimetics enhance anticancer immunosurveillance. *Cancer Cell*. 30 (1): 147–160 (cit. on p. 11).

Plovier, H., A. Everard, C. Druart, et al. (2017). A purified membrane protein from Akkermansia muciniphila or the pasteurized bacterium improves metabolism in obese and diabetic mice. *Nature Medicine*. 23 (1): 107–113 (cit. on p. 11).

Powers, E. T., R. I. Morimoto, A. Dillin, J. W. Kelly, and W. E. Balch (2009). Biological and chemical approaches to diseases of proteostasis deficiency. *Annual Review of Biochemistry*. 78 (1): 959–991 (cit. on p. 7).

Pradhan, A. D., J. E. Manson, N. Rifai, J. E. Buring, and P. M. Ridker (2001). C-reactive protein, interleukin 6, and risk of developing type 2 diabetes mellitus. *Journal of the American Medical Association*. 286 (3): 327–334 (cit. on p. 4).

Prakash, A., L. B. Gordon, M. E. Kleinman, et al. (2018). Cardiac abnormalities in patients with Hutchinson-Gilford progeria syndrome. *JAMA Cardiology*. 3 (4): 326 (cit. on pp. 19, 68, 73).

Puente, X. S., V. Quesada, F. G. Osorio, et al. (2011). Exome sequencing and functional analysis identifies BANF1 mutation as the cause of a hereditary progeroid syndrome. *American Journal of Human Genetics*. 88 (5): 650–656 (cit. on p. 11).

Pyo, J. O., S. M. Yoo, H. H. Ahn, et al. (2013). Overexpression of Atg5 in mice activates autophagy and extends lifespan. *Nature Communications*. 4 (1): 2300 (cit. on p. 9).

Quirós, P. M., A. Mottis, and J. Auwerx (2016). Mitonuclear communication in homeostasis and stress. *Nature Reviews Molecular Cell Biology*. 17 (4): 213–226 (cit. on p. 9).

Ragnauth, C. D., D. T. Warren, Y. Liu, et al. (2010). Prelamin A acts to accelerate smooth muscle cell senescence and is a novel biomarker of human vascular aging. *Circulation*. 121 (20): 2200–2210 (cit. on p. 17).

Rando, T. A. and H. Y. Chang (2012). Aging, rejuvenation, and epigenetic reprogramming: resetting the aging clock. *Cell*. 148 (1-2): 46–57 (cit. on p. 8).

Rao Kondapally Seshasai, S., S. Kaptoge, A. Thompson, et al. (2011). Diabetes mellitus, fasting glucose, and risk of cause-specific death. *New England Journal of Medicine*. 364 (9): 829–841 (cit. on p. 5).

Reddy, S. and L. Comai (2012). Lamin A, farnesylation and aging. *Experimental Cell Research*. 318 (1): 1–7 (cit. on p. 17).

Revêchon, G., N. Viceconte, T. McKenna, et al. (2017). Rare progerin-expressing preadipocytes and adipocytes contribute to tissue depletion over time. *Scientific Reports*. 7 (1): 4405 (cit. on p. 74).

Richardson, M. R., X. Lai, S. B. Mason, S. J. Miller, and F. A. Witzmann (2008). Differential protein expression during aging in ventricular myocardium of Fischer 344×Brown Norway hybrid rats. *Experimental Gerontology*. 43 (10): 909–918 (cit. on p. 69).

Righolt, C. H., M. L. van 't Hoff, B. J. Vermolen, I. T. Young, and V. Raz (2011). Robust nuclear lamina-based cell classification of aging and senescent cells. *Aging*. 3 (12): 1192–1201 (cit. on p. 16).

Rivera-Torres, J., R. Acín-Pérez, P. Cabezas-Sánchez, et al. (2013). Identification of mitochondrial dysfunction in Hutchinson-Gilford progeria syndrome through use of stable isotope labeling with amino acids in cell culture. *Journal of proteomics*. 91: 466–477 (cit. on pp. 16, 40, 69, 71).

Rivera-Torres, J., C. J. Calvo, A. Llach, et al. (2016). Cardiac electrical defects in progeroid mice and Hutchinson–Gilford progeria syndrome patients with nuclear lamina alterations. *Proceedings of the National Academy of Sciences*. 113 (46): E7250–E7259 (cit. on pp. 14, 19, 44, 68, 73).

Rodriguez, S., F. Coppedè, H. Sagelius, and M. Eriksson (2009). Increased expression of the Hutchinson-Gilford progeria syndrome truncated lamin A transcript during cell aging. *European journal of human genetics : EJHG*. 17 (7): 928–937 (cit. on pp. 17, 67).

Rosengardten, Y., T. McKenna, D. Grochová, and M. Eriksson (2011). Stem cell depletion in Hutchinson-Gilford progeria syndrome. *Aging Cell*. 10 (6): 1011–1020 (cit. on p. 17).

Roth, G. A., C. Johnson, A. Abajobir, et al. (2017). Global, regional, and national burden of cardiovascular diseases for 10 causes, 1990 to 2015. *Journal of the American College of Cardiology*. 70 (1): 1–25 (cit. on p. 1).

Ruf, T. and F. Geiser (2015). Daily torpor and hibernation in birds and mammals. *Biological Reviews*. 90 (3): 891–926 (cit. on p. 71).

Russell, S. J. and C. R. Kahn (2007). Endocrine regulation of ageing. *Nature Reviews Molecular Cell Biology*. 8 (9): 681–691 (cit. on p. 8).

Sahin, E. and R. A. Depinho (2010). Linking functional decline of telomeres, mitochondria and stem cells during ageing (cit. on p. 10).

Sahin, E., S. Colla, M. Liesa, et al. (2011). Telomere dysfunction induces metabolic and mitochondrial compromise. *Nature*. 470 (7334): 359–365 (cit. on p. 9).

Samuel, V. T., K. F. Petersen, and G. I. Shulman (2010). Lipid-induced insulin resistance: unravelling the mechanism (cit. on p. 5).

Santiago-Fernández, O., F. G. Osorio, V. Quesada, et al. (2019). Development of a CRISPR/Cas9-based therapy for Hutchinson–Gilford progeria syndrome. *Nature Medicine*.: 1 (cit. on pp. 15, 75).

Savji, N., C. B. Rockman, A. H. Skolnick, et al. (2013). Association between advanced age and vascular disease in different arterial territories. *Journal of the American College of Cardiology*. 61 (16): 1736–1743 (cit. on pp. 1, 67).

Sawaki, D., G. Czibik, M. Pini, et al. (2018). Visceral adipose tissue drives cardiac aging through modulation of fibroblast senescence by osteopontin production. *Circulation*. 138 (8): 809–822 (cit. on p. 4).

Scaffidi, P. (2006). Lamin A-dependent nuclear defects in human aging. *Science*. 312 (5776): 1059–1063 (cit. on pp. 16, 17, 67).

Scaffidi, P. and T. Misteli (2005). Reversal of the cellular phenotype in the premature aging disease Hutchinson-Gilford progeria syndrome. *Nature Medicine*. 11 (4): 440–445 (cit. on p. 15).

– (2008). Lamin A-dependent misregulation of adult stem cells associated with accelerated ageing. *Nature cell biology*. 10 (4): 452–459 (cit. on pp. 17, 40, 74).

Schnelle, M., N. Catibog, M. Zhang, et al. (2018). Echocardiographic evaluation of diastolic function in mouse models of heart disease. *Journal of Molecular and Cellular Cardiology*. 114: 20–28 (cit. on p. 28).

Sen, P., P. P. Shah, R. Nativio, and S. L. Berger (2016). Epigenetic mechanisms of longevity and aging. (Cit. on p. 69).

Shaw, A. C., S. Joshi, H. Greenwood, A. Panda, and J. M. Lord (2010). Aging of the innate immune system. *Current Opinion in Immunology*. 22 (4): 507–513 (cit. on p. 8).

Shin, H., Y. Ma, T. Chanturiya, et al. (2017). Lipolysis in brown adipocytes is not essential for cold-induced thermogenesis in mice. *Cell Metabolism*. 26 (5): 764–777 (cit. on pp. 62, 74).

Shumaker, D. K., T. Dechat, A. Kohlmaier, et al. (2006). Mutant nuclear lamin A leads to progressive alterations of epigenetic control in premature aging. *Proceedings of the National Academy of Sciences of the United States of America*. 103 (23): 8703–8708 (cit. on p. 16).

Shuster, A., M. Patlas, J. H. Pinthus, and M. Mourtzakis (2012). The clinical importance of visceral adiposity: a critical review of methods for visceral adipose tissue analysis. *The British Journal of Radiology*. 85 (1009): 1–10 (cit. on pp. 4, 70).

Signore, S., A. Sorrentino, G. Borghetti, et al. (2015). Late Na+ current and protracted electrical recovery are critical determinants of the aging myopathy. *Nature Communications*. 6 (1): 8803 (cit. on p. 68).

Silvera, V. M., L. B. Gordon, D. B. Orbach, et al. (2013). Imaging characteristics of cerebrovascular arteriopathy and stroke in Hutchinson-Gilford progeria syndrome. *American Journal of Neuroradiology*. 34 (5): 1091–1097 (cit. on p. 19).

Sinensky, M., K. S. Fantle, M. A. Trujillo, et al. (1994). The processing pathway of prelamin A. *Journal of Cell Science*. 107: 61–67 (cit. on p. 12).

Soto, M., L. Orliaguet, M. L. Reyzer, et al. (2018). Pyruvate induces torpor in obese mice. *Proceedings of the National Academy of Sciences of the United States of America*. 115 (4): 810–815 (cit. on p. 71).

Sousa-Victor, P., L. García-Prat, A. L. Serrano, E. Perdiguero, and P. Muñoz-Cánoves (2015). Muscle stem cell aging: regulation and rejuvenation. *Trends in Endocrinology & Metabolism*. 26 (6): 287–296 (cit. on p. 8).

Spadaccio, C., P. Mozetic, F. Nappi, et al. (2016). Cells and extracellular matrix interplay in cardiac valve disease: because age matters. *Basic Research in Cardiology*. 111 (2): 16 (cit. on p. 2).

Speakman, J. R. and K. R. Westerterp (2010). Associations between energy demands, physical activity, and body composition in adult humans between 18 and 96 y of age. *American Journal of Clinical Nutrition*. 92 (4): 826–834 (cit. on pp. 4, 70).

Speerschneider, T. and M. B. Thomsen (2013). Physiology and analysis of the electrocardiographic T wave in mice. *Acta Physiologica*. 209 (4): 262–271 (cit. on p. 26).

Stehbens, W. E., B. Delahunt, T. Shozawa, and E. Gilbert-Barness (2001). Smooth muscle cell depletion and collagen types in progeric arteries. *Cardiovascular Pathology*. 10 (3): 133–136 (cit. on p. 19).

Sullivan, T., D. Escalante-Alcalde, H. Bhatt, et al. (1999). Loss of A-type lamin expression compromises nuclear envelope integrity leading to muscular dystrophy. *The Journal of Cell Biology*. 147 (5): 913–920 (cit. on p. 15).

Sun, K., J. Tordjman, K. Clément, and P. E. Scherer (2013). Fibrosis and adipose tissue dysfunction. *Cell metabolism*. 18 (4): 470–477 (cit. on p. 4).

Sun, Z. (2015). Aging, arterial stiffness, and hypertension. *Hypertension*. 65 (2): 252–256 (cit. on p. 3).

Takahashi, K. and S. Yamanaka (2006). Induction of pluripotent stem cells from mouse embryonic and adult fibroblast cultures by defined factors. *Cell*. 126 (4): 663–676 (cit. on p. 10).

Talens, R. P., K. Christensen, H. Putter, et al. (2012). Epigenetic variation during the adult lifespan: cross-sectional and longitudinal data on monozygotic twin pairs. *Aging Cell*. 11 (4): 694–703 (cit. on p. 7).

Taylor, J. A. and C. O. Tan (2014). BP regulation VI: elevated sympathetic outflow with human aging: hypertensive or homeostatic? *European Journal of Applied Physiology*. 114 (3): 511–519 (cit. on p. 3).

Tchkonia, T., T. Thomou, Y. Zhu, et al. (2013). Mechanisms and metabolic implications of regional differences among fat depots (cit. on pp. 4, 20, 70).

Thibault, H. B., B. Kurtz, M. J. Raher, et al. (2010). Noninvasive assessment of murine pulmonary arterial pressure: validation and application to models of pulmonary hypertension. *Circulation: Cardiovascular Imaging*. 3 (2): 157–163 (cit. on p. 28).

Toribio-Fernández, R., V. Zorita, V. Rocha-Perugini, et al. (2018). Lamin A/C augments Th1 differentiation and response against vaccinia virus and Leishmania major. *Cell Death & Disease*. 9 (1): 9 (cit. on p. 17).

Trevisan-Herraz, M., N. Bagwan, F. García-Marqués, et al. (2018). SanXoT: a modular and versatile package for the quantitative analysis of high-throughput proteomics experiments. *Bioinformatics*. (May). Ed. by A. Valencia (cit. on pp. 40, 49).

Tschöp, M. H., J. R. Speakman, J. R. S. Arch, et al. (2011). A guide to analysis of mouse energy metabolism. *Nature Methods*. 9 (1): 57–63 (cit. on pp. 31, 71).

Ugalde, A. P., A. J. Ramsay, J. de la Rosa, et al. (2011). Aging and chronic DNA damage response activate a regulatory pathway involving miR-29 and p53. *The EMBO Journal*. 30 (11): 2219–2232 (cit. on p. 16).

Ullrich, N. J. and L. B. Gordon (2015). Hutchinson–Gilford progeria syndrome. *Handbook of Clinical Neurology*. 132: 249–264 (cit. on pp. 12, 17).

Vaidya, A., Z. Mao, X. Tian, et al. (2014). Knock-in reporter mice demonstrate that DNA repair by non-homologous end joining declines with age. *PLoS Genetics*. 10 (7). Ed. by P. Hasty: e1004511 (cit. on p. 6).

Varela, I., J. Cadiñanos, A. M. Pendás, et al. (2005). Accelerated ageing in mice deficient in Zmpste24 protease is linked to p53 signalling activation. *Nature*. 437 (7058): 564–568 (cit. on pp. 14, 16).

Varela, I., S. Pereira, A. P. Ugalde, et al. (2008). Combined treatment with statins and aminobisphosphonates extends longevity in a mouse model of human premature aging. *Nature medicine*. 14 (7): 767–772 (cit. on pp. 15, 75).

Varga, R., M. Eriksson, M. R. Erdos, et al. (2006). Progressive vascular smooth muscle cell defects in a mouse model of Hutchinson-Gilford progeria syndrome. *Proceedings of the National Academy of Sciences of the United States of America*. 103 (9): 3250–3255 (cit. on p. 14).

Verdin, E. (2015). NAD+ in aging, metabolism, and neurodegeneration. *Science*. 350 (6265): 1208–1213 (cit. on p. 9).

Villa-Bellosta, R., J. Rivera-Torres, F. G. Osorio, et al. (2013). Defective extracellular pyrophosphate metabolism promotes vascular calcification in a mouse model of Hutchinson-Gilford progeria syndrome that is ameliorated on pyrophosphate treatment. *Circulation*. 127 (24): 2442–2451 (cit. on pp. 14, 43, 58, 67).

Villeda, S. A., J. Luo, K. I. Mosher, et al. (2011). The ageing systemic milieu negatively regulates neurogenesis and cognitive function. *Nature*. 477 (7362): 90–94 (cit. on p. 9).

Volkert, D. and C. C. Sieber (2011). Protein requirements in the elderly. *International Journal for Vitamin and Nutrition Research*. 81 (2-3): 109–119 (cit. on pp. 4, 70).

Walther, D. M. and M. Mann (2011). Accurate quantification of more than 4000 mouse tissue proteins reveals minimal proteome changes during aging. *Molecular & Cellular Proteomics*. 10 (2): M110.004523 (cit. on p. 68).

Wang, L., W. Yang, W. Ju, et al. (2012). A proteomic study of Hutchinson-Gilford progeria syndrome: Application of 2D-chromotography in a premature aging disease. *Biochemical and Biophysical Research Communications*. 417 (4): 1119–1126 (cit. on p. 40).

Wang, M., R. E. Monticone, and E. G. Lakatta (2014). Proinflammation of aging central arteries: a mini-review. *Gerontology*. 60 (6): 519–529 (cit. on p. 3).

Wiśniewski, J. R., A. Zougman, N. Nagaraj, and M. Mann (2009). Universal sample preparation method for proteome analysis. *Nature Methods*. 6 (5): 359–362 (cit. on pp. 37, 47).

Wong, J., R. Chabiniok, A. DeVecchi, et al. (2016). Age-related changes in intraventricular kinetic energy: a physiological or pathological adaptation? *American Journal of Physiology-Heart and Circulatory Physiology*. 310 (6): H747–H755 (cit. on pp. 2, 68).

Worman, H. J. (2012). Nuclear lamins and laminopathies. *The Journal of Pathology*. 226 (2): 316–325 (cit. on pp. 6, 11).

Xiong, Z. M., C. LaDana, D. Wu, and K. Cao (2013). An inhibitory role of progerin in the gene induction network of adipocyte differentiation from iPS cells. *Aging*. 5 (4): 288–303 (cit. on p. 74).

Xu, M., A. K. Palmer, H. Ding, et al. (2015). Targeting senescent cells enhances adipogenesis and metabolic function in old age. *eLife*. 4 (December): e12997 (cit. on p. 9).

Yancy, C. W., M. Jessup, B. Bozkurt, et al. (2013). 2013 ACCF/AHA guideline for the management of heart failure. *Journal of the American College of Cardiology*. 62 (16): e147–e239 (cit. on p. 2).

Yang, S. H., M. O. Bergo, J. I. Toth, et al. (2005). Blocking protein farnesyltransferase improves nuclear blebbing in mouse fibroblasts with a targeted Hutchinson-Gilford progeria syndrome mutation. *Proceedings of the National Academy of Sciences of the United States of America*. 102 (29): 10291–10306 (cit. on pp. 14, 15).

Yang, S. H., M. D. Meta, X. Qiao, et al. (2006). A farnesyltransferase inhibitor improves disease phenotypes in mice with a Hutchinson-Gilford progeria syndrome mutation. *Journal of Clinical Investigation*. 116 (8): 2115–2121 (cit. on p. 15).

Yang, S. H., S. Y. Chang, S. Ren, et al. (2011). Absence of progeria-like disease phenotypes in knock-in mice expressing a non-farnesylated version of progerin. *Human Molecular Genetics*. 20 (3): 436–444 (cit. on p. 12).

Yin, W., E. Carballo-Jane, D. G. McLaren, et al. (2012). Plasma lipid profiling across species for the identification of optimal animal models of human dyslipidemia. *Journal of lipid research*. 53 (1): 51–65 (cit. on p. 70).

Yu, Q., Y. V. Katlinskaya, C. J. Carbone, et al. (2015). DNA-damage-induced type I interferon promotes senescence and inhibits stem cell function. *Cell Reports*. 11 (5): 785–797 (cit. on p. 9).

Yun, C., A. Stanhill, Y. Yang, et al. (2008). Proteasomal adaptation to environmental stress links resistance to proteotoxicity with longevity in Caenorhabditis elegans. *Proceedings of the National Academy of Sciences of the United States of America*. 105 (19): 7094–7099 (cit. on p. 7).

Zahn, J. M., S. Poosala, A. B. Owen, et al. (2007). AGEMAP: A gene expression database for aging in mice. *PLoS Genetics*. 3 (11): 2326–2337 (cit. on p. 40).

Zhang, C. and A. M. Cuervo (2008). Restoration of chaperone-mediated autophagy in aging liver improves cellular maintenance and hepatic function. *Nature Medicine*. 14 (9): 959–965 (cit. on p. 7).

Zhang, G., J. Li, S. Purkayastha, et al. (2013). Hypothalamic programming of systemic ageing involving IKK-β, NF-κB and GnRH. *Nature*. 497 (7448): 211–216 (cit. on p. 8).

Zhang, J., Q. Lian, G. Zhu, et al. (2011). A human iPSC model of hutchinson gilford progeria reveals vascular smooth muscle and mesenchymal stem cell defects. *Cell Stem Cell*. 8 (1): 31–45 (cit. on p. 74).

Zoghbi, W. A. and M. A. Quinones (1986). Determination of cardiac output by Doppler echocardiography: a critical appraisal. *Herz*. 11 (5): 258–268 (cit. on p. 28).

Zoni-Berisso, M., F. Lercari, T. Carazza, and S. Domenicucci (2014). Epidemiology of atrial fibrillation: European perspective. *Clinical Epidemiology*. 6: 213 (cit. on p. 3).

Zwighaft, Z., R. Aviram, M. Shalev, et al. (2015). Circadian clock control by polyamine levels through a mechanism that declines with age. *Cell Metabolism*. 22 (5): 874–885 (cit. on pp. 8, 10).

List of Figures

List of Tables

Colophon

This thesis was typeset with LaTeX 2_ε by modifying the *Clean Thesis* style (Ricardo Langner). The artwork in the epigraph and in figure 4 was designed by Mercedes Collantes.